Ensemble Smoother with Multiple Data Assimilation to parameterize subsidence by phreatic groundwater level lowering in the South Flevoland Polder, the Netherlands

Manon Anna Maria Verberne[1], Kay Koster[2], Aris Lourens[2], Jan Gunnink[3], Thibault Candela[4], and Peter A. Fokker[4]

[1]Utrecht University
[2]TNO - Geological Survey of the Netherlands
[3]TNO-Geological Survey of the Netherlands
[4]TNO

December 15, 2022

Abstract

This research targets disentangling shallow causes of anthropogenically-induced subsidence in a reclaimed and urbanized coastal plain. The study area is around the city of Almere, in the South Flevoland polder, the Netherlands, which is among the countries' fastest subsiding areas. The procedure consists of integrating synthetic Interferometric Synthetic Aperture Radar (InSAR) data with high-resolution phreatic groundwater and lithoclass models, and a database containing construction details. The two main parts of the workflow are isolation of the InSAR points of structures without a pile foundation and a data assimilation procedure by Ensemble Smoothing with Multiple Data Assimilation. The shrinkage of surficial clay beds by phreatic groundwater level lowering is identified to be the main cause of shallow subsidence in the area, with an average contribution of 6 mm/year. The history-matched physics-based model predicts that one meter drop in phreatic groundwater level now translates into 10 millimeter of subsidence in the next five years. Also, this study showed that a groundwater deficiency due to severe dry periods should be considered as an accelerator of subsidence in both the short- and long-term planning. To ensure a robust network to estimate future subsidence, we advise on a consistent monitoring strategy of the phreatic groundwater level.

Ensemble Smoother with Multiple Data Assimilation to parameterize subsidence by phreatic groundwater level lowering in the South Flevoland Polder, the Netherlands

Subtitle: Disentangling Shallow Subsidence Sources by Data Assimilation in a Reclaimed Ubanized Coastal Plain

Manon Verberne[1,2], Kay Koster[3], Aris Lourens[3], Jan Gunnink[3], Thibault Candela[2] and Peter A. Fokker[1,2]

[1] Utrecht University, Geosciences, Utrecht, The Netherlands
[2] TNO Applied Geoscience, Utrecht, The Netherlands
[3] TNO Geomodelling, Utrecht, The Netherlands

Corresponding author: Manon Verberne (manon.verberne@tno.nl)

Key Points:

- Interferometric Synthetic Aperture Rader data on objects constructed on soft soil without a foundation are used for subsidence measurements
- Shrinkage of clay by aeration as a result of artificially lowered phreatic groundwater levels is identified as the main source of subsidence
- One meter drop in phreatic groundwater level now translates into one centimeter of subsidence in five years

Abstract

This research targets disentangling shallow causes of anthropogenically-induced subsidence in a reclaimed and urbanized coastal plain. The study area is around the city of Almere, in the South Flevoland polder, the Netherlands, which is among the countries' fastest subsiding areas. The procedure consists of integrating Interferometric Synthetic Aperture Radar (InSAR) data with high-resolution phreatic groundwater and lithoclass models, and a database containing construction details. The two main parts of the workflow are isolation of the InSAR points of structures without a pile foundation and a data assimilation procedure by Ensemble Smoothing with Multiple Data Assimilation. The shrinkage of surficial clay beds by phreatic groundwater level lowering is identified to be the main cause of shallow subsidence in the area, with an average contribution of 6 mm/year. The history-matched physics-based model predicts that one meter drop in phreatic groundwater level now translates into 10 millimeter of subsidence in the next five years. Also, this study showed that a groundwater deficiency due to severe dry periods should be considered as an accelerator of subsidence in both the short- and long-term planning. To ensure a robust network to estimate future subsidence, we advise on a consistent monitoring strategy of the phreatic groundwater level.

Plain Language Summary

The city of Almere, in the Netherlands, is part of a polder that was reclaimed in 1968. Land reclamation is accompanied by lowering of groundwater levels, which can cause land subsidence. Almere is situated on top of ~9 meters of soft soil layers. These layers were deposited after the last ice age and consist predominantly of clay and peat. It is important to understand and quantify the subsidence processes in these Holocene layers, to be able to mitigate subsidence.

By lowering the groundwater level, the soft soil layers are dried. Clay shrinks when it dries out and organic material (within peat) oxidizes. Lowering the groundwater level also causes the load of the layers below to increase, which can result in compaction of the layers (reduction in size by pressing together). This study targets the behavior of these processes.

Results of our study indicate that the shrinkage of clay is the dominant driver of subsidence in Almere. One meter lowering in groundwater level now results in approximately one centimeter subsidence in five years. To improve our understanding of the non-trivial link between groundwater fluctuations and subsidence, higher spatial-temporal resolution groundwater monitoring is required.

1 Introduction

Over half a billion people live in coastal plains and deltas threatened by anthropogenically induced subsidence, and this number is expected to increase in the foreseeable future (Neumann, 2015; Schmidt, 2015). Many anthropogenic subsurface activities in coastal areas and delta plains result in subsidence, thereby amplifying relative sea-level rise and flood risks, inflicting damage to infrastructure, and overall, reducing the viability of these low-lying areas (Dinar et al., 2021; Guo and Jiao, 2007; Syvitski et al., 2009). Examples of subsurface activities are resources extraction, such as groundwater (Jones et al., 2016) and deep hydrocarbons (Chaussard et al., 2013), and surficial processes related to land use, primarily phreatic groundwater level management (Koster, Stafleu and Stouthamer, 2018), and sediment deficit (Eslami et al., 2019).

Some heavily populated coastal plains and deltas require engineered extension of their surface area by land reclamation, to accommodate population growth, and increase the surface area of arable land, e.g. China, Belgium, Japan, Dubai, U.S. and Singapore (e.g. Declerq et al., 2021; Li et al., 2022; Martín-Antón et al, 2016; Wang et al., 2014). When land is gained along sea or lake shorelines by drainage of open water, this in essence means exposing waterlogged sediments to the atmosphere, thereby instigating various subsidence processes, primarily by shrinkage, compaction, and oxidation of fine grained and organic deposits.

The dense population of Hong Kong for instance, prompted the government to reclaim land since the nineteenth century. There, rates of subsidence are around 20 mm/year, resulting in major damage to the built environment by differential settlements (Sun et al., 2018; Wang et al., 2016). In Bangladesh, reclamation primarily serves the purpose of gaining arable land, resulting in subsidence rates up to 10 mm/year in these reclaimed areas. This catalyzes a rise in social inequality as especially low-income farmers are not able to cover adaptation costs for the negative effects of these high subsidence rates (Barbour et al., 2002; Steckler et al., 2022).

The Netherlands is a prime example of a country that has extended its coastal plains by land reclamation. In total, the Netherlands has 443 reclaimed former lakes located in its coastal plains, with a cumulative surface area of 3123.60 km^2 (Schultz, 1987). The centuries-long tradition of reclaiming land, referred to as ‘polder’, can be divided into three main periods of lake drainage. The first stage comprised the sixteenth to seventeenth century, when many small lakes within the back-barrier peatlands were drained with windmills. Secondly, in the nineteenth century, larger lakes in the coastal plain were drained with steam pumping stations. Lastly, in the twentieth century, Lake IJssel, the countries’ largest lake that was created by the damming of a tidal inlet, was reclaimed, resulting in the largest polders of all: the Lake IJssel polders (Fig. 1a).

The focus of this study is on understanding and predicting shallow causes of subsidence in the reclaimed urbanized South Flevoland Polder (430 km^2), which is part of the Lake IJssel polders (Fig. 1). The polder was created in 1968 by constructing a ring-dike around the water body to be reclaimed. This enclosed water body was subsequently drained until the water level dropped below the former lakes’ floor. Subsidence immediately commenced when the waterlogged deposits experienced aeration for the first time and pore water progressively evaporated (De Glopper, 1969). Ultimately, the polder has experienced locally one to two meters of subsidence since its reclamation (Barciela Rial, 2019; De Glopper, 1973; De Glopper 1984; De Lange et al., 2012; De Lange, 2015; Fokker et al., 2019).

Paradoxically, severe water pumping has been ongoing to this day, as it is required to keep phreatic water levels low, thereby preventing the polder from flooding due to its low-lying position relative to adjacent Lake IJssel water level and increasing the load-bearing capacity of the former lake floor. The area thus continues to subside as waterlogged sediments are progressively exposed to the atmosphere. Besides flood risks, differential subsidence in the urbanized areas of the South Flevoland polder causes stress on structures, which results in damage to the built environment, leading to major costs. This especially accounts for the ‘Regenboogbuurt’, which is a neighborhood that onlaps the thickest sequence of soft soil deposits in the area (Maas, 2021). Additionally, the severe drought events that have been striking

Northwestern Europe during recent summers, pose the threat of accelerated subsidence to the area by increasing evaporation of pore water from fine grained and organic deposits. To the best of our knowledge, no study has been reported on the effects of severe drought in South Flevoland, although Hoogland et al. (2020) showed that subsidence may be slowed down by proactively saturating shallow peat beds within the area. Understanding, quantifying, and predicting subsidence, both spatially and temporally in the South Flevoland polder is therefore from a socio-economic as well as a hazard-prevention point of view of immense importance.

The artificial lowering of phreatic water levels in the South Flevoland polder results in shrinkage of clay and oxidation of peat in the unsaturated zone (i.e. above the annually averaged lowest phreatic groundwater level). Clay shrinks as water that is adsorbed to charged platy clay particles evaporates and organic matter mixed within the clay oxidizes (Barciela Rial et al., 2020). This leads to volumetric loss and is largely irreversible. Peat oxidation regards the breakdown of organic components by microbial activity, is completely irreversible, and results in the emission of carbon dioxide (Koster et al., 2020). Further, there are subsidence processes in the saturated zone: the consolidation of clay and peat layers due to an increase in effective stress by lowering the hydrostatic pressure when phreatic water levels are lowered (De Glopper and Ritzema, 1994). Consolidation and oxidation have been addressed regularly in other areas in the Netherlands that experience shallow subsidence (e.g. Kooi, 2000; Van Asselen et al., 2009; Van Asselen et al., 2018). On the contrary, shrinkage of clay in the context of subsidence has been poorly covered (Fokker et al., 2019). However, in other countries, subsidence by clay shrinkage is considered as a major issue. In France and Great Britain for example, potential damage to the built environment inflicted by clay shrinkage as a result of drought and climate change has been studied in terms of cost per annum in the light of the insurance industry for decades (e.g. Burnol et al., 2021; Charpentier et al., 2021; Pritchard et al., 2015).

Most recent studies focus on establishing physics-based subsidence forecasts using input parameters derived by field- and laboratory measurements (Koster, Stafleu and Stouthamer, 2018; Mayoral et al., 2017; Nusantara et al., 2018; Schothorst, 1982; Van Asselen et al., 2018). This approach inherently renders the subsidence estimates to be strongly dependent on used models and input soil parameters. A step forward regards the coupling of the different processes. Allison et al. (2016) for instance, stressed that developing an integrated model with coupled behavior of the different subsidence processes is critical for reliable subsidence estimates. Only by considering the behavior of all subsidence processes combined with real observations can the full impact of subsidence be understood.

Optimizing the relation between coupled subsidence processes and measured subsidence can improve subsidence forecasts. A history matching procedure by correlation and/or trial-and-error is often employed (e.g. Caló et al., 2017; Castellazzi et al., 2016; Teatini et al., 2006). For larger areas, or areas where multiple subsidence processes are superimposed, a more formal approach is considered more efficient (e.g. Candela and Koster, 2022; Fokker et al., 2019). A mathematically driven approach such as data assimilation can cover the entire range of uncertainty of all the parameters, to seek the optimal solution.

Data assimilation combines models and observations to obtain the best possible description of the system (Evensen, 2009; Evensen et al., 2022). This approach is customary practice in a wide range of disciplines such as subsurface modelling (Candela et al., 2022; Chang et al., 2010; Evensen et al., 2022; Fokker et al., 2016; Gazolla et al., 2021), weather predictions (Navon, 2009; Thépaut, 2003) and oceanographic simulations (Carton and Giese 2008; Ghil and Malanotte-Rizzoli, 1991), but for interpreting shallow causes of subsidence this method has not yet been applied widely. Peduto et al. (2017; 2020) presented examples of shallow subsidence studies that apply a form of data assimilation to a geotechnical problem. Their studies show the benefit of combining multiple datasets. Li et al. (2017) applied data assimilation with an Ensemble Kalman Filter and showed the strength of data assimilation procedures, although they did not emphasize the subsidence models in their study.

Data assimilation procedures have also been applied in studies on polders in the Netherlands (Fokker et al., 2019; Muntendam-Bos et al., 2009). Fokker et al., 2019 used Ensemble Smoothing with Multiple Data Assimilation (ES-MDA) for ten distinct locations in the South Flevoland polder with a few dozens of timesteps over a period from reclamation until recent, combined with coring for lithological data and phreatic groundwater level measurements. They focused on the agricultural areas of the South Flevoland polder, over a longer timescale with a small number of locations. Therefore, their results are not directly applicable to the subsidence in the urbanized areas of the South Flevoland polder, where the urbanization might have had inhibitory effect on shrinkage and layers might have undergone more severe compaction in the past. Additionally, corings of individual locations were used in Fokker et al., 2019, whilst in this study we introduce an automated procedure including a lithological and groundwater model, making it possible to apply this methodology to larger areas.

We here aimed to quantify the subsidence processes within urbanized areas of the South Flevoland polder in relation to phreatic groundwater level changes and to showcase the added value of combining large observational data sets with numerical models to improve parameter estimations for shallow subsidence processes. We deployed data assimilation on a dataset comprising thousands of locations with hundreds of timesteps derived from satellite observations, high-resolution 3D models of subsurface lithology and groundwater to quantify the contribution of the different shallow subsidence processes. We studied multiple subsidence processes at the same time to understand the full impact of subsidence and to identify the relative contributions of the different processes. Such information is critical for policymakers and spatial planners to design strategies to mitigate subsidence in the South Flevoland polder.

1.2 Study area

The South Flevoland polder is situated in the central Netherlands in the partly reclaimed Lake IJssel (Fig. 1). The Holocene sequence of the polder is underlain by several hundreds of meters thick Pleistocene sediments, consisting of a complex of alternating sandy to clayey marine, fluvial, and (peri-)glacial deposits (Menke et al., 1999; Peeters et al., 2015; TNO, 2022). The uppermost Pleistocene unit consists of a several meters thick aeolian sand bed, which grades from ca. -5 to -12 m below NAP (i.e. the Dutch ordinance datum, approximately corresponding to the mean sea level) in northwestern direction, locally incised by the Eem brook paleo-valley or elevated by dune formation (Fig. 1).

During the Holocene, the South Flevoland Polder became part of the landward margin of a coastal plain. The base of the Holocene sequence consists of a basal peat bed, formed between

6000- and 7000-year BP under influence of inland groundwater level rise in tandem with post-glacial sea-level changes (Koster et al., 2017; Makaske et al., 2003). These peatlands drowned and transformed into an open tidal basin under the influence of continuous sea-level rise (Vos, 2015). The tidal basin deposits consist of alternating sand-clay beds, with local erosion of the underlying basal peat. When around 5500-year BP eustatic sea-level rise decreased, the open tidal basin was closed off by the formation of a beach-barrier, transforming the area into a freshwater swamp with large-scale peat formation (Beets and Van der Spek, 2000; Makaske et al., 2003). In parallel, the area remained connected in the west to the North-Sea by several smaller tidal inlets, making the Eem brook part of a branched network of freshwater tidal channels (Vos, 2015). The peatland itself was characterized by a series of open lakes (Menke et al., 1999). From the north, this lake system was connected to the Waddensea. When the peatlands deteriorated as a combination of natural and anthropogenic causes, the open sea connection in the north expanded southwards, thereby gradually drowning the peatlands and turning the area into a partly enclosed inland sea (Van den Biggelaar et al., 2014). The inland sea was dammed off and became Lake IJssel in 1932, to protect the surrounding areas against flooding. After the damming several parts of the newly formed lake were reclaimed from 1939 onwards. The South Flevoland polder is the final area that was reclaimed.

Almere is a large urban conglomerate in the polder of South Flevoland (Fig. 1), with a population of ca. 200,000. Almere was founded in 1976, approximately eight years after reclamation to account for the first years of subsidence, for which it was predicted to be the highest (up to 70 centimeters in total) (Hoeksma, 2007). Almere has been partly built on top of the paleo-valley of the Eem brook system, which incised several meters into underlying deposits of Pleistocene age. Therefore, the thickness of the Holocene sequence underneath Almere strongly varies, with thicknesses between <1 and 10 meter. The thickest sequence can be found over the course of the former Eem brook system. Generally, basal peat in the Netherlands, like underneath Almere, has undergone substantial compression by the overburden, and consequently has mechanical characteristics that deviate from the younger peat beds (Koster, De Lange et al., 2018). Due to sea-ingressions that drowned the peatlands, the paleo-valley infill on top of the basal peat consists of marine clay with sandy infills overlain by organic clay, gyttja and peat, interfingered with some sand (Menke et al, 1999).

Subsidence was expected after reclamation (De Glopper, 1969), therefore, regular monitoring campaigns were conducted, including regular levelling measurements, corings, and soil sampling (De Glopper, 1984**;** Van Dooremolen et al., 1996). Within 25 years, the a priori expected subsidence for the South Flevoland polder was exceeded, in some places by 0.5 m (Van Dooremolen et al., 1996), resulting in complications for the drainage of the area. Most buildings have a concrete pile foundation in sandy, less compressible layers of Pleistocene age, and consequently do not subside in parallel with the overlying Holocene sequence. On the contrary, public structures, such as (local) roads, squares, sport fields and playgrounds are often lacking a pile foundation and are constructed immediately on top of the Holocene sequence. The consequential differential subsidence between structures with and without a concrete pile foundation inflicts stress on pipeline structures, belowground electrical and network cables, and the connection from buildings to the roads in general, potentially causing damage. Currently, the city of Almere, lying ~4 meters below NAP, must deal with damage to buildings and infrastructure because of the ongoing differential subsidence (Lambert et al., 2016).

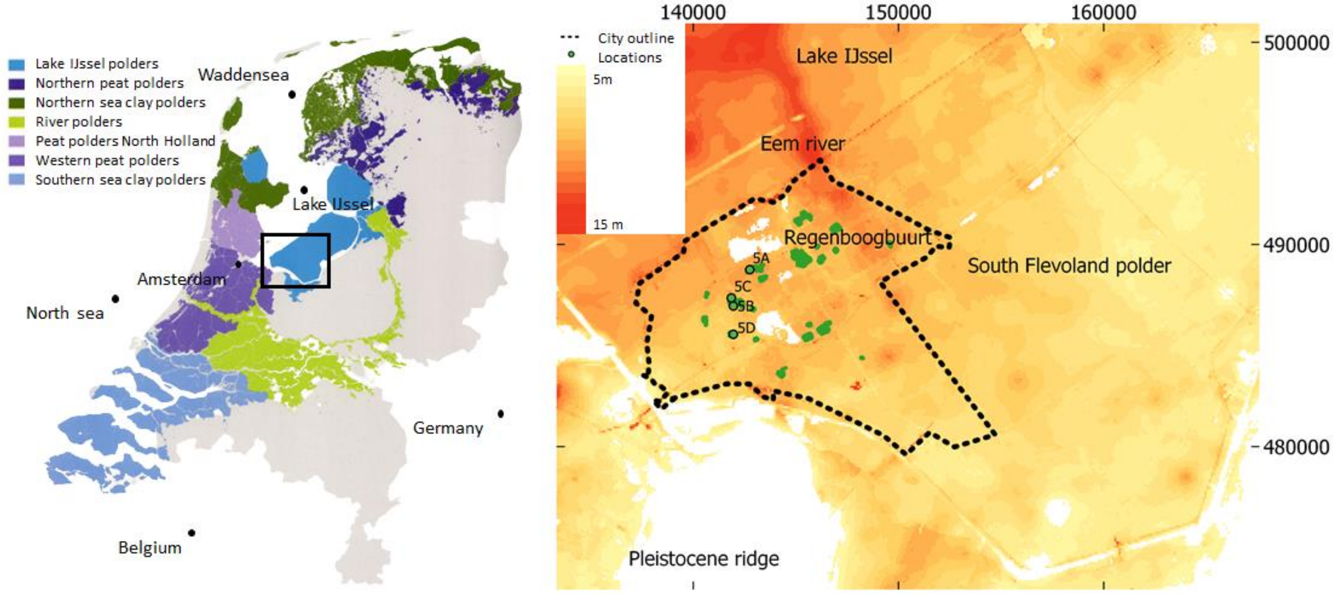

Figure 1 a: Map of the Netherlands showing all the areas that accommodate polders (adjusted from Steenbergen et al., 2009). b: Map of the area of Almere and its surroundings projected on a map showing the thickness of the Holocene sequence (TNO, 2022). The thickness decreases towards the south-east. The incised course of the Eem River, in the northeast of the city Almere is reflected by an increased Holocene thickness. The map is plotted on the Rijksdriehoek coordinate system. The green dots indicate the locations of the data points included in this study. The locations of the graphs of Figure 5a-5d are denoted.

2 Materials and Methods

We used a data assimilation procedure combining the use of InSAR data with 3D lithological and phreatic groundwater level models. Figure 2 depicts the complete workflow, with the different colors indicating the different steps. In green, three classes of input data are displayed: (1) data in the form of previously developed geological and groundwater level models (paragraph 2.1.3 and 2.1.4.), (2) estimates of input parameters necessary for the forward model, based on a literature search (paragraphs 2.2), and (3) satellite data for actual surface movement estimates (paragraph 2.1.1).

We defined three steps of the subsidence estimation algorithm:

1. The preprocessing the InSAR data to filter the appropriate measurements points from the full data set (paragraph 2.1).
2. The forward model in which we calculated subsidence for all locations and timesteps in this study (paragraph 2.2).
3. The data assimilation step, where the subsidence measurements derived from InSAR were combined with the forward model, to optimize the forward model by changing the input parameters (paragraphs 2.3).

Lastly, the output of our analysis is defined into two classes; (1) refined estimated parameters. As a result of the data assimilation approach, refined estimated parameters are the optimized values for the input parameters, and (2) a subsidence prediction. The outcome of the forward model is a subsidence prediction for all the locations and timesteps.

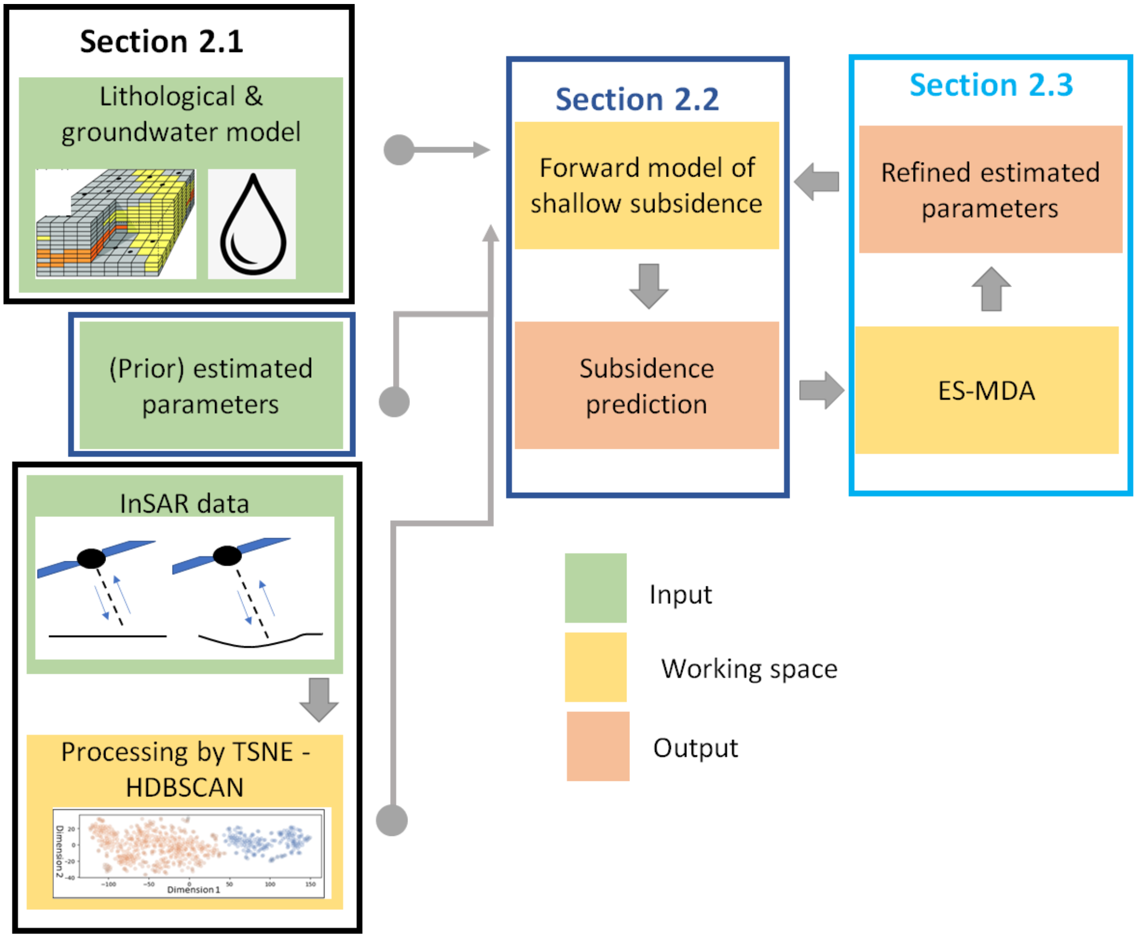

Figure 2: Workflow of the different steps of the methodology divided into: input, working space and output. The steps of the workflow are explained in corresponding sections. The parameters of the physical models that estimate subsidence are optimized towards measured relative subsidence from satellite data, with the use of a groundwater model and a lithological model (GeoTOP). InSAR points measured on top of unfounded objects are separated by a data selection process (Fig. 3). A prior estimate of the parameters part of the forward model is initially made, whereafter the forward model and optimization with data assimilation is repeated multiple times. The image of lithological grid model is adjusted from Van der Meulen et al. (2007).

2.1 Input data

2.1.1 InSAR data

The InSAR data consists of Sentinel-1 images for one ascending and one descending track, ranging over the period March 2015 until June 2020 and November 2015 until June 2020 respectively. The sampling interval of the data points varies temporarily by the availability of the 6- or 12-days repeat pass (Wegmüller et al., 2015). One of the key issues of InSAR data is loss of signal coherence, both in space and time. Spatial decorrelation is caused by changes in the acquisition baseline, resulting in a different phase between two images and causing phase wrapping errors that reduce the coherence. This implies that spatially decorrelated data is less suitable for subsidence research. Temporal decorrelation is caused by atmospheric variability and changes in the physical and geometric properties of the scatter points, e.g. due to seasonal changes in vegetation which result in landcover changes (Ferretti et al, 2007; Hanssen, 2001). As a result, vegetation-rich areas are suboptimal for the analysis of subsidence by satellite imaging (Conroy et al., 2022). Therefore, the focus of this study is on man-made structures, because these scatter points face less decorrelation issues.

The ascending and descending tracks were processed and analyzed separately. This yielded two results of subsidence estimations and associated fits, which were compared for an additional quality check of the workflow. The line-of-sight movement was projected in the vertical direction with the use of the incident angle as part of the processing. We assume no significant horizontal displacements, because of the shallow character of the cause of subsidence.

2.1.2 InSAR processing by TSNE-HDBSCAN

InSAR locations were selected based on two main criteria, forming the first step in the point-selection procedure of Figure 3. We selected PS-InSAR points in the built-up area of Almere without a pile foundation. Buildings in the area typically have a pile foundation reaching depths of ca. –7 to –20 m with respect to NAP, i.e. piles driven in Pleistocene sand beds with load bearing capacity (Spikker, 2010). Consequently, buildings with a pile foundation are less suitable to reflect subsidence processes that happen within the Holocene sequence. We therefore focused on large reflective objects (~>10 reflection points) without pile foundations. These objects range from large parking lots around shopping centers and business parks, to playgrounds, concrete sport fields, and artificial grass turfs.

The next selection criterium was that the structures without foundations had been built at least 10 years before the first InSAR acquisition dates. Therefore, only objects constructed before the year 2005 were considered. This choice was made to reduce the effect of consolidation due to construction of the objects without foundations on the subsidence signal. Because no register exists for the construction date of parking lots, playgrounds and sport fields, the year of construction of the associated buildings was used. The construction year of all buildings in the Netherlands are registered in ‘Basisregistratie Adressen en Gebouwen’ (BAG) (Kadaster, 2022), which was used to verify the construction year of objects in the selected areas.

Reflection points on top of structures without a pile foundation that meet above stated criteria were isolated from the ones on top of structures with a pile foundation using a statistical visualization method. Firstly, data points were separated with time Distributed Stochastic Neighbor Embedding (t-SNE) (Van der Maaten and Hinton, 2008), subsequently data points were appointed to a cluster using HDBSCAN (Campello et al., 2014). This two-steps approach based on unsupervised machine learning enables isolating time series that measure the same processes. In the case of Almere, no significant subsidence below the level of the pile foundations was expected. Hence, objects with a pile foundation should show negligible subsidence, whilst other nearby objects without a foundation were expected to show subsidence. This would result in differently behaving timeseries for points measured on top of objects with and without a pile foundation. This step formed the second step in the point selection procedure of figure 3

The practice of dimensionality reduction followed by clustering is common for large input data and has been applied to SAR datasets (Van de Kerkhof et al., 2020), and for a wide range of other date types (Fernández Llamas et al., 2019; Harrison et al. 2019; Kahloot and Ekler, 2019). T-SNE is a dimensionality reduction method that can group similarly behaving timeseries of height measurements of the different reflection points (Van der Maaten and Hinton, 2008). For the present study, clustering was conducted with Hierarchical Density-Based Spatial Clustering of Applications with Noise (HDBSCAN). HDBSCAN provides significant clusters, where the clusters can vary in density threshold. The method maximizes the stability of the selected clusters by calculating the optimal solution (Campello et al., 2014).

To ensure that the selected clusters represent the time series of measurements on top of objects without a pile foundation, the clusters were verified by checking the time series of all the clusters and their location in a geographic information system. This is the third procedure of Figure 3.

The last step in Figure 3 entails the optimization of the selected InSAR points for the subsidence optimization procedure. InSAR data points in a single lithological grid cell (see section 2.2. about lithological modelling) were averaged. Reducing the number of points by averaging reduces the computational time, whilst still incorporating the uncertainty for the InSAR data for each grid cell. The variance of this average was added to the chosen standard deviation squared of 0.01 m^2, to ensure that the uncertainty of variance in the subsidence measurements was incorporated. A 0.01 m^2 standard deviation for each epoch aims to capture both the uncertainty in the model and measuring space, as the true standard deviation is unknown. To prevent a disproportionate weight of the first measurement in time, an average of the first ten measurements in time was taken as the first time step in our post-processing timeseries data.

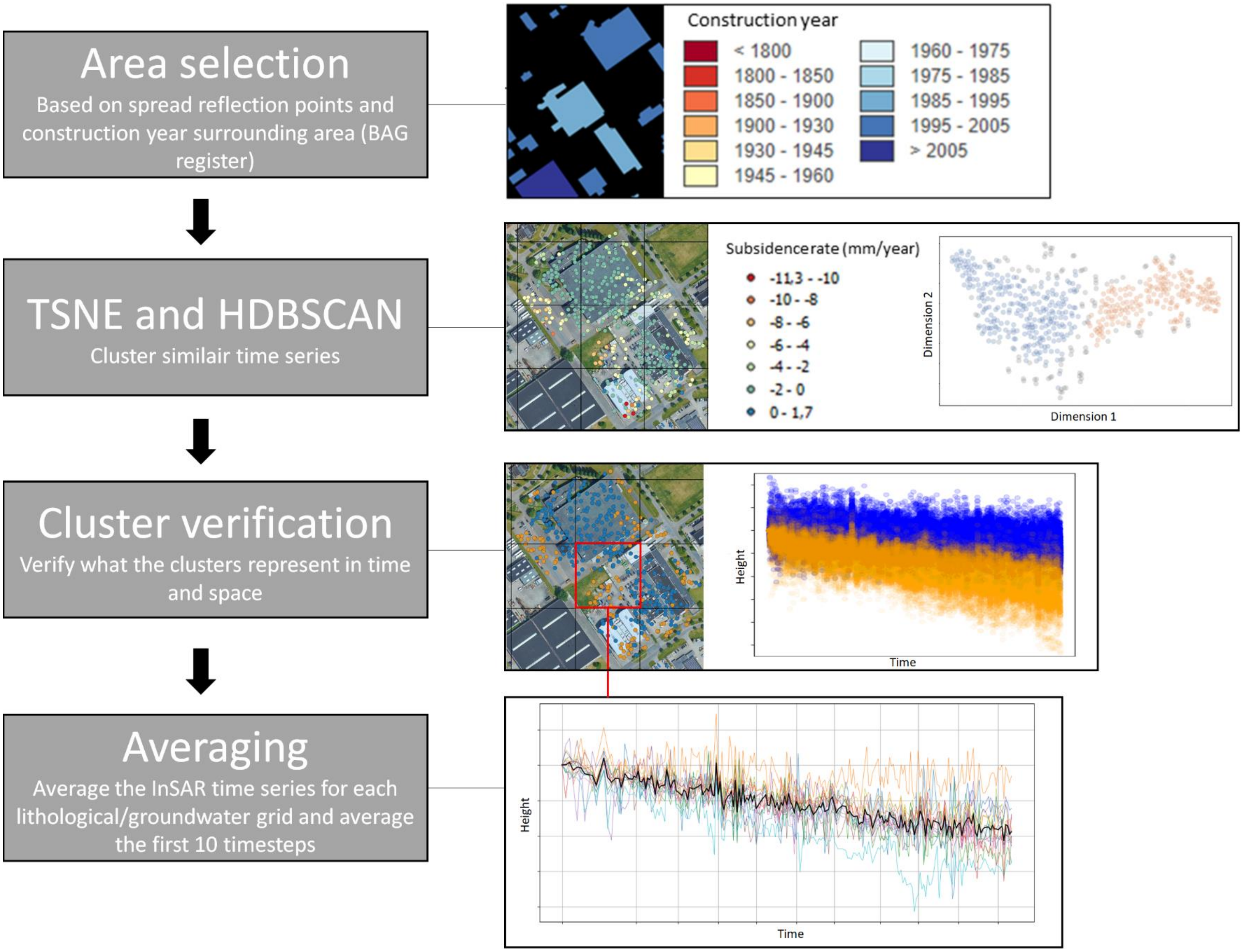

Figure 3: Workflow for selecting InSAR points. Firstly, areas with a significant amount of data points, potentially on top of structure without a pile foundation are selected. With the BAG register (Kadaster, 2022), the construction date of the area is verified. The image shows the construction years of the buildings in the example area (image adjusted from Spaan, 2015).. The remaining areas follow dimensionality reduction by T-SNE, followed by a clustering method HDBSCAN. At the second processing step, the average yearly subsidence rate of the selected InSAR points of the sample area are shown on the left. On the right, the result of the T-SNE dimension reduction is plotted, where the colors refer to the clusters each point is assigned to. The number of dimensions of the initial data set is equal to the number of locations. Thirdly, the clusters are visualized as scatter points for each time step and in a geographic information system, to verify the clusters and select the cluster representing the scatter points on top of unfounded man-made structures. The clusters from the second time step, in their corresponding colors are plotted spatially on the left image and over time on the right. Lastly, for each grid cell corresponding to the lithological and groundwater model, an average of the selected InSAR points within the cell is taken This is depicted in the graph belonging to the last processing step, where the thick black line represents the average of the InSAR timeseries falling into the grid cell. To not give a disproportionate high weight to the first measurement of the InSAR series, an average has been taken of the first 10 timesteps, which forms the first timestep in our post processing time series.

2.1.3 Lithoclass model

A previously released 3D lithoclasses (classes of different grainsize compositions) voxel model for the province of Flevoland that covers the entire study area was used as input for numerical modeling (Fig. 4b) (Gunnink, 2021). The model was initially developed for high-resolution hydraulic resistance modelling for groundwater flows within the Holocene sequence and had been constructed based on 31.000 digitalized borehole logs and 4250 Cone Penetration Tests that had been derived from the freely accessible online data portal of the Geological Survey of the Netherlands (TNO-GSN, 2022). The boreholes are sufficiently distributed throughout the province of Flevoland, whereas the Cone Penetration Test are primarily clustered in urbanized areas and along infrastructural elements.

The 3D model had been created by interpolation via spatial kriging, following a similar procedure as explained in Van der Meulen et al. (2013). The voxel x,y,z dimensions are 100x100x0.5 meter and the model ranges from the surface to the top of geological units of Pleistocene age, thereby encompassing the entire Holocene sequence. The different lithoclasses (sand, sandy clay, clay, peat, and basal peat – the latter being in a more compressed state than peat) are described with their probability of occurrence for each voxel, based on 100 realizations of the interpolation. The highest probability was taken as the truth scenario for this study.

2.1.4 Groundwater model

Changes in groundwater heads form an important explanatory variable for shallow sources of subsidence. Therefore, time series of this data are needed all over the study area. Unfortunately, this was only sparsely available at locations with observation wells. Therefore, a model was developed to estimate the required time series (TNO-GSN, 2022; Zaadnoordijk et al., 2018): monthly phreatic water level values for grid cells of x,y 100x100 meter (Fig. 4a) from the year 2000 until 2020. The applied method was an interpolation in two steps. The first step was an interpolation of the groundwater heads within the time series to obtain for all well locations an observation on the same day (28th) of each month. This yielded interpolated heads including variances. The second step comprised a spatial (kriging) interpolation, applying a sequential Gaussian simulation (Deutsch and Journel, 1998, p.170), which yielded for each month a map of the interpolated heads. Since the observation wells were sparse, their observed heads could not fully describe the spatial variation in the groundwater heads. Therefore, a trend surface was used with a spatial interpolation performed on the residuals (observation minus trend surface). To honor the seasonal fluctuation of the groundwater heads, each month had a separate trend surface. Herewith, one hundred equiprobable interpolations of phreatic groundwater levels for each month were created. We used the average of the 100 realizations as the truth scenario for the phreatic surface model in space and time.

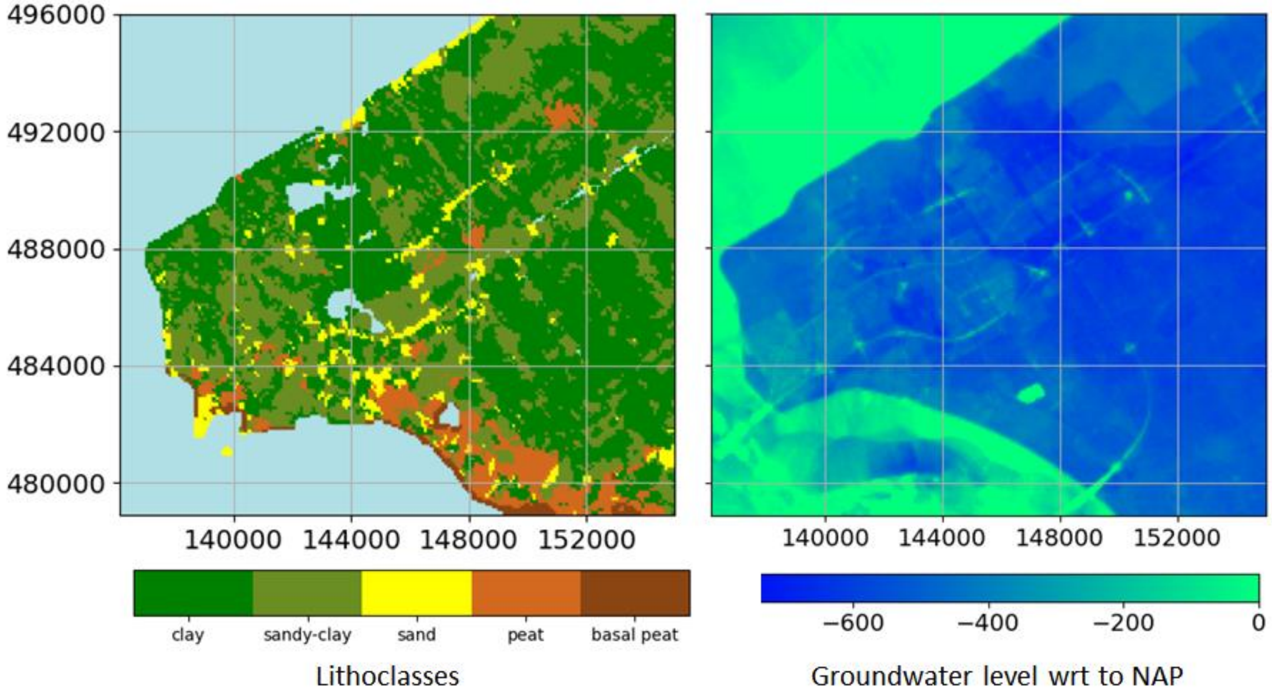

Figure 4: Left: Map of the South Flevoland polder lithologies according to GeoTOP at 5 meters below NAP. Right: Map of phreatic surface level in the South Flevoland polder in January 2015. The scale is in cm with respect to NAP. The polder itself lies ~400 cm below NAP (Dutch ordinance level ~ sea level). The areas that lie at NAP are the lake IJssel area and in the left bottom the Dutch mainland.

2.2 Forward model

The different shallow subsidence processes initiated by human-induced phreatic groundwater level lowering in the South Flevoland polder are described in forward models. These forward models include physical relations that describe the subsidence processes and thereby, with an estimate of the parameters, provide an estimate of the subsidence. The groundwater and lithoclass models are used to describe which lithology is present and to what depth the sediments are saturated. Previous studies identified oxidation of peat, shrinkage of clay, and compression of clay and peat as the main subsidence processes in the area (De Lange et al., 2012; Fokker et al., 2019; Lambert et al, 2016; Van Dooremolen et al., 1996)**.**

Fokker et al. (2019), described a subsidence model with a relation between shrinkage and equivalent age using linear-strain fits and time series of land levelling subsidence observations in the South Flevoland polder from 1967 to 2012. They used an exponential relation of clay shrinkage processes to fit the model to the data. Furthermore, they described that well-established compression functions of consolidation and creep (Den Haan, 1996; Visschendijk and Trompille, 2009) did not fit with the observed subsidence trend. Given the results of the study of Fokker et al. (2019), subsidence by compression was expected to be negligible in comparison to the processes of shrinkage and oxidation for the timing after reclamation and due to the length of our study period. We have therefore not modelled compression as a separate process in this study. Note also here that compression by the overburden weight of building material was assumed to have a negligible effect on the selected InSAR time series, because all the locations included in this study have undergone settlement due to loading by construction for minimal >10 years (cf. CUR, 1992).

2.2.1 Oxidation model

The applied equation for the oxidation model is widely applied to describe peat oxidation in the Netherlands (Fokker et al., 2019; Koster, Stafleu and Stouthamer, 2018; Van den Akker, 2008; Van Hardeveld et al., 2017; Van der Meulen et al., 2007). It provides a relative annual oxidation rate for peat above the phreatic groundwater level. Since only organic matter oxidizes, admixed sediments remain, albeit on average 3 to 4 % of the total volume (Koster, Stafleu and Stouthamer, 2018). Hence, a residual thickness is considered.

Firstly, for a unit above the phreatic groundwater level the part susceptible to oxidation needs to be determined.

$$h_{ox,0} = h_{ox}(t=0) = (1 - R_{ox})h_0 \tag{1}$$

If part of a unit has already been reduced, we have $h_{ox}(t) = h(t) - R_{r,ox}h_0$. The original thickness of the unit is unknown, since collection of the data used in this study started ~50 years after reclamation. Hence, we simply assumed h equals h_0 at t=0. This results in a higher residual height than for completely virgin soil, as the original units are (partly) reduced in thickness already. The oxidation rate can be calculated as follows:

$$\frac{dh}{dt} = \frac{dh_{ox}}{dt} = -V_{ox}\, h_{ox} \tag{2}$$

Over time Δt the thickness reduction of a layer can be written as:

$$\begin{aligned} \Delta h = h_{ox}(t) - h_{ox}(t + \Delta t) &= (1 - e^{-V_{ox}\Delta t}) \cdot h_{ox}(t) \\ &= (1 - e^{-V_{ox}\Delta t}) \cdot (h(t) - R_{ox}h_0) \end{aligned} \tag{3}$$

Incorporating units that are partly aerated, the part susceptible of oxidation is corrected for the wet part of the voxel:

$$\Delta h_{ox} = (1 - e^{-V_{ox}\Delta t})(h(t) - h_{wet} - R_{ox}\,[h_0 - h_{wet}]) \tag{4}$$

In which V_{ox} is the shrinkage rate and R_{ox} the residual height.

2.2.2 Shrinkage model

Time-dependent shrinkage models have not been documented for the Netherlands yet. Typically, shrinkage is expressed as a function of clay mineral content, organic matter, and calcareous admixture (e.g. Barciela Rial, 2019; De Glopper, 1969). To overcome this, Fokker et al. (2019) designed a simple shrinkage relation, inspired by Equation 4, which enabled good matches between the subsidence model and the observed subsidence. This relation assumes that the shrinkage rate is proportional to the volume sensitive to shrinkage. A lithology-dependent residual height was assumed to indicate an asymptotic value to which the shrinkage can lead.

The process of clay swelling has been ignored in this study. Furthermore, seasonal swelling effects of clay by a relative increase in precipitation during autumn and winter were not observed in the InSAR data. Most likely, if present, a swelling capacity is suppressed in the urbanized area by structure overburden. In general, the South Flevoland polder is subjected to net groundwater level lowering; this is reflected in net subsidence, visible as a decreasing trend without a large swelling effect in the InSAR data. Furthermore, previous studies reported that the clay beds in our study area have a relatively high irreversible character regarding shrinkage (Bronswijk et al., 1990; Kim et al., 1993).

The equation for shrinkage (Eq. 5):

$$\Delta h_{sh} = (1 - e^{-V_{sh}\Delta t})(h(t) - h_{wet} - R_{sh}\,[h_0 - h_{wet}]) \tag{5}$$

In which V_{sh} is the shrinkage rate and R_{sh} the residual height.

2.2.3 The prior estimated parameters

The parameters aimed to optimize are the shrinkage and oxidation rate and their respective residual heights (see first column of table 2). The prior estimated values take into account the results of Fokker et al., (2019). The rates were lowered, because a significant amount of time (~50 years) has passed since reclamation (and the start of the study of Fokker et al., 2019), decreasing the void ratio of deposits and increasing the stiffness. Additionally, there is a potential inhibitory effect of shrinkage and oxidation rate in the urbanized area, compared to the agricultural area of Fokker et al. (2019).

The rates of shrinkage and oxidation are closely related to the associated residual heights. Due to the brief period of the surface elevation data (~4-5 years), the exponential relation between relative residual height and reduction (shrinkage or oxidation) rate cannot be established absolutely: an increase in subsidence rates can have the same effect on total subsidence as a reduction in residual height. As a result, the contribution of relative residual height and reduction cannot be distinguished. If one of the two parameters increases, the other should increase as well, to reach the same value for total subsidence. From Equations 1 and 2 we can derive:

$$\frac{dh}{dt} = h_0 v\ (1 - R)e^{-vt} \tag{6}$$

Therefore, if a certain height reduction rate is acting it can be the result of different combinations of v and R, as long as the right-hand side of Eq. (10) gives the same number. The exponential in this equation can be neglected because the compaction (order of mm) is very small with respect to the layer thickness (order of m). Different combinations with the same value of $C = v(1 - R)$, or $R = 1 - \frac{C}{v}$ therefore, give equally good fits, with no time dependence in the expression. This equation was hence fitted to the posterior result of the residual height and rate of oxidation and shrinkage for the different lithologies, utilizing an automated least squares polynomial fit.

2.3 ES-MDA

Parameters have been estimated with Ensemble Smoother with Multiple Data Assimilation (ES-MDA) (Emerick and Reynolds, 2016; Evensen et al., 2022). Earlier accounts for the method to estimate parameters for shallow subsidence can be found in Fokker et al. (2019); the method has also been applied to estimate the parameters for deep subsidence processes (gas production) (e.g. Fokker et al., 2016; Gazolla et al., 2021).

An ensemble refers to a collection of members that are the result of a Monte Carlo analysis. Members are single realizations of the model with specific values for the different parameters. ES-MDA is thus based on a parameter description of the properties that describe the physical processes in the subsurface. A forward model takes the parameters and calculates the subsidence in space and time for each member of the ensemble. The ES-MDA algorithm minimizes the mismatch between the measured data and the estimated subsidence values by changing the parameters of the ensemble members in an organized manner. The multiple data assimilation notion of ES-MDA indicates that the assimilation process is repeated several times. The newly estimated parameters are taken to create a new ensemble of members, with each step increasing the confidence in the parameters.

ES-MDA can be mathematically described as follows. The parameters collected form the vector **m**. The subsidence data is put into a vector **d**, this vector has the length of the number of data points in the area multiplied by the time steps taken at each location. Operation of the forward model is indicated by **G**(**m**); it calculates the subsidence as a function of time for each individual location, based on the parameters in **m**. We want to estimate the vector **m** for which **G**(**m**) has the smallest misfit with the data **d.** To do so, for a single member, as set of prior parameters is created ($\mathbf{m_0}$), with covariance in a matrix $\mathbf{C_m}$. Another covariance matrix is created for the data ($\mathbf{C_d}$). Following Tarantola (2005), the least square solution is acquired by maximizing *J* in the following function:

$$J = \exp\left(-\frac{1}{2}[\boldsymbol{m}-\boldsymbol{m_0}]^T \boldsymbol{C}_m^{-1}\,[\boldsymbol{m}-\ \boldsymbol{m_0}] - \frac{1}{2}\,[\boldsymbol{d}-\boldsymbol{G}(\boldsymbol{m})]^T \boldsymbol{C}_d^{-1}[\boldsymbol{d}-\boldsymbol{G}(\boldsymbol{m})]\right) \qquad (7)$$

In the ensemble procedure, the values of the members are derived from a prior estimate with a standard deviation of the parameters. An ensemble consists of N_e vectors of **m**; $\mathbf{M} = (\mathbf{m_1}, \mathbf{m_2}, \ldots, \mathbf{m_{Ne}})$. Similarly, an ensemble of data vectors is created by adding random noise to the data following the uncertainty of the data points: $\mathbf{D} = (\mathbf{d_1}, \mathbf{d_2}, \ldots, \mathbf{d_{Ne}})$.

To solve the least square solution for the entire ensemble at once, **GM** replaces **G**(**m**) in equation 5. **GM** is the result of the parameters of all ensemble members operating in the forward model and is the collection of realizations of surface elevations through time. **GM’** is defined as the difference between **GM** and the average of **GM**. **M’** is the difference with the prior mean for each ensemble member: $\mathbf{M'} = \mathbf{M} - \mathbf{m_0}$. The covariance matrix is defined as: $\mathbf{C_m} = \mathbf{M'}\mathbf{M'^T}/(N_e\text{-}1)$. The new set of parameters for the ensemble is given by:

$$\begin{aligned}\widehat{\boldsymbol{M}} &= \boldsymbol{M} + \boldsymbol{M}'[\boldsymbol{GM}']^T(\boldsymbol{GM}'[\boldsymbol{GM}']^T + (N_e-1)\boldsymbol{C}_d)^{-1}(\boldsymbol{D}-\boldsymbol{GM})\\ &= \boldsymbol{M} + \boldsymbol{M}'\left([\boldsymbol{GM}']^T\boldsymbol{C}_d^{-1}\boldsymbol{GM}' + (N_e-1)\mathbf{I}\right)^{-1}[\boldsymbol{GM}']^T\boldsymbol{C}_d^{-1}(\boldsymbol{D}-\boldsymbol{GM}) \qquad (8)\end{aligned}$$

Depending on the number of parameters versus number of data points one of the two equivalent expressions might be more appropriate to use. $\widehat{\boldsymbol{M}}$ is the estimated ensemble of parameters.

The ensemble smoother technique with a new estimate of parameters can be applied repetitively to obtain a better estimate of parameters in the case of non-linear forward models (Emerick and Reynolds, 2013). The set of parameters is updated with each subsequent step. The data remains the same over the entire procedure. To compensate for the effect of multiple applications with the same data, the covariance of the data is increased with each step of the optimization. This is done with a factor α_i, where the following condition is met: $\sum_{i=1}^{nI}\frac{1}{\alpha_i} = 1$. nI is the number of assimilation steps (Fokker et al., 2019). We used a factor α_i that decreases every step with a factor q to ensure increasing influence of subsequent assimilations.

$$\alpha_i = \alpha_0 \cdot q^i \qquad (9)$$

With i being the assimilation step. The above summation condition is met with:

$$\alpha_0 = \frac{1 - q^{nI}}{q^{nI-1} - q^{nI}} \tag{10}$$

To verify the results and determine the actual improvement of the parameter estimation procedure, a test function is applied, considering the covariance of the data and the estimate parameters after the last assimilation step:

$$\chi^2 = \left(\widehat{\boldsymbol{GM}} - \boldsymbol{d}\right)^T (\boldsymbol{C}_d + \boldsymbol{C}_{\widehat{GM}})^{-1} \left(\widehat{\boldsymbol{GM}} - \boldsymbol{d}\right) \tag{11}$$

The outcome of this equation should be around the degree of freedom (N_d), so that $\frac{\chi^2}{Nd} \approx 1.$

The parameters for this study are summarized in table 1. The number of grid cells equals the number of lithological and groundwater voxel cells the InSAR data points cover. In the result section, we present key examples of individual voxel cell locations, the values of the optimized parameters and correlations between different parameters.

Table 1: Parameters for the data assimilation procedure of this study.

Number of ensemble members (-)	200
Number of assimilations (-)	4
q (-)	0.666667
Covariance data (m)	0.01
Number of InSAR data points (-)	3747 (descending), 2846 (ascending)
Number of voxel locations (-)	199 (descending), 158 (ascending)
Number of points in time (-)	208 (descending), 212 (ascending)
Number of model parameters	6

3 Results

Our ES-MDA based workflow yielded 357 individual scatter point locations. To provide a representative summary of the results on point location scale, we present 4 key examples below (Fig. 5). Additionally, we present four key indicators for parameter covariance (Fig. 6), values for the estimated parameters (Table 1), and the average contribution to subsidence for clay and peat (Table 2). The estimated parameters consist of the four model parameters for the shrinkage of clay (shrinkage rate and relative residual thickness for clay and sandy clay), and two model parameters for oxidation (oxidation velocity and relative residual thickness of peat).

The four key examples of the results of the simultaneous assimilation are presented in Figure 5. The time series of the prior ensemble is not indicated in Figure 5. Because they have a high variance, they would not fit into the scale of the figure. The red time series in Figure 5 are the 200 modelled surface movement developments for the ensemble of assimilated parameters. The black dots are the InSAR data points, and the grey area represents the uncertainty given to each data point, as described in section 2.1. On the right y-axis in the same plot the phreatic groundwater level variation is plotted. The lithological column and the location of the column with respect to the phreatic groundwater level is indicated on the right of the plot. The time series and the estimated subsidence correspond well, regardless of lithology, except for Figure 5a. The prior and estimated parameters are presented in Table 2.

Table 2 provides the estimates prior and posterior to the data assimilation with their standard deviation. Results are given for the descending and ascending satellite tracks separately. The two tracks provide comparable estimated parameters as a result of the data assimilation. A few of the parameters are plotted against each other in Figure 6. For each assimilation step, the 200 estimates of the parameters are plotted against each other. The figure indicates the ensemble spread in the prior estimates and the operation of the smoother by molding the cloud of parameter values. A clear relationship between different parameters evolves, along the lines of the argument in the previous paragraph: different combinations of the shrinkage and oxidation rate and the associated residual height give identical outcomes, as long as they follow the relationship $R = 1 - \frac{C}{v}$. The final ensembles have been fitted to this relationship, as indicated with the dotted black line. The resulting constant C is given in the figure description.

In summary, Table 3 provides the overview of the average contribution to subsidence in mm for the different lithologies for both the ascending and descending satellite tracks.

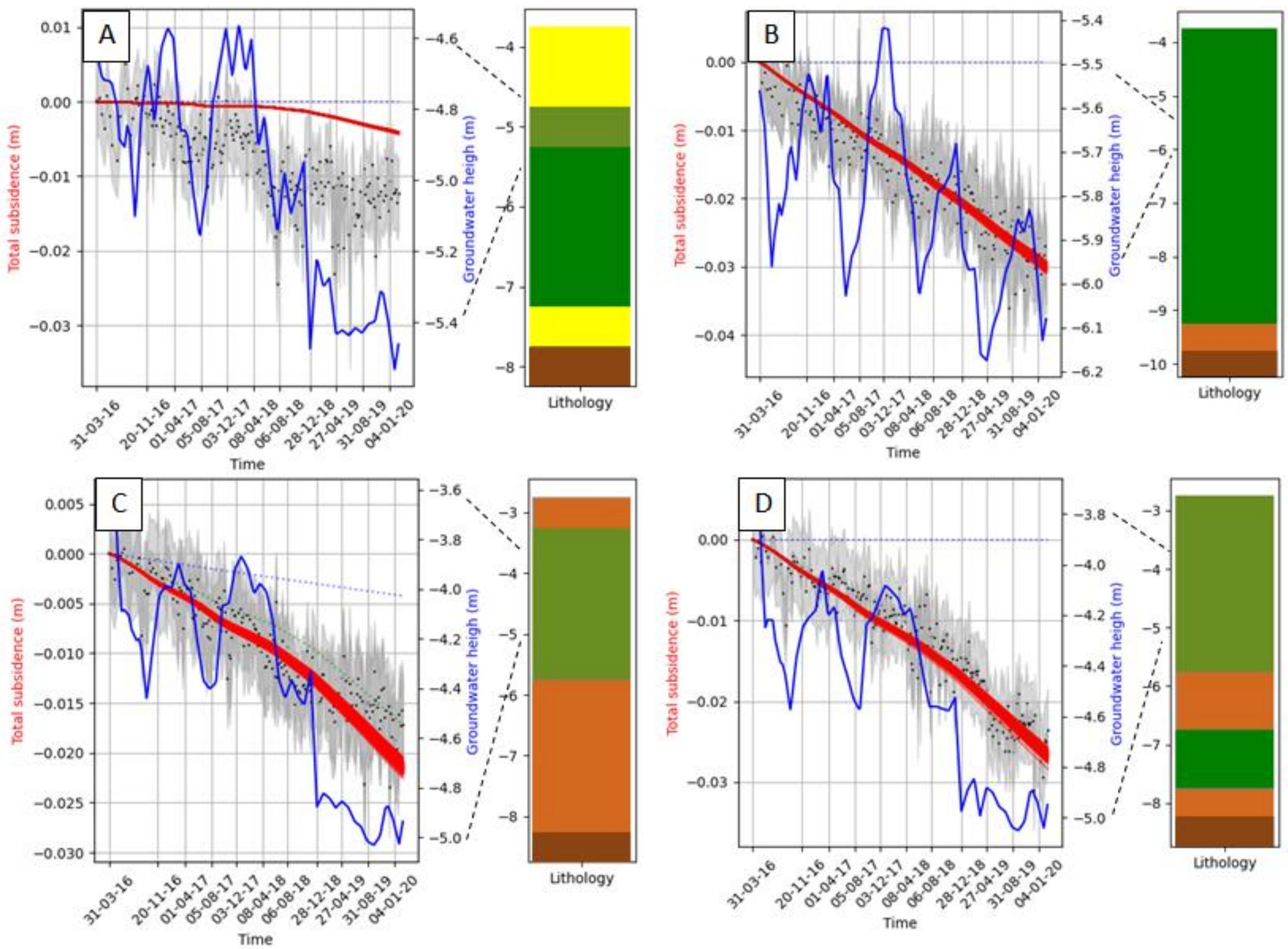

Figure 5: Comparison of surface movements, groundwater levels and lithology for 4 example locations. All figures show the InSAR-derived surface movements (black points) on the scale of the left y-axis. The uncertainty around them is depicted in gray. It was determined as described in section 2.1. The red lines are the 200 ensemble members of the optimized fit after 4 assimilation steps, also on the scale of the left y-axis. The groundwater is the blue line and is with respect to the right y-axis. Next to the graph a stratigraphic column for that specific location is given, according to GeoTOP. The legend of the column is the same as for figure 4. All y-axes are in meters with respect to NAP.

a: descending track, this location shows in increase in subsidence rate once the phreatic surface is below the sandy layers, which happens from spring 2018 onwards. b: ascending track. Shows the fit of subsidence, where the phreatic surface steadily drops under a seasonal trend. There was no significant increase in subsidence rate. d: descending track. Combination of subsidence due to peat and clay. Enhanced subsidence rate from spring/summer 2018 onwards is clear. d: descending track. Seemingly linear subsidence, with a slight acceleration from spring/summer 2018 onwards.

Table 1: The parameters that are optimized in this study for all the locations at the same time. The optimized fit of the ascending and descending track are result of separate data assimilation procedures, but the results are similar. The pre parameters were chosen based on the study of Fokker et al. (2019). The chi-squared error of the ascending track data set has been reduced from 5.2 (prior) to 1.01 (posterior); for the descending track data set it has been reduced from 3.6 (prior) is 3.6 to 0.77 (posterior).

PARAMETER	PRE	POST (ASCENDING)	POST (DESCENDING)
V_{SH} CLAY	0.02 ± 0.005	0.017 ± 0.0012	0.018 ± 0.001
R_H CLAY	0.6 ± 0.05	0.79 ± 0.017	0.78 ± 0.019
V_{SH} SANDY CLAY	0.02 ± 0.005	0.017 ± 0.0015	0.018 ± 0.0016
R_H SANDY CLAY	0.6 ± 0.05	0.77 ± 0.02	0.77 ± 0.025
V_{OX} PEAT	0.01 ± 0.005	0.009 ± 0.003	0.02 ± 0.007
R_H PEAT	0.9 ± 0.05	0.89 ± 0.04	0.88 ± 0.04

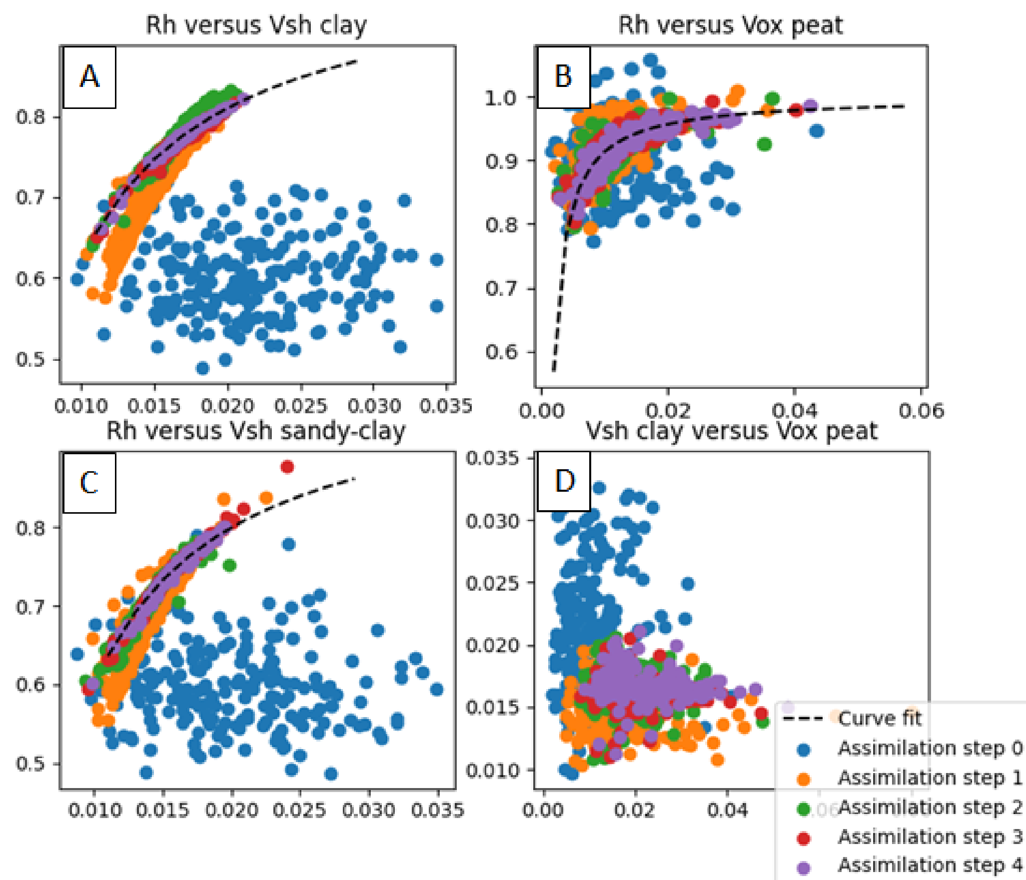

Figure 6: Several of the optimized parameters are plotted against each other for the pre-scenario (assimilation step 0) until the optimized result for the parameters (assimilation step 4) for the ascending satellite track. For all lithoclasses there is a strong correlation between the residual height (Rh) and the rate of subsidence (V). There is no clear correlation between the different lithoclasses, as indicated in figure 6d. For all the lithoclasses the relation of equation 12 is optimized for assimilation step 4, using an automated least squares polynomial fit. The constants for the line in figure a is $C = v(1 - R) = 0.0038\ \mathrm{yr}^{-1}$; for b it is $C = v(1 - R) = 0.0021\ \mathrm{yr}^{-1}$ and for c $C = v(1 - R) = 0.0040\ \mathrm{yr}^{-1}$.

Table 2: The average contribution of clay shrinkage versus peat 21oxidation for all the locations is provided below, in mm/year . Clay incorporates both clay and sandy clay lithoclasses from the GeoTOP model.

	Ascending	Descending
Average contribution clay shrinkage (mm/year)	5.7 ± 2.0	5.8 ± 2.3
Average contribution peat oxidation (mm/year)	0.07 ± 0.17	0.2 ± 0.42

4. Discussion

4.1 Future estimates and spatial pattern of subsidence

This study has demonstrated the possibility to make reliable estimates of subsidence related to phreatic groundwater level changes and lithoclass layering. The study area was the urbanized Almere area of the reclaimed South Flevoland polder. For relatively short timescales, this enables making estimates of future subsidence, providing indications to drivers and hence tools for designing mitigation strategies. To provide information on expected future subsidence rates, four scenarios for the next five years were simulated. The first scenario was to continue the average rate of phreatic groundwater level change towards the future (red in figure 7b), the second scenario was to fix the level at the average height from April 2018 until the end of the research period (blue in Figure 7b) – no more lowering is allowed. The third scenario fixed the phreatic groundwater level at the average height of the phreatic surface for the research period until April 2018 (green in figure 7b): the phreatic level is brought back to higher values. The last scenario, finally, increased the water level even further by adding to the third scenario an extra 20 centimeters. No seasonal trends were added to the scenarios, it is a mere indication of phreatic groundwater level elevation effects on subsidence until 2025.

Figure 7a shows the spatial distribution of the total absolute increase in subsidence since the start of the study related to the different scenarios. The difference between a continuous decrease versus the average level of before March 2018 +0.2 m can be up to 2 centimeters in 5 years. The spatial plotting also makes apparent that most of the subsidence is expected in the southwest and northeast of the city of Almere. The area in the northeast part coincides with the course of the Eem paleovalley (Fig. 1), where the thickest Holocene sequence is present. Naturally, as this study does not provide a continuous image of subsidence, local alternating Holocene sequences are not accounted for. The spatial relation of subsidence with Holocene thickness or groundwater level is not a result straightforward relation, where clay thickness or groundwater level alone determines the subsidence rate. From our results, we see that not one single factor influences the spatial pattern of subsidence. This amplifies our need for subsidence modelling on the urban scale.

Figure 7B provides predictions for one randomly chosen location, to give an idea of what subsidence looks like over time. The phreatic groundwater level is a key factor in the subsidence rates. From our analysis it follows that one meter drop in the phreatic surface will lead to one centimeter of additional subsidence in five years. This relationship can help in decisions concerning groundwater management, the single key factor of human influence on the subsidence rate. The result of this study can be used to support science-based mitigation measures.

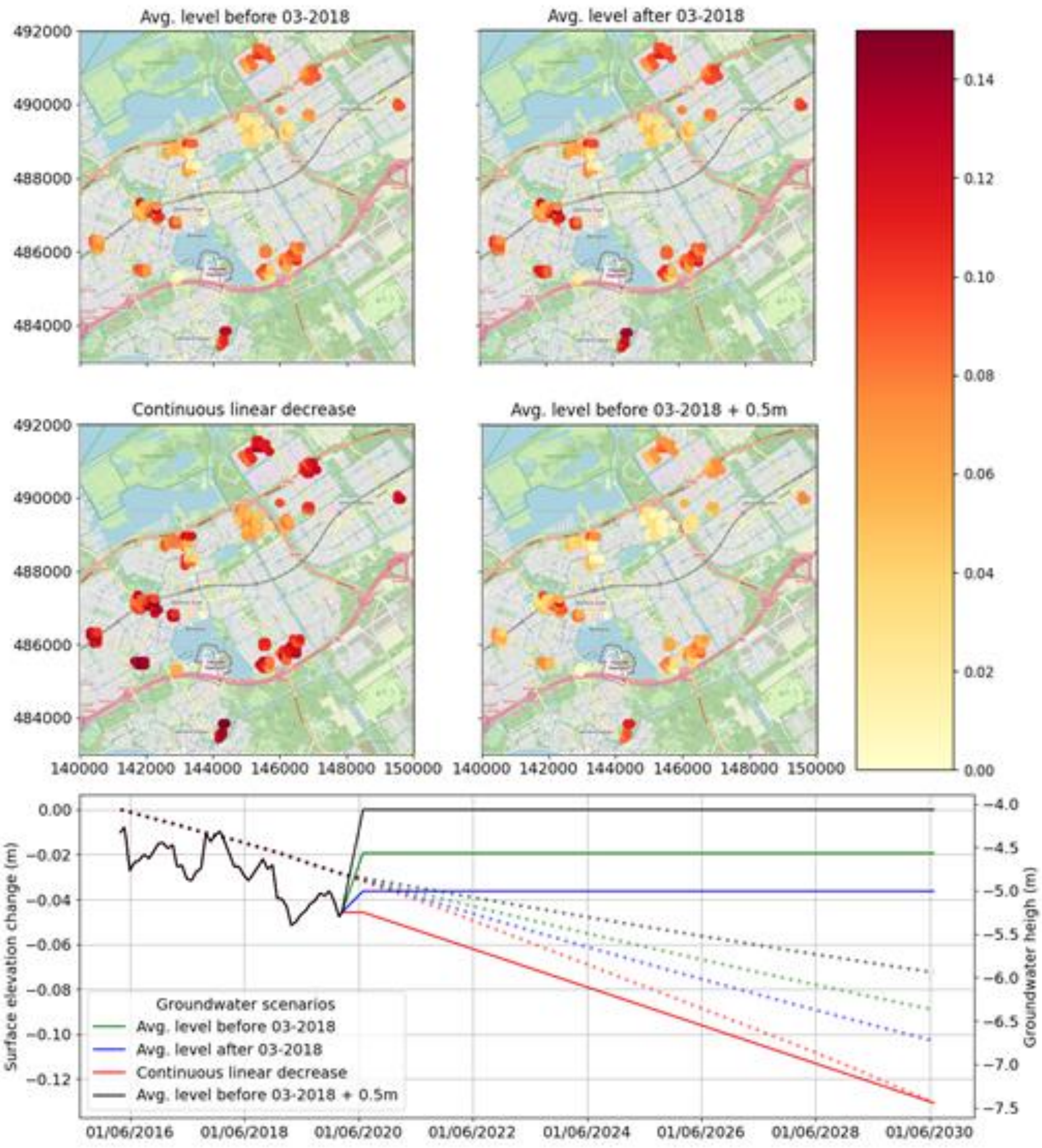

Figure 7: Future estimates of subsidence. Figure 7a plots the expected subsidence since the start of the study for different scenarios of groundwater development. The scenarios range from largest to smallest drop in the phreatic surface, and hence largest to smallest expected subsidence. Locations are the same as in Figure 1. 7b shows the subsidence development of one individual location over time, from the start of the study period until 5 years after the end of the study period. The continuous lines show the phreatic surface, on the right y-axis, the dashed line shows the modelled subsidence, with height on the left y-axis In red the continuous decrease of subsidence is

modelled, in blue the average groundwater level from March 2018 until the end of the study period, the green line the average groundwater level of the study period until March 2018 and the black line is the green groundwater level plus 0.2 meters.

4.2 Comparison to other subsidence regions

The Flevoland Polder is unique in the Netherlands in the sense that subsidence is dominated by shrinkage of clay. Clay-shrinkage dominated subsidence is however observed in many other regions in the world. An example is the northern Nile Delta plain in Egypt, where Holocene clay related subsidence is enhanced by climate change that affects the Nile's flow regime (Stanley and Clemente, 2014). There, subsidence ranges from 3.7-8.4 mm/year, which are comparable to the subsidence by clay derived in this study for the South-Flevoland polder.

In and around Venice, Italy there is ongoing subsidence caused by compression of the natural lagoon (0.0-0.5 mm/year). More recently, there is human-induced subsidence (> 2.5 mm/year) due to groundwater withdrawals (Tosi et al., 2013). Parallels with the South Flevoland polder can be found in the reducing natural consolidation over time and significant subsidence induced by groundwater withdrawals. Both areas must deal with irreversible land lowering caused by groundwater withdrawals which are required to prevent the area from flooding.

The same comparison can be made with the Vietnamese Mekong Delta, where groundwater lowering by withdrawals is the main driver of subsidence. The rates of groundwater withdrawal and subsidence are significantly higher in the Mekong Delta. Compaction rates are estimated at an average of 16 mm/year and total subsidence rates, including the subsidence as a result of groundwater withdrawal, can locally be up to 40 mm/year (Erban et al., 2014).

Despite the differences between these areas in rates of subsidence and groundwater withdrawal, the common thread is that all areas are affected by groundwater lowering, either by climate change or anthropogenic causes. Understanding the importance of groundwater level changes to subsidence is therefore of major importance for all these coastal regions across the world. The method presented in this study, and the results in relation to clay behavior of the reclaimed land and the response to groundwater lowering can be of help to tackle this problem.

4.3 Subsidence by drought

In the results, a slight acceleration of subsidence around summer 2018 is visible. This acceleration is related to relative deep lowering of the phreatic groundwater level. At some locations, this acceleration is more profound than in others, as this is influenced by litholoclass and fluctuations of the phreatic levels as well. As shown in Figure 5, this relative low elevation of the phreatic groundwater level influences the processes responsible for subsidence. Namely, due to a lowered groundwater level, deep peat layers are temporarily aerated, resulting in oxidation and volumetric loss. Furthermore, a deeply lowered groundwater level can therefore instigate subsidence at locations that were previously not subsiding.

These temporary deeply lowered phreatic groundwater levels are the results of climate change related drought events, such as the summers of 2018 and 2019 (Hari et al., 2020). Observed accelerated subsidence due to drought is new in the context of the Netherlands. Studies in other (Northwestern) European countries have recently linked drought to increased shrinkage in clay and associated damage to the built environment (e.g. Charpentier et al., 2021; Gruslin et al., 2022). With global warming resulting in more frequent droughts, establishing these relationships becomes increasingly more important.

The results for the effects of drought in this study, however, must be viewed with care. As the number of groundwater datapoints decreases with time, the uncertainty increases. Our results are indicators of drought having an effect, but more extensive and consistent measuring of the phreatic surface is essential to assess groundwater related subsidence. Especially the effect of drought on the phreatic surface height is an important link for future scenarios of subsidence and mitigation strategies.

4.4 Implications

Current governmental attention in the Netherlands for shallow subsidence is predominantly focusing on peat oxidation (Van Nieuwenhuizen Wijbenga, 2019). Therefore, the current study fills a gap in the Netherlands knowledge base. Quantifying the process of clay-driven subsidence is important for optimal decision making regarding shallow subsidence in Almere. Additionally, showing that drought enhances subsidence rates is important for focusing future measures to mitigate subsidence, and connects the problem to climate change. Furthermore, phreatic surface lowering exposing deeper peat beds also increases carbon dioxide emissions by peat oxidation (e.g. Koster et al., 2020).

This study would not have been possible without a structure of nation-wide freely available data on the construction of buildings, relative elevation measurements, geology, and groundwater. Still, more data will help to corroborate our findings. Investments in a network to monitor phreatic groundwater level changes and shallow extensometers able to measure volumetric loss within the Holocene sequence is critical herein (cf. Van Asselen et al., 2020). For improved processing of geodetic data, a network of corner reflectors is required to measure surface movement of the ground level (e.g. Yu et al., 2013). Such investments should be conducted in close collaboration with policy makers and spatial planners.

4.5 A comparison of parameters with previous studies

The South Flevoland polder is unique in the Netherlands with respect to the progressively increasing number of clay and peat beds that encounter contact with atmosphere for the first time since their formation. The estimated subsidence rates are therefore not directly comparable to other polder areas in the Netherlands that have been reclaimed centuries ago.

Earlier studies on subsidence in the South Flevoland polder determined the rates of subsidence due to shrinkage after reclamation estimated based on a few measurements of non-urbanized locations across the South Flevoland polder (De Lange et al., 2012; De Lange, 2015; Fokker et al., 2019). The estimated subsidence in those regions was larger than what we have observed here in the urbanized areas. A reasonable explanation would be that construction has an inhibitory effect on the shrinkage of clay (and when applicable oxidation of organic material) (De Lange, 2015). This study focuses on an urbanized area to estimate the contribution of the different background subsidence processes in urbanized settings.

The residual height estimated by Fokker et al., 2019 lies between 0.50 and 0.67 for clay. However, as mentioned before, the start of modelling subsidence is ~50 years after reclamation in our study, whereas Fokker et al., 2019 start modelling from reclamation onwards, hence the layers still have their original thickness. The values found in this study are higher; ~0.78. Due to the length of the modelling period, only a relation between residual height and reduction rate could be established (Fig. 6). A higher residual height can be explained when layers already have partly undergone shrinkage before the start of the observations. Indeed, in our study, the reference is not at the start of exposure to air but a long time later in the compaction history.

A good match between the estimated parameters and the InSAR time series was found for our spatiotemporal model of subsidence in the city of Almere, quantified with the calculated chi-square error, whilst incorporating groundwater levels, lithology, and the physical models. In line with literature, the shrinkage rates of clay are larger than the oxidation rates of peat (Fokker et al, 2019; Schothorst, 1982).

The same value for uncertainty is currently attributed to each InSAR-derived data point in space and time. There was no covariance matrix available for the dataset. Accurate covariance matrices could increase our ability to fit parameters and models to the data, by reducing the weight given to less reliable data points and incorporating interdependencies.

4.6 Correlations between parameters

We found correlations between the residual height and reduction rate parameters for the same soil types. This correlation could have been expected from the form of their presence in the forward model. The relationship, as shown in Figure 6, helps in future subsidence estimates. By parameterizing the average behavior of the three lithological types, prediction on future behavior with respect to phreatic groundwater changes can be made even when the individual values of the parameters are rather uncertain.

There is no correlation between the shrinkage rate of clay and the oxidation rate of peat (Fig. 6), because lithoclasses act independently. Clay and sandy clay show similar behavior (Figure 6 and Table 2). In the South Flevoland polder, sandy clay is the product of tidal dynamics, and consists of mm-thick alternating clay and sand beds. The comparable behavior between these thin-bedded sandy-clay and clay deposits indicates the dominance of clay shrinkage within the sandy-clay cells. Apparently, the presence of sand is only minimally preventing these deposits from volumetric loss by shrinkage.

Figure 5a shows a scenario in which the average phreatic groundwater level is located within the uppermost sand bed. Here, the model underestimated observed subsidence. We think the mismatch is related to short drought events not captured by our monthly updated groundwater model. Phreatic groundwater levels that are temporally lowered, result in shrinkage of clay directly underneath the upper sand bed, resulting in enhanced subsidence. This explanation is corroborated by the increase in subsidence rate in Figure 5a that coincides with the phreatic surface drop into the clay layer.

5 Conclusions

We have presented a novel data processing and data assimilation workflow with an unprecedented dataset to identify processes resulting in anthropogenically-induced subsidence around the city of Almere in the reclaimed South Flevoland polder in the Netherlands. The workflow integrates lithoclass, phreatic groundwater level changes, and InSAR data, with information on construction dates of structures, and a suite of physical models. The assimilation exercise has enabled us to quantify the drivers of subsidence.

Our results have revealed that shrinkage of shallow clay beds induced by artificial lowering of phreatic groundwater levels is the dominant subsidence process in the South Flevoland polder, with rates up to 6 mm/yr. In line with previous research in the South Flevoland polder, the subsidence rates due to clay shrinkage are significantly higher than those due to peat oxidation, which are up to 0.2 mm/yr. The rates depend critically on the development of phreatic water levels – drought has therefore been identified in this study as an important catalyzer of subsidence. At longer timescales we estimated that one meter drop in groundwater level results in 10 millimeter of subsidence in the urbanized area of Almere.

Groundwater governance is the single human activity influencing land subsidence in Almere. Our study highlights the necessity of high-quality data in order to make trustworthy analyses of subsidence processes and support such governance. Data is obtained by measuring campaigns and continuous monitoring. This includes lithology, groundwater development and surface level changes. Robust analyses of subsidence processes and quality predictions are possible through the application of an approach that integrates all available data with knowledge on physical processes in a dedicated data assimilation procedure.

Acknowledgments

We are grateful to Joana Esteves-Martins for providing aid with the initial InSAR dataset for this study. The research presented in this paper is part of the project Living on soft soils: subsidence and society (grantnr.: NWA.1160.18.259). This project is funded through the Dutch Research Council (NWO-NWA-ORC), Utrecht University, Wageningen University, Delft University of Technology, Ministry of Infrastructure & Water Management, Ministry of the Interior & Kingdom Relations, Deltares, Wageningen Environmental Research, TNO-Geological Survey of The Netherlands, STOWA, Water Authority: Hoogheemraadschap de Stichtse Rijnlanden, Water Authority: Drents Overijsselse Delta, Province of Utrecht, Province of Zuid-Holland, Municipality of Gouda, Platform Soft Soil, Sweco, Tauw BV, NAM.

Open Research

Data from the geological survey of the Netherlands (TNO-GSN, 2022) is used to construct the lithological and groundwater model. Kadaster (2022) has been used to verify the age of the buildings. From Rijkswaterstaat (2022) InSAR data products were retrieved. Figures were made with Matplotlib v.3.4.3 (Caswell et al., 2022) available under the matplotlib license at https://matplotlib.org and QGIS v3.24 (QGIS Development team, 2022).

References

Allison, M., Yuill, B., Törnqvist, T., Amelung, F., Dixon, T.H., Erkens, G., Stuurman, R., Jones, C., Milne, G., Steckler, M., Syvitski, J. & Teatini, P. (2016) Global risks and research priorities for coastal subsidence. *Eos* 97, 22-27. https://doi.org/10.1029/2016EO055013.

Barbour, E.J., Adnan, M.S.G., Borgomeo, E., Paprocki, K., Shah Alam Khan, M., Salehin, M. & Hall, J. W. (2022) The unequal distribution of water risks and adaptation benefits in coastal Bangladesh *Nature Sustainability* 5, 295-302, https://doi.org/10.1038/s41893-021-00846-9

Barciela Rial, M. (2019). Consolidation and drying of slurries: A building with nature study for the Marker Wadden. (Doctoral dissertation) Delft: TU Delft https://doi.org/10.4233/uuid:ae11c3e7-86f2-4c6a-8d53-ee8781d56a72

Barciela-Rial, M., van Paassen, L. A., Griffioen, J., van Kessel, T. & Winterwerp, J. C. (2020). The effect of solid-phase composition on the drying behavior of Markermeer sediment. *Vadose Zone Journal*, 19(1), doi:10.1002/vzj2.20028

Beets, D. & Van der Spek, A. (2000). The Holocene evolution of the barrier and the back-barrier basins of Belgium and the Netherlands as a function of late Weichselian morphology, relative sea-level rise and sediment supply. Netherlands Journal of Geosciences - Geologie En Mijnbouw, 79(1), 3-16. doi:10.1017/S0016774600021533

Bronswijk, J. J. B. & Evers-Vermeer, J. J. (1990). Shrinkage of Dutch clay soil aggregates. *Netherlands Journal of Agricultural Science*, 38(2), 175-194.

Burnol, A., Foumelis, M., Gourdier, S., Deparis, J. & Raucoules, D. (2021) Monitoring of expansive clays over drought-rewetting cycles using satellite remote sensing. *Atmosphere* 12 (10), 1262. https://doi.org/ 10.3390/atmos12101262

Caló, F., Notti, D., Galve, J.P, Abdikan, S., Görüm, T., Pepe, A. & Balik Şanli, F. (2017) DInSAR-based detection of land subsidence and correlation with groundwater depletion in Konya Plain, Turkey. *Remote Sensing Volume* 9 (83). https://doi.org/10.3390/rs9010083

Campello, R.J.G.B., Moulavi, D. & Sander, J. (2013) Density-based clustering based on hierarchical density estimates. *Conference: Pacific-Asia Conference on Knowledge Discovery and Data Mining.* https://doi.org/10.1007/978-3-642-37456-2_14

Candela, T., Chitu, C.G., Peters, E., Pluymaekers, M., Hegen, D., Koster, K. & Peter, A.F. (2022) Subsidence induced by gas extraction: A data assimilation framework to constrain the driving rock compaction process at depth. *Frontiers in Earth Science.* 10. https://doi.org/10.3389/feart.2022.713273

Candela, T. & Koster, K. (2022) The many faces of anthropogenic subsidence. *Science*. 376(6600):1381-1382. https://doi.org/10.1126/science.abn3676.

Chang, H., Chen, Y. & Zhang, D. (2010) Data assimilation of coupled fluid flow and geomechanics using the ensemble Kalman Filter. *SPE Journal*. 15 (2010): 382–394. https://doi.org/10.2118/118963-PA.

Carton, J. A. & Giese, B. S. (2008). A reanalysis of ocean climate using simple ocean data assimilation (SODA), *Monthly Weather Review*, 136(8), 2999-3017. doi:10.1175/2007MWR1978.1.

Castellazzi, P., Martel, R., Galloway, D., Longuevergne, L. & Rivera, A. (2016). Assessing groundwater depletion and dynamics using GRACE and InSAR: Potential and Limitations. *Groundwater.* 54. https://doi.org/10.1111/gwat.12453.

Chaussard, E., Amelung, F., Abidin, H. & Hong, S. (2013) Sininking cities in Indonesia: ALOS PALSAR detects rapid subsidence due to groundwater and gas extraction. *Remote Sensing of Environment.* Volume 218, pp: 150-161. https://doi.org/10.1016/j.rse.2012.10.015

Charpentier, A., James, M.R. & Hani, A. (2021) Predicting drought and subsidence risks in France, *Natural Hazards and Earth System Science Discussions* doi:10.5194/nhess-2021-214

Conroy, P., Van Diepen, S. A. N., Van Asselen, S., Erkens, G., Van Leijen, F. J. & Hanssen, R. F. (2022). Probabilistic Estimation of InSAR displacement phase guided by contextual information and artificial intelligence. *IEEE Transactions on Geoscience and Remote Sensing*, 1-11. https://doi.org/10.1109/TGRS.2022.3203872

CUR (1992). Construeren met grond (In Dutch). CUR Rapport 162, pp. 411

Declercq, P., Gérard, P., Pirard, E., Walstra, J. & Devleeschouwer, X. (2021) Long-term subsidence monitoring of the alluvial plain of the Scheldt river in Antwerp (Belgium) Using Radar Interferometry. *Remote Sensing.* 12, 1160, https://doi.org/10.3390/rs13061160

Deutsch, C. and Journel, A.G. (1998) GSLIB Geostatistical software library and user guide, Second Edition. New York: Oxford University Press.

Dinar, A., Esteban, E., Calvo, E., Herrera, G., Teatini, P., Tomás, R., et al. (2021) We lose ground: Global assessment of land subsidence impact extent. *Science of The Total Environment.* 768, doi:10.1016/j.scitotenv.2021.147415

De Lange, G., Gunnink, J., Houthuessen, Y. & Muntjewerff, R. (2012), Bodemdalingskaart Flevoland. *Grontmij*; GM-0042778.

De Lange, G. (2015), Analyse bodemdaling en zetting Almere. *Deltares Rapport*; 1210761-000.

De Glopper, R.J. (1969) Shrinkage of subaqueuous sediments of Lake IJssel (the Netherlands) after reclamation. *Proceedings First International Symposium On Land Subsidence*, IAH, Tokyo, 192-201

De Glopper, R.J. (1973) Subsidence after drainge of the deposits in the former Zuyder Zee and in the brackish and marine forelands in The Netherlands. *Van Zee tot Land* 50, pp. 205.

De Glopper, R.J. (1984) Subsidence in the recently reclaimed IJsselmeerpolder "Flevoland". *Proc. Third International Symposium On Land Subsidence*, IAHS, Venice, 487-496

De Glopper, R.J. & Ritzema, H.P. (1994) Land Subsidence. *Drainage Principles and Applications.* vol. 16 (2). ILRI, pp. 41

Den Haan, E. (January 1996). A compression model for non-brittle soft clays and peat. *Géotechnique*, 46(1), 1– 16. https://doi.org/10.1680/geot.1996.46.1.1

Emerick, A. & Reynolds, A.C. (2013), Ensemble smoother with multiple data assimilation, *Computational Geoscience.*, 55, 3-15, doi:10.1016/j.cageo2012.03.011.

Erban, L.E., Gorelick, S.M. & Zebker, H.A. (2014) Groundwater extraction, land subsidence and sea-level rise in the Mekong Delta, Vietnam. *Environmental Research Letters.* 9 https://doi.org/10.1088/1748-9326/9/8/084010

Eslami, S., Hoekstra, P., Nguyen Trung, N., Ahmed Kantoush, S., Van Binh, D., Duc Dung, D., et al. (2019). Tidal amplification and salt intrusion in the Mekong Delta driven by anthropogenic sediment starvation. *Scientific Reports*, 9(1). https://doi.org/10.1038/s41598-019-55018-9

Evensen, G. (2009). *Data assimilation, The Ensemble Kalman Filter* (2nd ed.). Berlin: Springer.

Evensen, G., Vossepoel, F.C. & Van Leeuwen, P.J. (2022) *Data Assimilation Fundementals, A Unified Formulation of the State and Parameter Estimation Problem.* Berlin: Springer. https://doi.org/10.1007/978-3-030-96709-3_1

Fernández Llamas, A., Martínez, D., Hernández, P., Cristóbal, S., Schwaiger, F., Nuñez, J. & Ruiz, J. (2019). Flight Data Monitoring (FDM) Unknown Hazards detection during Approach Phase using Clustering Techniques and AutoEncoders. *Conference paper SESAR* ISSN 0770-1268

Ferretti, A., Monti-Guarnieri, A., Prati, C. & Rocca, F. (2007), InSAR Principles: Guidelines for SAR Interferometry Processing and Interpretation, *ESA Publications*, ESTEC

Fokker, P.A., Wassing, B., Van Leijen, F.J., Hanssen, R.F. & Nieuwland, D. (2016), Application of an ensemble smoother with multiple data assimilation of the Bergermeer gas field, using PS-InSAR. *Geomechanics for Energy and the Environment*, 5, 183-187.

Fokker, P.A., Gunnink, J., Koster, K. & de Lange, G. (2019), Disentangling and Parameterizing Shallow Sources of Subsidence: Application to a Reclaimed Coastal Area, Flevoland, The Netherlands. *Journal of Geophysical Research: Earth Surface*, https://doi.org/10.1029/2018jf004975.

Gazzola, L., Ferronato, M., Frigo, M., Carlo, J., Pietro, T., Zoccarato, C., et al. (2021) A novel methodological approach for land subsidence prediction through data assimilation techniques. *Computational Geoscience. 25*, 1731–1750. https://doi.org/10.1007/s10596-021-10062-1

Ghil, M. & Malanotte-Rizzoli, P. (1991) Data Assimilation in Meteorology and Oceanography. *Advances in Geophysics*. 33, pp: 141-266. https://doi.org/10.1016/S0065-2687(08)60442-2.

Guo, H. & Jiao, J.J. (2007) Impact of Coastal Land Reclamation on Ground Water Level and the Sea Water Interface. *Groundwater.* 45, 3, pp: 362-367. https://doi.org/10.1111/j.1745-6584.2006.00290.x

Hanssen, R. F. (2001). *Radar interferometry: data interpretation and error analysis* (Vol. 2). Springer Science & Business Media.

Hari, V., Rakovec, O. , Markonis, Y. Hanel, M. & Kumar, R. (2020) Increased future occurrences of the exceptional 2018-2019 Central European drought under global warming. *Scientific reports.* 10, 12207. https://doi.org/10.1038/s41598-020-68872-9

Harrison, R., Hol, E.A. & De Graef, M. (2019) On the use of 2D moment invariants in the classification of additive manufacturing powder feedstock. *Material Characterization.* 149, 255-263. https://doi.org/10.1016/j.matchar.2019.01.019

Hoeksema, R. J. (2007). Three stages in the history of land reclamation in the Netherlands. *Irrigation and Drainage*, 56(S1), S113–S126. https://doi.org/10.1002/ird.340

Hoogland, F., Roelandse, A. S., de La Loma González, B., Waterloo, M. J., Mooij, P. W., Verhagen, S. A. & Velstra, J. (2020) Investigating the effectiveness of drain infiltration to minimize peat oxidation in agricultural fields in Flevoland, the Netherlands. *Proceedings of the International Association of Hydrological Sciences.* 382, 747–753, https://doi.org/10.5194/piahs-382-747-2020

Hoogland, T., Van Den Akker, J.J.H. & Brus, D.J. (2012) Modelling the subsidence of peat soils in the Dutch coastal area. *Geoderma* 171-172, 92-97, https://doi.org/10.1016/j.geoderma.2011.02.013

Jones, C.E., An, K., Blom, R.G., Kent, J.D., Ivins, E.R. & Bekaert, D. (2016) Anthropogenic and geologic influences on subsidence in the vicinity of New Orleans, Louisiana. *Journal of Geophysical Research Solid Earth* Volume 121, 5, pp: 3867-3887. https://doi.org/10.1002/2015JB012636

Kadaster (2022) Basisregistratie Adressen en Gebouwen – BAG, URL: www.kadaster.nl/zakelijk/registraties/basisregistraties/bag

Kahloot, K. & Ekler, P. (2019) Improving t-SNE clustering and visualization. *Computer science*, Cropus ID: 229360049

Kim, D. J., Feyen, J., Vereecken, H., Boels, D., & Bronswijk, J. J. B. (1993). Quantification of physical ripening in an unripe marine clay soil. *Geoderma*, 58(1-2), 67–77. https://doi.org/10.1016/0016-7061(93)90085-y

Kooi, H. (2000) Land subsidence due to compaction in the coastal area of the Netherlands: the role of lateral fluid flow and constraints from well-log data. *Global and Planetery Change.* 27, 1-4, pp: 207-222. https://doi.org/10.1016/S0921-8181(01)00067-4

Koster, K., Stafleu, J. & Cohen, K. (2016) Generic 3D interpolation of Holocene base-level rise and provision of accommodation space, developed for the Netherlands coastal plain and infilled palaeovalleys. *Basin Research.* Volume 29. https://doi.org/10.1111/bre.12202

Koster, K., Stafleu, J. & Stouthamer, E. (2018), Differential subsidence in the urbanized coastal-deltaic plain of the Netherlands. *Netherlands Journal of Geosciences*, 1-13. https://doi.org/10.1017/njg2018.11

Koster, K., Stafleu, J., Cohen, K.M., Stouthamer, E., Busschers, F.S. & Middelkoop, H. (2018) Three-dimensional distribution of organic matter in coastal-deltaic peat: Implications for subsidence and carbon dioxide emissions by human-induced peat oxidation. *Anthropocene.* 22, pp: 1-9, https://doi.org/10.1016/j.ancene.2018.03.001

Koster, K., De Lange, G., Harting, R., De Heer, E. & Middelkoop, H. (2018) Characterizing void ratio and compressibility of Holocene peat with CPT for assessing coastal–deltaic subsidence. *Quarterly Journal of Engineering Geology and Hydrogeology*, 51(2), 210–218. https://doi.org/qjegh2017-120

Koster, K., Frumau, A., Stafleu, J., Dijkstra, J., Hensen, A., Velzeboer, I., et al. (2020) Greenhouse Peat: a model linking CO_2 emissions from subsiding peatlands to changing groundwater levels, *Proceedings of* *the International Association of Hydrological Sciences.* 382, 609-614, https://doi.org/10.5194/piahs-382-609-2020

Lambert, J.W.M., Nieal, L., Stoorvogel-van der Horst, S., Verheijen, E. & Woning, M. (2016) Bodemdaling Almere: consequenties voor gemeentelijke infrastructuur. *Rapport Circulair Cities, TO2.*

Li, D., Li, B., Zhang, Y., Fan, C., Xu, H. and Hou, X. (2022) Spatial and temporal characteristics analysis for land subsidence in Shanghai coastal reclamation area using PSInSAR method. Frontiers in Marine Science. 9:1000523. https://doi.org/10.3389/fmars.2022.1000523

Maas, M. (2021) Ook Almere worstelt met bodemdaling. *Binnenlands bestuur* nr. 12

Makaske, B., Van Smeerdijk, D., Peeters, H., Mulder, J., & Spek, T. (2003). Relative water-level rise in the Flevo lagoon (The Netherlands), 5300-2000 cal. yr BC: An evaluation of new and existing basal peat time-depth data. *Netherlands Journal of Geosciences*. 82(2), 115-131. https://doi.org/10.1017/S0016774600020680

Martín-Antón, M., Negro, V., del Campo, J.M., López-Gutiérrez, J.S. & Esteban M.D., 2016. Review of coastal Land Reclamation situation in the World. *Journal of Coastal Research, Special Issue*, No. 75, pp. 667–671. https://doi.org/10.2112/SI75-133.1

Mayoral, J. M., Castañon, E., & Albarran, J. (2017). Regional subsidence effects on seismic soil-structure interaction in soft clay. *Soil Dynamics and Earthquake Engineering*, 103, 123–140. https://doi.org/10.1016/j.soildyn.2017.09.014

Menke, U., van Laar, E. & Lenselink, G. (1999), De Geologie en Bodem van Zuidelijk Flevoland. *Flevobericht* 415, ISBN: 90-3691-2202

Muntendam-Bos, A. G., Kleuskens, M. H. P., Bakr, M., de Lange, G., & Fokker, P. A. (2009). Unraveling shallow causes of subsidence. *Geophysical Research Letters*, 36(10). https://doi.org/10.1029/2009gl037190

Navon, I.M. (2009). Data Assimilation for Numerical Weather Prediction: A Review. In: Park, S.K., Xu, L. (eds) *Data Assimilation for Atmospheric, Oceanic and Hydrologic Applications.* Berlin: Springer. https://doi.org/10.1007/978-3-540-71056-1_2

Neumann, B., Vafeidis, A.T., Zimmermann, J. & Nicholls, R.J. (2015) Future coastal population growth and exposure to sea-level rise and coastal flooding – a global assessment. *PLoS One*, 10 (3), Article e0118571

Nieuwenhuis, H.S. & Schokking, F. (1997) Land subsidence in drained peat areas of the Province of Friesland, The Netherlands. *Quarterly Journal of Engineering Geology and Hydrology.* 30, 37-48, https://doi.org/10.1144/GSL.QJEGH.1997.030.P1.04

Nusantara, R. W., Hazriani, R., & Suryadi, U. E. (2018). Water-table Depth and Peat Subsidence Due to Land-use Change of Peatlands. *IOP Conference Series: Earth and Environmental Science*, 145, 012090. https://doi.org/10.1088/1755-1315/145/1/012090

Peduto, D., Huber, M., Speranza, G., van Ruijven, J., & Cascini, L. (2017). DInSAR data assimilation for settlement prediction: case study of a railway embankment in the Netherlands. *Canadian Geotechnical Journal*, 54(4), 502-517.

Peduto, D., Giangreco, C., & Venmans, A. A. (2020). Differential settlements affecting transition zones between bridges and road embankments on soft soils: Numerical analysis of maintenance scenarios by multi-source monitoring data assimilation. *Transportation Geotechnics*, 24, 100369.

Peeters, J., Busschers, F.S. & Stouthamer, E. (2015) Fluvial evolution of the Rhine during the last interglacial-glacial cycle in the southern North Sea basin: A review and look forward. *Quaternary International.* Volume 357, pp: 176-188. https://doi.org/10.1016/j.quaint.2014.03.024

Pritchard, O.G., Hallett, S.H. & Farewell, T.S. (2015) Probabilistic soil moisture projections to assess Great Britain's future clay-related subsidence hazard. *Climate Change*. 133, 635-650. https://doi.org/ 10.1007/s10584-015-1486-z

Schmidt, C.W. (2015) Delta Subsidence: An Imminent Threat to Coastal Populations. *Environmental Health Perspectives.* 123 (8): A204-A209. https://doi.org/10.1289/ehp.123-A204

Schothorst, C.J., (1982). Drainage and behavior of peat soils. In: *Proceedings of the symposium on peat lands below sea level*, edited by H. de Bakker & M.W. van den Berg. ILRI-publication 30: 130-163.

Schultz, E. (1983). From Natural to Reclaimed Land. *Water International*, 8(2), 55–60. https://doi.org/10.1080/02508068308686007

Spaan, B. (2015). Buildings, *Waag Society*. URL: https://code.waag.org/buildings/

Spikker, M. (2010) Funderen in Almere. *Msc. Thesis TU Delft*

Stanley, J.D. & Clemente, P.L. (2014) Clay Distributions, Grain Sizes, Sediment Thickness and Compaction Rates to Interpret Subsidence in Egypt's Northern Nile Delta. *Journal Of Coastal Research*, 30 (1), 88-101. https://doi.org/10.2112/JCOASTRES-D-13-00146.1

Steckler, M.S., Oryan, B., Wilson, C.A., Grall, C., Nooner, S.L., Mondal, D.R., et al. (2022) Synthesis of the distribution of subsidence of the lower Ganges-Brahmaputra Delta, Bangladesh. *Earth-Science Reviews* 224, https://doi.org/10.1016/j.earscirev.2021.103887

Steenbergen, C., Reh, W., Nijhuis, S. & Pouderoijen, M. (2009) The Polder Atlas of The Netherlands – Pantheon of the Low Lands. *THOTH*, ISBN: 978-90-6868-519-0

Sun, Q., Jiang, L., Jiang, M., Lin, H., Ma, P. & Wang, H. (2018) Monitoring Coastal Reclamation Subsidence in Hong Kong with Distributed Scatterer Interferometry. *Remote Sensing* 10 (11), pp:1738. https://doi.org/10.3390/rs10111738

Syvitski, J., Kettner, A., Overeem, I., Hutton E., Hannon, M., Brakenridge, R., et al. (2009) Sinking deltas due to human activities. *Nature Geoscience* 2, 681–686 https://doi.org/10.1038/ngeo629

Teatini, P., Ferronato, M., Gambolati, G. & Gonella, M. (2006). Groundwater pumping and land subsidence in the Emilia-Romagna coastland, Italy: Modeling the past occurrence and the future trend. *Water Resources Research* 42. https://doi.org/10.1029/2005WR004242.

Thépaut, J. N. (2003). *Satellite data assimilation in numerical weather prediction: An overview. In Proceedings of ECMWF Seminar on Recent Developments in Data Assimilation for Atmosphere and Ocean*, Reading UK: ECMWF. (pp. 8-12).

TNO (2022) REGIS II, hydrogeologisch model (HGM). *Basisregistratie Ondergrond (BRO).* URL: REGIS II, hydrogeologisch model (HGM) - Basisregistratieondergrond

Tarantola, A. (2005), *Inverse Problem Theory and Method for Model Parameter Estimation*. Paris; SIAM.

TNO-GSN (2022) DINOloket, https://www.dinoloket.nl/

Tosi, L., Teatini, P. & Strozzi, T. (2013) Natural versus anthropogenic subsidence of Venice. *Scientific Reports* 3: 2710. https://doi.org/10.1038/srep02710

Van Asselen, S., Stouthamer, E. & Van Asch, Th.W.J. (2009) Effect of peat compaction on delta evolution: A review on processes, respones, measuring and modeling. *Earth-science Reviews* 92-1, pp: 35-51. https://doi.org/10.1016/j.earscirev.2008.11.001

Van Asselen, S., Erkens, G., Stouthamer, E., Woolderink, H.A.G., Geeraerts, R.E.E. & Hefting, M.M. (2018), The relative contribution of peat compaction and oxidation to subsidence in built-up areas in the Rhine-Meuse delta, The Netherlands. *Science of the Total Environment* 636, 177-191. https://doi.org/10.1016/j.scitotenv.2018.04.141

Van Asselen, S., Erkens, G. & de Graaf, F. (2020) Monitoring shallow subsidence in cultivated peatlands. *Proceedings of the International Association of Hydrological Sciences*. 382, 189-194. https://doi.org/10.5194/piahs-382-189-2020

Van den Biggelaar, D.F.A.M., Kluiving, S.J., Van Balen, R.T., Kasse, C., Troelstra, S.R. & Prins, M.A. (2014) Storms in a lagoon: flooding history during the last 1200 years derived from geological and historical archives of Schokland (Noordoostpolder, the Netherlands) *Netherlands Journal of Geosciences*. 93, 175-196, https://doi.org/10.1017/njg.2014.14

Van Dooremolen, W.A., van der Scheer, A. & Winkels, H.J. (1996), Waarnemingen en Prognoses van maaiveldsdaling in Flevoland, *Flevobericht* 388, ISBN: 90-369-1161-3

Van de Kerkhof, B., Pankratius, V., Chang, L, van Swol, R. & Hanssen, R.F. (2020), Individual Scatterer Model Learning for Satellite Interferometry. *IEEE Transactions on Geoscience and Remote Sensing.* 58-2, https://doi.org/10.1109/TGRS.2019.2945370.

Van den Akker, J.J.H., Kuikman, P.J., De Vries, F., Hoving, I., Pleijter, M., Hendriks, R.F. A., et al. (2008) *Emission of CO2 from agricultural peat soils in the Netherlands and ways to limit this emission.* In: Farrell, C., Feehan, J. (Eds.), Proceedings of the 13th International Peat Congress., pp. 1–6.

Van der Maaten, L. & Hinton, G. (2008), Visualizing Data using t-SNE, *Journal of Machine Learning Research* 9, 2579-2605

Van der Meulen, M., Maljers, D., Gesssel, S.F. & Gruijters, S.H.L.L. (2007) Clay resources in the Netherlands, *Geologie en Mijnbouw, Netherlands Journal of Geosciences.* https://doi.org/10.1017/S001677460002312X

Van der Meulen, M., Doornenbal, J., Gunnink, J., Stafleu, J., Schokker, J., Vernes, R., et al. (2013). 3D geology in a 2D country: Perspectives for geological surveying in the Netherlands. *Netherlands Journal of Geosciences - Geologie En Mijnbouw*, 92(4), 217-241. https://doi.org/10.1017/S0016774600000184

Van Hardeveld, H. A., Driessen, P. P. J., Schot, P. P., & Wassen, M. J. (2017). An integrated modelling framework to assess management strategies steering soil subsidence in peatlands. *Environmental Impact Assesssment Review*, 66, 66– 77. https://doi.org/10.1016/j.eiar.2017.06.007

Van Nieuwenhuizen Wijbenga, C. (2019) Rijksbrede inzet op bodemdaling. *Ministerie van Infrastructuur en Waterstaat:* IENW/BSK-2019/135551.

Viscchedijk, M.A.T. & Trompille,V. (2009) MSettle Version 8.2. Emankment design and soil settlement prediction. *Deltares report*

Vos, P.C. (2015), Origin of the Duthc coastal landscape. Long-term landscape evolution of the Netherlands during the Holocene, described and visualized in national, regional and local palaeogeographical map series. (Doctoral Dissertation) Retrieved from: Utrecht University Repository. (https://dspace.library.uu.nl/handle/1874/315553) Utrecht: Utrecht University

Wang, M., Li, T. & Jiang, L. (2016) Monitoring reclaimed land subsidence in Hong Kong with InSAR technique by persistent and distributed scatters. *Natural Hazards* 82, pp 531-543. https://doi.org/10.1007/s11069-016-2196-1

Wang, W., Liu, H., Li, Y. & Su, J. (2014) Development and management of land reclamation in China. *Ocean & Coastal Management* 102B, pp: 415-425. https://doi.org/10.1016/j.ocecoaman.2014.03.009.

Wegmüller, U, Santoro, M., Werner, C. & Cartus, O. (2015) On the estimation and interpretation of Sentinel-1 tops InSAR coherence. *Proc. 'Fringe 2015 Workshop'*

Yu, B., Liu, G., Li, Z., Zhang, R., Jia, H., Wang, X., & Cai, G. (2013). Subsidence detection by TerraSAR-X interferometry on a network of natural persistent scatterers and artificial corner reflectors. *Computers & Geosciences*, 58, 126–136. https://doi.org/10.1016/j.cageo.2013.04.020

Zaadnoordijk, W.J., Bus, S.A.R., Lourens, A. & Berendrecht, W.L. (2018) Automated Time Series Modelling for Piezometers in the National Database of the Netherlands. *Groundwater*. https://doi.org/10.1111/gwat.12819

Ensemble Smoother with Multiple Data Assimilation to parameterize subsidence by phreatic groundwater level lowering in the South Flevoland Polder, the Netherlands

Subtitle: Disentangling Shallow Subsidence Sources by Data Assimilation in a Reclaimed Ubanized Coastal Plain

Manon Verberne[1,2], Kay Koster[3], Aris Lourens[3], Jan Gunnink[3], Thibault Candela[2] and Peter A. Fokker[1,2]

[1] Utrecht University, Geosciences, Utrecht, The Netherlands
[2] TNO Applied Geoscience, Utrecht, The Netherlands
[3] TNO Geomodelling, Utrecht, The Netherlands

Corresponding author: Manon Verberne (manon.verberne@tno.nl)

Key Points:

- Interferometric Synthetic Aperture Rader data on objects constructed on soft soil without a foundation are used for subsidence measurements
- Shrinkage of clay by aeration as a result of artificially lowered phreatic groundwater levels is identified as the main source of subsidence
- One meter drop in phreatic groundwater level now translates into one centimeter of subsidence in five years

Abstract

This research targets disentangling shallow causes of anthropogenically-induced subsidence in a reclaimed and urbanized coastal plain. The study area is around the city of Almere, in the South Flevoland polder, the Netherlands, which is among the countries' fastest subsiding areas. The procedure consists of integrating Interferometric Synthetic Aperture Radar (InSAR) data with high-resolution phreatic groundwater and lithoclass models, and a database containing construction details. The two main parts of the workflow are isolation of the InSAR points of structures without a pile foundation and a data assimilation procedure by Ensemble Smoothing with Multiple Data Assimilation. The shrinkage of surficial clay beds by phreatic groundwater level lowering is identified to be the main cause of shallow subsidence in the area, with an average contribution of 6 mm/year. The history-matched physics-based model predicts that one meter drop in phreatic groundwater level now translates into 10 millimeter of subsidence in the next five years. Also, this study showed that a groundwater deficiency due to severe dry periods should be considered as an accelerator of subsidence in both the short- and long-term planning. To ensure a robust network to estimate future subsidence, we advise on a consistent monitoring strategy of the phreatic groundwater level.

Plain Language Summary

The city of Almere, in the Netherlands, is part of a polder that was reclaimed in 1968. Land reclamation is accompanied by lowering of groundwater levels, which can cause land subsidence. Almere is situated on top of ~9 meters of soft soil layers. These layers were deposited after the last ice age and consist predominantly of clay and peat. It is important to understand and quantify the subsidence processes in these Holocene layers, to be able to mitigate subsidence.

By lowering the groundwater level, the soft soil layers are dried. Clay shrinks when it dries out and organic material (within peat) oxidizes. Lowering the groundwater level also causes the load of the layers below to increase, which can result in compaction of the layers (reduction in size by pressing together). This study targets the behavior of these processes.

Results of our study indicate that the shrinkage of clay is the dominant driver of subsidence in Almere. One meter lowering in groundwater level now results in approximately one centimeter subsidence in five years. To improve our understanding of the non-trivial link between groundwater fluctuations and subsidence, higher spatial-temporal resolution groundwater monitoring is required.

1 Introduction

Over half a billion people live in coastal plains and deltas threatened by anthropogenically induced subsidence, and this number is expected to increase in the foreseeable future (Neumann, 2015; Schmidt, 2015). Many anthropogenic subsurface activities in coastal areas and delta plains result in subsidence, thereby amplifying relative sea-level rise and flood risks, inflicting damage to infrastructure, and overall, reducing the viability of these low-lying areas (Dinar et al., 2021; Guo and Jiao, 2007; Syvitski et al., 2009). Examples of subsurface activities are resources extraction, such as groundwater (Jones et al., 2016) and deep hydrocarbons (Chaussard et al., 2013), and surficial processes related to land use, primarily phreatic groundwater level management (Koster, Stafleu and Stouthamer, 2018), and sediment deficit (Eslami et al., 2019).

Some heavily populated coastal plains and deltas require engineered extension of their surface area by land reclamation, to accommodate population growth, and increase the surface area of arable land, e.g. China, Belgium, Japan, Dubai, U.S. and Singapore (e.g. Declerq et al., 2021; Li et al., 2022; Martín-Antón et al, 2016; Wang et al., 2014). When land is gained along sea or lake shorelines by drainage of open water, this in essence means exposing waterlogged sediments to the atmosphere, thereby instigating various subsidence processes, primarily by shrinkage, compaction, and oxidation of fine grained and organic deposits.

The dense population of Hong Kong for instance, prompted the government to reclaim land since the nineteenth century. There, rates of subsidence are around 20 mm/year, resulting in major damage to the built environment by differential settlements (Sun et al., 2018; Wang et al., 2016). In Bangladesh, reclamation primarily serves the purpose of gaining arable land, resulting in subsidence rates up to 10 mm/year in these reclaimed areas. This catalyzes a rise in social inequality as especially low-income farmers are not able to cover adaptation costs for the negative effects of these high subsidence rates (Barbour et al., 2002; Steckler et al., 2022).

The Netherlands is a prime example of a country that has extended its coastal plains by land reclamation. In total, the Netherlands has 443 reclaimed former lakes located in its coastal plains, with a cumulative surface area of 3123.60 km^2 (Schultz, 1987). The centuries-long tradition of reclaiming land, referred to as ‘polder’, can be divided into three main periods of lake drainage. The first stage comprised the sixteenth to seventeenth century, when many small lakes within the back-barrier peatlands were drained with windmills. Secondly, in the nineteenth century, larger lakes in the coastal plain were drained with steam pumping stations. Lastly, in the twentieth century, Lake IJssel, the countries’ largest lake that was created by the damming of a tidal inlet, was reclaimed, resulting in the largest polders of all: the Lake IJssel polders (Fig. 1a).

The focus of this study is on understanding and predicting shallow causes of subsidence in the reclaimed urbanized South Flevoland Polder (430 km^2), which is part of the Lake IJssel polders (Fig. 1). The polder was created in 1968 by constructing a ring-dike around the water body to be reclaimed. This enclosed water body was subsequently drained until the water level dropped below the former lakes’ floor. Subsidence immediately commenced when the waterlogged deposits experienced aeration for the first time and pore water progressively evaporated (De Glopper, 1969). Ultimately, the polder has experienced locally one to two meters of subsidence since its reclamation (Barciela Rial, 2019; De Glopper, 1973; De Glopper 1984; De Lange et al., 2012; De Lange, 2015; Fokker et al., 2019).

Paradoxically, severe water pumping has been ongoing to this day, as it is required to keep phreatic water levels low, thereby preventing the polder from flooding due to its low-lying position relative to adjacent Lake IJssel water level and increasing the load-bearing capacity of the former lake floor. The area thus continues to subside as waterlogged sediments are progressively exposed to the atmosphere. Besides flood risks, differential subsidence in the urbanized areas of the South Flevoland polder causes stress on structures, which results in damage to the built environment, leading to major costs. This especially accounts for the ‘Regenboogbuurt’, which is a neighborhood that onlaps the thickest sequence of soft soil deposits in the area (Maas, 2021). Additionally, the severe drought events that have been striking

Northwestern Europe during recent summers, pose the threat of accelerated subsidence to the area by increasing evaporation of pore water from fine grained and organic deposits. To the best of our knowledge, no study has been reported on the effects of severe drought in South Flevoland, although Hoogland et al. (2020) showed that subsidence may be slowed down by proactively saturating shallow peat beds within the area. Understanding, quantifying, and predicting subsidence, both spatially and temporally in the South Flevoland polder is therefore from a socio-economic as well as a hazard-prevention point of view of immense importance.

The artificial lowering of phreatic water levels in the South Flevoland polder results in shrinkage of clay and oxidation of peat in the unsaturated zone (i.e. above the annually averaged lowest phreatic groundwater level). Clay shrinks as water that is adsorbed to charged platy clay particles evaporates and organic matter mixed within the clay oxidizes (Barciela Rial et al., 2020). This leads to volumetric loss and is largely irreversible. Peat oxidation regards the breakdown of organic components by microbial activity, is completely irreversible, and results in the emission of carbon dioxide (Koster et al., 2020). Further, there are subsidence processes in the saturated zone: the consolidation of clay and peat layers due to an increase in effective stress by lowering the hydrostatic pressure when phreatic water levels are lowered (De Glopper and Ritzema, 1994). Consolidation and oxidation have been addressed regularly in other areas in the Netherlands that experience shallow subsidence (e.g. Kooi, 2000; Van Asselen et al., 2009; Van Asselen et al., 2018). On the contrary, shrinkage of clay in the context of subsidence has been poorly covered (Fokker et al., 2019). However, in other countries, subsidence by clay shrinkage is considered as a major issue. In France and Great Britain for example, potential damage to the built environment inflicted by clay shrinkage as a result of drought and climate change has been studied in terms of cost per annum in the light of the insurance industry for decades (e.g. Burnol et al., 2021; Charpentier et al., 2021; Pritchard et al., 2015).

Most recent studies focus on establishing physics-based subsidence forecasts using input parameters derived by field- and laboratory measurements (Koster, Stafleu and Stouthamer, 2018; Mayoral et al., 2017; Nusantara et al., 2018; Schothorst, 1982; Van Asselen et al., 2018). This approach inherently renders the subsidence estimates to be strongly dependent on used models and input soil parameters. A step forward regards the coupling of the different processes. Allison et al. (2016) for instance, stressed that developing an integrated model with coupled behavior of the different subsidence processes is critical for reliable subsidence estimates. Only by considering the behavior of all subsidence processes combined with real observations can the full impact of subsidence be understood.

Optimizing the relation between coupled subsidence processes and measured subsidence can improve subsidence forecasts. A history matching procedure by correlation and/or trial-and-error is often employed (e.g. Caló et al., 2017; Castellazzi et al., 2016; Teatini et al., 2006). For larger areas, or areas where multiple subsidence processes are superimposed, a more formal approach is considered more efficient (e.g. Candela and Koster, 2022; Fokker et al., 2019). A mathematically driven approach such as data assimilation can cover the entire range of uncertainty of all the parameters, to seek the optimal solution.

Data assimilation combines models and observations to obtain the best possible description of the system (Evensen, 2009; Evensen et al., 2022). This approach is customary practice in a wide range of disciplines such as subsurface modelling (Candela et al., 2022; Chang et al., 2010; Evensen et al., 2022; Fokker et al., 2016; Gazolla et al., 2021), weather predictions (Navon, 2009; Thépaut, 2003) and oceanographic simulations (Carton and Giese 2008; Ghil and Malanotte-Rizzoli, 1991), but for interpreting shallow causes of subsidence this method has not yet been applied widely. Peduto et al. (2017; 2020) presented examples of shallow subsidence studies that apply a form of data assimilation to a geotechnical problem. Their studies show the benefit of combining multiple datasets. Li et al. (2017) applied data assimilation with an Ensemble Kalman Filter and showed the strength of data assimilation procedures, although they did not emphasize the subsidence models in their study.

Data assimilation procedures have also been applied in studies on polders in the Netherlands (Fokker et al., 2019; Muntendam-Bos et al., 2009). Fokker et al., 2019 used Ensemble Smoothing with Multiple Data Assimilation (ES-MDA) for ten distinct locations in the South Flevoland polder with a few dozens of timesteps over a period from reclamation until recent, combined with coring for lithological data and phreatic groundwater level measurements. They focused on the agricultural areas of the South Flevoland polder, over a longer timescale with a small number of locations. Therefore, their results are not directly applicable to the subsidence in the urbanized areas of the South Flevoland polder, where the urbanization might have had inhibitory effect on shrinkage and layers might have undergone more severe compaction in the past. Additionally, corings of individual locations were used in Fokker et al., 2019, whilst in this study we introduce an automated procedure including a lithological and groundwater model, making it possible to apply this methodology to larger areas.

We here aimed to quantify the subsidence processes within urbanized areas of the South Flevoland polder in relation to phreatic groundwater level changes and to showcase the added value of combining large observational data sets with numerical models to improve parameter estimations for shallow subsidence processes. We deployed data assimilation on a dataset comprising thousands of locations with hundreds of timesteps derived from satellite observations, high-resolution 3D models of subsurface lithology and groundwater to quantify the contribution of the different shallow subsidence processes. We studied multiple subsidence processes at the same time to understand the full impact of subsidence and to identify the relative contributions of the different processes. Such information is critical for policymakers and spatial planners to design strategies to mitigate subsidence in the South Flevoland polder.

1.2 Study area

The South Flevoland polder is situated in the central Netherlands in the partly reclaimed Lake IJssel (Fig. 1). The Holocene sequence of the polder is underlain by several hundreds of meters thick Pleistocene sediments, consisting of a complex of alternating sandy to clayey marine, fluvial, and (peri-)glacial deposits (Menke et al., 1999; Peeters et al., 2015; TNO, 2022). The uppermost Pleistocene unit consists of a several meters thick aeolian sand bed, which grades from ca. -5 to -12 m below NAP (i.e. the Dutch ordinance datum, approximately corresponding to the mean sea level) in northwestern direction, locally incised by the Eem brook paleo-valley or elevated by dune formation (Fig. 1).

During the Holocene, the South Flevoland Polder became part of the landward margin of a coastal plain. The base of the Holocene sequence consists of a basal peat bed, formed between

6000- and 7000-year BP under influence of inland groundwater level rise in tandem with post-glacial sea-level changes (Koster et al., 2017; Makaske et al., 2003). These peatlands drowned and transformed into an open tidal basin under the influence of continuous sea-level rise (Vos, 2015). The tidal basin deposits consist of alternating sand-clay beds, with local erosion of the underlying basal peat. When around 5500-year BP eustatic sea-level rise decreased, the open tidal basin was closed off by the formation of a beach-barrier, transforming the area into a freshwater swamp with large-scale peat formation (Beets and Van der Spek, 2000; Makaske et al., 2003). In parallel, the area remained connected in the west to the North-Sea by several smaller tidal inlets, making the Eem brook part of a branched network of freshwater tidal channels (Vos, 2015). The peatland itself was characterized by a series of open lakes (Menke et al., 1999). From the north, this lake system was connected to the Waddensea. When the peatlands deteriorated as a combination of natural and anthropogenic causes, the open sea connection in the north expanded southwards, thereby gradually drowning the peatlands and turning the area into a partly enclosed inland sea (Van den Biggelaar et al., 2014). The inland sea was dammed off and became Lake IJssel in 1932, to protect the surrounding areas against flooding. After the damming several parts of the newly formed lake were reclaimed from 1939 onwards. The South Flevoland polder is the final area that was reclaimed.

Almere is a large urban conglomerate in the polder of South Flevoland (Fig. 1), with a population of ca. 200,000. Almere was founded in 1976, approximately eight years after reclamation to account for the first years of subsidence, for which it was predicted to be the highest (up to 70 centimeters in total) (Hoeksma, 2007). Almere has been partly built on top of the paleo-valley of the Eem brook system, which incised several meters into underlying deposits of Pleistocene age. Therefore, the thickness of the Holocene sequence underneath Almere strongly varies, with thicknesses between <1 and 10 meter. The thickest sequence can be found over the course of the former Eem brook system. Generally, basal peat in the Netherlands, like underneath Almere, has undergone substantial compression by the overburden, and consequently has mechanical characteristics that deviate from the younger peat beds (Koster, De Lange et al., 2018). Due to sea-ingressions that drowned the peatlands, the paleo-valley infill on top of the basal peat consists of marine clay with sandy infills overlain by organic clay, gyttja and peat, interfingered with some sand (Menke et al, 1999).

Subsidence was expected after reclamation (De Glopper, 1969), therefore, regular monitoring campaigns were conducted, including regular levelling measurements, corings, and soil sampling (De Glopper, 1984**;** Van Dooremolen et al., 1996). Within 25 years, the a priori expected subsidence for the South Flevoland polder was exceeded, in some places by 0.5 m (Van Dooremolen et al., 1996), resulting in complications for the drainage of the area. Most buildings have a concrete pile foundation in sandy, less compressible layers of Pleistocene age, and consequently do not subside in parallel with the overlying Holocene sequence. On the contrary, public structures, such as (local) roads, squares, sport fields and playgrounds are often lacking a pile foundation and are constructed immediately on top of the Holocene sequence. The consequential differential subsidence between structures with and without a concrete pile foundation inflicts stress on pipeline structures, belowground electrical and network cables, and the connection from buildings to the roads in general, potentially causing damage. Currently, the city of Almere, lying ~4 meters below NAP, must deal with damage to buildings and infrastructure because of the ongoing differential subsidence (Lambert et al., 2016).

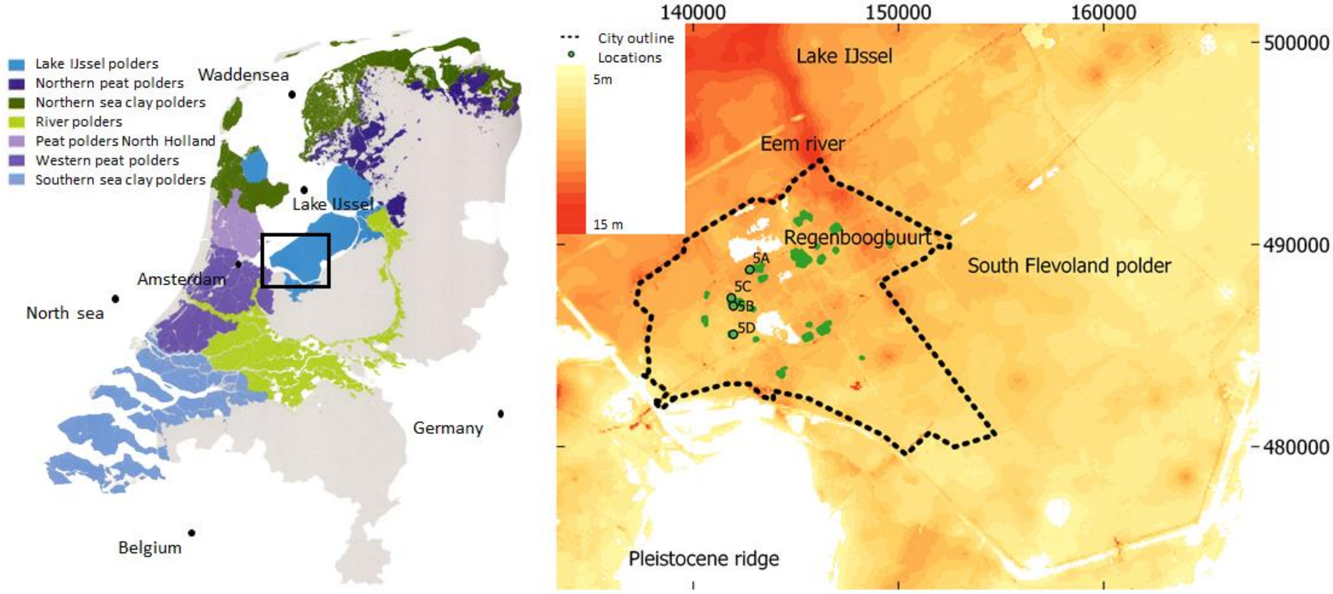

Figure 1 a: Map of the Netherlands showing all the areas that accommodate polders (adjusted from Steenbergen et al., 2009). b: Map of the area of Almere and its surroundings projected on a map showing the thickness of the Holocene sequence (TNO, 2022). The thickness decreases towards the south-east. The incised course of the Eem River, in the northeast of the city Almere is reflected by an increased Holocene thickness. The map is plotted on the Rijksdriehoek coordinate system. The green dots indicate the locations of the data points included in this study. The locations of the graphs of Figure 5a-5d are denoted.

2 Materials and Methods

We used a data assimilation procedure combining the use of InSAR data with 3D lithological and phreatic groundwater level models. Figure 2 depicts the complete workflow, with the different colors indicating the different steps. In green, three classes of input data are displayed: (1) data in the form of previously developed geological and groundwater level models (paragraph 2.1.3 and 2.1.4.), (2) estimates of input parameters necessary for the forward model, based on a literature search (paragraphs 2.2), and (3) satellite data for actual surface movement estimates (paragraph 2.1.1).

We defined three steps of the subsidence estimation algorithm:

1. The preprocessing the InSAR data to filter the appropriate measurements points from the full data set (paragraph 2.1).
2. The forward model in which we calculated subsidence for all locations and timesteps in this study (paragraph 2.2).
3. The data assimilation step, where the subsidence measurements derived from InSAR were combined with the forward model, to optimize the forward model by changing the input parameters (paragraphs 2.3).

Lastly, the output of our analysis is defined into two classes; (1) refined estimated parameters. As a result of the data assimilation approach, refined estimated parameters are the optimized values for the input parameters, and (2) a subsidence prediction. The outcome of the forward model is a subsidence prediction for all the locations and timesteps.

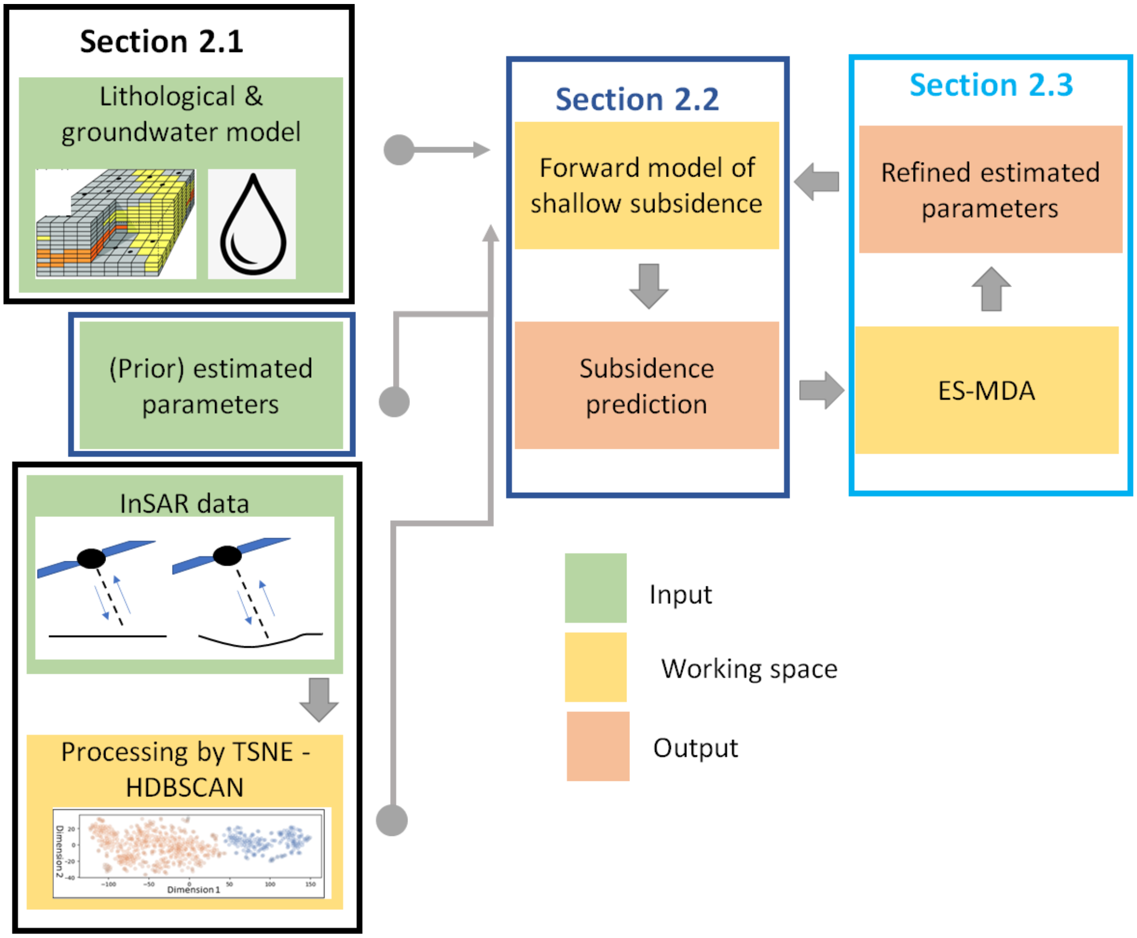

Figure 2: Workflow of the different steps of the methodology divided into: input, working space and output. The steps of the workflow are explained in corresponding sections. The parameters of the physical models that estimate subsidence are optimized towards measured relative subsidence from satellite data, with the use of a groundwater model and a lithological model (GeoTOP). InSAR points measured on top of unfounded objects are separated by a data selection process (Fig. 3). A prior estimate of the parameters part of the forward model is initially made, whereafter the forward model and optimization with data assimilation is repeated multiple times. The image of lithological grid model is adjusted from Van der Meulen et al. (2007).

2.1 Input data

2.1.1 InSAR data

The InSAR data consists of Sentinel-1 images for one ascending and one descending track, ranging over the period March 2015 until June 2020 and November 2015 until June 2020 respectively. The sampling interval of the data points varies temporarily by the availability of the 6- or 12-days repeat pass (Wegmüller et al., 2015). One of the key issues of InSAR data is loss of signal coherence, both in space and time. Spatial decorrelation is caused by changes in the acquisition baseline, resulting in a different phase between two images and causing phase wrapping errors that reduce the coherence. This implies that spatially decorrelated data is less suitable for subsidence research. Temporal decorrelation is caused by atmospheric variability and changes in the physical and geometric properties of the scatter points, e.g. due to seasonal changes in vegetation which result in landcover changes (Ferretti et al, 2007; Hanssen, 2001). As a result, vegetation-rich areas are suboptimal for the analysis of subsidence by satellite imaging (Conroy et al., 2022). Therefore, the focus of this study is on man-made structures, because these scatter points face less decorrelation issues.

The ascending and descending tracks were processed and analyzed separately. This yielded two results of subsidence estimations and associated fits, which were compared for an additional quality check of the workflow. The line-of-sight movement was projected in the vertical direction with the use of the incident angle as part of the processing. We assume no significant horizontal displacements, because of the shallow character of the cause of subsidence.

2.1.2 InSAR processing by TSNE-HDBSCAN

InSAR locations were selected based on two main criteria, forming the first step in the point-selection procedure of Figure 3. We selected PS-InSAR points in the built-up area of Almere without a pile foundation. Buildings in the area typically have a pile foundation reaching depths of ca. –7 to –20 m with respect to NAP, i.e. piles driven in Pleistocene sand beds with load bearing capacity (Spikker, 2010). Consequently, buildings with a pile foundation are less suitable to reflect subsidence processes that happen within the Holocene sequence. We therefore focused on large reflective objects (~>10 reflection points) without pile foundations. These objects range from large parking lots around shopping centers and business parks, to playgrounds, concrete sport fields, and artificial grass turfs.

The next selection criterium was that the structures without foundations had been built at least 10 years before the first InSAR acquisition dates. Therefore, only objects constructed before the year 2005 were considered. This choice was made to reduce the effect of consolidation due to construction of the objects without foundations on the subsidence signal. Because no register exists for the construction date of parking lots, playgrounds and sport fields, the year of construction of the associated buildings was used. The construction year of all buildings in the Netherlands are registered in 'Basisregistratie Adressen en Gebouwen' (BAG) (Kadaster, 2022), which was used to verify the construction year of objects in the selected areas.

Reflection points on top of structures without a pile foundation that meet above stated criteria were isolated from the ones on top of structures with a pile foundation using a statistical visualization method. Firstly, data points were separated with time Distributed Stochastic Neighbor Embedding (t-SNE) (Van der Maaten and Hinton, 2008), subsequently data points were appointed to a cluster using HDBSCAN (Campello et al., 2014). This two-steps approach based on unsupervised machine learning enables isolating time series that measure the same processes. In the case of Almere, no significant subsidence below the level of the pile foundations was expected. Hence, objects with a pile foundation should show negligible subsidence, whilst other nearby objects without a foundation were expected to show subsidence. This would result in differently behaving timeseries for points measured on top of objects with and without a pile foundation. This step formed the second step in the point selection procedure of figure 3

The practice of dimensionality reduction followed by clustering is common for large input data and has been applied to SAR datasets (Van de Kerkhof et al., 2020), and for a wide range of other date types (Fernández Llamas et al., 2019; Harrison et al. 2019; Kahloot and Ekler, 2019). T-SNE is a dimensionality reduction method that can group similarly behaving timeseries of height measurements of the different reflection points (Van der Maaten and Hinton, 2008). For the present study, clustering was conducted with Hierarchical Density-Based Spatial Clustering of Applications with Noise (HDBSCAN). HDBSCAN provides significant clusters, where the clusters can vary in density threshold. The method maximizes the stability of the selected clusters by calculating the optimal solution (Campello et al., 2014).

To ensure that the selected clusters represent the time series of measurements on top of objects without a pile foundation, the clusters were verified by checking the time series of all the clusters and their location in a geographic information system. This is the third procedure of Figure 3.

The last step in Figure 3 entails the optimization of the selected InSAR points for the subsidence optimization procedure. InSAR data points in a single lithological grid cell (see section 2.2. about lithological modelling) were averaged. Reducing the number of points by averaging reduces the computational time, whilst still incorporating the uncertainty for the InSAR data for each grid cell. The variance of this average was added to the chosen standard deviation squared of 0.01 m^2, to ensure that the uncertainty of variance in the subsidence measurements was incorporated. A 0.01 m^2 standard deviation for each epoch aims to capture both the uncertainty in the model and measuring space, as the true standard deviation is unknown. To prevent a disproportionate weight of the first measurement in time, an average of the first ten measurements in time was taken as the first time step in our post-processing timeseries data.

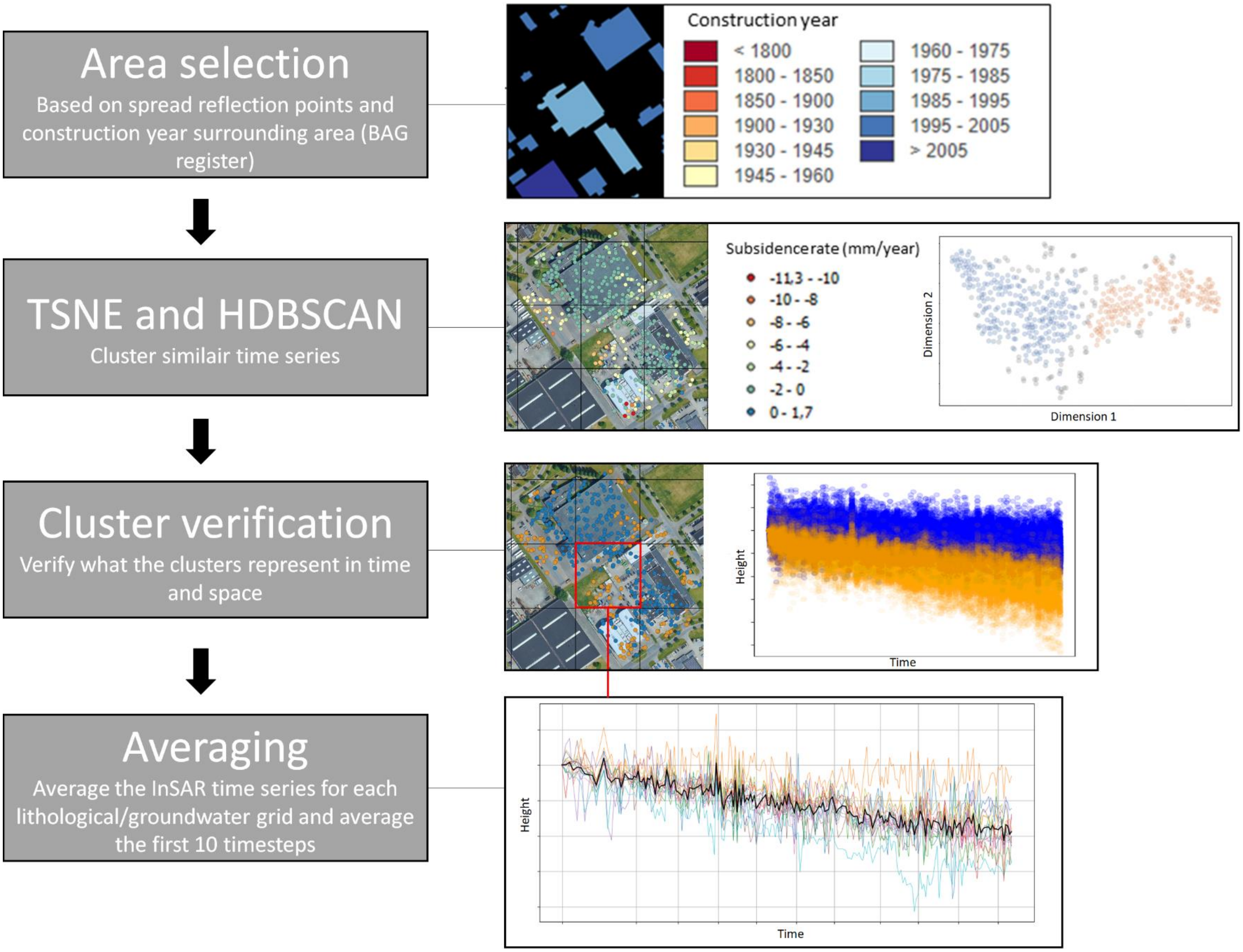

Figure 3: Workflow for selecting InSAR points. Firstly, areas with a significant amount of data points, potentially on top of structure without a pile foundation are selected. With the BAG register (Kadaster, 2022), the construction date of the area is verified. The image shows the construction years of the buildings in the example area (image adjusted from Spaan, 2015).. The remaining areas follow dimensionality reduction by T-SNE, followed by a clustering method HDBSCAN. At the second processing step, the average yearly subsidence rate of the selected InSAR points of the sample area are shown on the left. On the right, the result of the T-SNE dimension reduction is plotted, where the colors refer to the clusters each point is assigned to. The number of dimensions of the initial data set is equal to the number of locations. Thirdly, the clusters are visualized as scatter points for each time step and in a geographic information system, to verify the clusters and select the cluster representing the scatter points on top of unfounded man-made structures. The clusters from the second time step, in their corresponding colors are plotted spatially on the left image and over time on the right. Lastly, for each grid cell corresponding to the lithological and groundwater model, an average of the selected InSAR points within the cell is taken This is depicted in the graph belonging to the last processing step, where the thick black line represents the average of the InSAR timeseries falling into the grid cell. To not give a disproportionate high weight to the first measurement of the InSAR series, an average has been taken of the first 10 timesteps, which forms the first timestep in our post processing time series.

2.1.3 Lithoclass model

A previously released 3D lithoclasses (classes of different grainsize compositions) voxel model for the province of Flevoland that covers the entire study area was used as input for numerical modeling (Fig. 4b) (Gunnink, 2021). The model was initially developed for high-resolution hydraulic resistance modelling for groundwater flows within the Holocene sequence and had been constructed based on 31.000 digitalized borehole logs and 4250 Cone Penetration Tests that had been derived from the freely accessible online data portal of the Geological Survey of the Netherlands (TNO-GSN, 2022). The boreholes are sufficiently distributed throughout the province of Flevoland, whereas the Cone Penetration Test are primarily clustered in urbanized areas and along infrastructural elements.

The 3D model had been created by interpolation via spatial kriging, following a similar procedure as explained in Van der Meulen et al. (2013). The voxel x,y,z dimensions are 100x100x0.5 meter and the model ranges from the surface to the top of geological units of Pleistocene age, thereby encompassing the entire Holocene sequence. The different lithoclasses (sand, sandy clay, clay, peat, and basal peat – the latter being in a more compressed state than peat) are described with their probability of occurrence for each voxel, based on 100 realizations of the interpolation. The highest probability was taken as the truth scenario for this study.

2.1.4 Groundwater model

Changes in groundwater heads form an important explanatory variable for shallow sources of subsidence. Therefore, time series of this data are needed all over the study area. Unfortunately, this was only sparsely available at locations with observation wells. Therefore, a model was developed to estimate the required time series (TNO-GSN, 2022; Zaadnoordijk et al., 2018): monthly phreatic water level values for grid cells of x,y 100x100 meter (Fig. 4a) from the year 2000 until 2020. The applied method was an interpolation in two steps. The first step was an interpolation of the groundwater heads within the time series to obtain for all well locations an observation on the same day (28th) of each month. This yielded interpolated heads including variances. The second step comprised a spatial (kriging) interpolation, applying a sequential Gaussian simulation (Deutsch and Journel, 1998, p.170), which yielded for each month a map of the interpolated heads. Since the observation wells were sparse, their observed heads could not fully describe the spatial variation in the groundwater heads. Therefore, a trend surface was used with a spatial interpolation performed on the residuals (observation minus trend surface). To honor the seasonal fluctuation of the groundwater heads, each month had a separate trend surface. Herewith, one hundred equiprobable interpolations of phreatic groundwater levels for each month were created. We used the average of the 100 realizations as the truth scenario for the phreatic surface model in space and time.

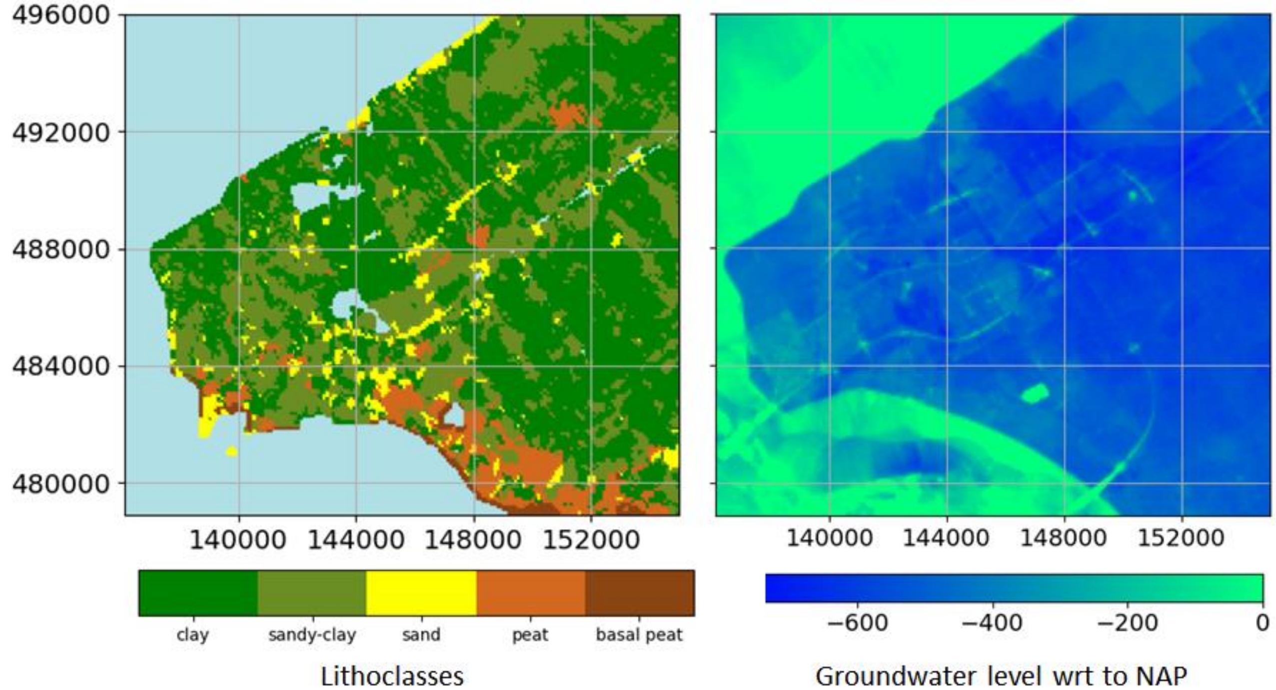

Figure 4: Left: Map of the South Flevoland polder lithologies according to GeoTOP at 5 meters below NAP. Right: Map of phreatic surface level in the South Flevoland polder in January 2015. The scale is in cm with respect to NAP. The polder itself lies ~400 cm below NAP (Dutch ordinance level ~ sea level). The areas that lie at NAP are the lake IJssel area and in the left bottom the Dutch mainland.

2.2 Forward model

The different shallow subsidence processes initiated by human-induced phreatic groundwater level lowering in the South Flevoland polder are described in forward models. These forward models include physical relations that describe the subsidence processes and thereby, with an estimate of the parameters, provide an estimate of the subsidence. The groundwater and lithoclass models are used to describe which lithology is present and to what depth the sediments are saturated. Previous studies identified oxidation of peat, shrinkage of clay, and compression of clay and peat as the main subsidence processes in the area (De Lange et al., 2012; Fokker et al., 2019; Lambert et al, 2016; Van Dooremolen et al., 1996)**.**

Fokker et al. (2019), described a subsidence model with a relation between shrinkage and equivalent age using linear-strain fits and time series of land levelling subsidence observations in the South Flevoland polder from 1967 to 2012. They used an exponential relation of clay shrinkage processes to fit the model to the data. Furthermore, they described that well-established compression functions of consolidation and creep (Den Haan, 1996; Visschendijk and Trompille, 2009) did not fit with the observed subsidence trend. Given the results of the study of Fokker et al. (2019), subsidence by compression was expected to be negligible in comparison to the processes of shrinkage and oxidation for the timing after reclamation and due to the length of our study period. We have therefore not modelled compression as a separate process in this study. Note also here that compression by the overburden weight of building material was assumed to have a negligible effect on the selected InSAR time series, because all the locations included in this study have undergone settlement due to loading by construction for minimal >10 years (cf. CUR, 1992).

2.2.1 Oxidation model

The applied equation for the oxidation model is widely applied to describe peat oxidation in the Netherlands (Fokker et al., 2019; Koster, Stafleu and Stouthamer, 2018; Van den Akker, 2008; Van Hardeveld et al., 2017; Van der Meulen et al., 2007). It provides a relative annual oxidation rate for peat above the phreatic groundwater level. Since only organic matter oxidizes, admixed sediments remain, albeit on average 3 to 4 % of the total volume (Koster, Stafleu and Stouthamer, 2018). Hence, a residual thickness is considered.

Firstly, for a unit above the phreatic groundwater level the part susceptible to oxidation needs to be determined.

$$h_{ox,0} = h_{ox}(t=0) = (1 - R_{ox})h_0 \tag{1}$$

If part of a unit has already been reduced, we have $h_{ox}(t) = h(t) - R_{r,ox}h_0$. The original thickness of the unit is unknown, since collection of the data used in this study started ~50 years after reclamation. Hence, we simply assumed h equals h_0 at t=0. This results in a higher residual height than for completely virgin soil, as the original units are (partly) reduced in thickness already. The oxidation rate can be calculated as follows:

$$\frac{dh}{dt} = \frac{dh_{ox}}{dt} = -V_{ox}\, h_{ox} \tag{2}$$

Over time Δt the thickness reduction of a layer can be written as:

$$\begin{aligned}\Delta h = h_{ox}(t) - h_{ox}(t + \Delta t) &= (1 - e^{-V_{ox}\Delta t}) \cdot h_{ox}(t) \\ &= (1 - e^{-V_{ox}\Delta t}) \cdot (h(t) - R_{ox}h_0)\end{aligned} \tag{3}$$

Incorporating units that are partly aerated, the part susceptible of oxidation is corrected for the wet part of the voxel:

$$\Delta h_{ox} = (1 - e^{-V_{ox}\Delta t})(h(t) - h_{wet} - R_{ox}\,[h_0 - h_{wet}]) \tag{4}$$

In which V_{ox} is the shrinkage rate and R_{ox} the residual height.

2.2.2 Shrinkage model

Time-dependent shrinkage models have not been documented for the Netherlands yet. Typically, shrinkage is expressed as a function of clay mineral content, organic matter, and calcareous admixture (e.g. Barciela Rial, 2019; De Glopper, 1969). To overcome this, Fokker et al. (2019) designed a simple shrinkage relation, inspired by Equation 4, which enabled good matches between the subsidence model and the observed subsidence. This relation assumes that the shrinkage rate is proportional to the volume sensitive to shrinkage. A lithology-dependent residual height was assumed to indicate an asymptotic value to which the shrinkage can lead.

The process of clay swelling has been ignored in this study. Furthermore, seasonal swelling effects of clay by a relative increase in precipitation during autumn and winter were not observed in the InSAR data. Most likely, if present, a swelling capacity is suppressed in the urbanized area by structure overburden. In general, the South Flevoland polder is subjected to net groundwater level lowering; this is reflected in net subsidence, visible as a decreasing trend without a large swelling effect in the InSAR data. Furthermore, previous studies reported that the clay beds in our study area have a relatively high irreversible character regarding shrinkage (Bronswijk et al., 1990; Kim et al., 1993).

The equation for shrinkage (Eq. 5):

$$\Delta h_{sh} = (1 - e^{-V_{sh}\Delta t})(h(t) - h_{wet} - R_{sh}\,[h_0 - h_{wet}]) \quad (5)$$

In which V_{sh} is the shrinkage rate and R_{sh} the residual height.

2.2.3 The prior estimated parameters

The parameters aimed to optimize are the shrinkage and oxidation rate and their respective residual heights (see first column of table 2). The prior estimated values take into account the results of Fokker et al., (2019). The rates were lowered, because a significant amount of time (~50 years) has passed since reclamation (and the start of the study of Fokker et al., 2019), decreasing the void ratio of deposits and increasing the stiffness. Additionally, there is a potential inhibitory effect of shrinkage and oxidation rate in the urbanized area, compared to the agricultural area of Fokker et al. (2019).

The rates of shrinkage and oxidation are closely related to the associated residual heights. Due to the brief period of the surface elevation data (~4-5 years), the exponential relation between relative residual height and reduction (shrinkage or oxidation) rate cannot be established absolutely: an increase in subsidence rates can have the same effect on total subsidence as a reduction in residual height. As a result, the contribution of relative residual height and reduction cannot be distinguished. If one of the two parameters increases, the other should increase as well, to reach the same value for total subsidence. From Equations 1 and 2 we can derive:

$$\frac{dh}{dt} = h_0 v\ (1 - R)e^{-vt} \quad (6)$$

Therefore, if a certain height reduction rate is acting it can be the result of different combinations of v and R, as long as the right-hand side of Eq. (10) gives the same number. The exponential in this equation can be neglected because the compaction (order of mm) is very small with respect to the layer thickness (order of m). Different combinations with the same value of $C = v(1 - R)$, or $R = 1 - \frac{C}{v}$ therefore, give equally good fits, with no time dependence in the expression. This equation was hence fitted to the posterior result of the residual height and rate of oxidation and shrinkage for the different lithologies, utilizing an automated least squares polynomial fit.

2.3 ES-MDA

Parameters have been estimated with Ensemble Smoother with Multiple Data Assimilation (ES-MDA) (Emerick and Reynolds, 2016; Evensen et al., 2022). Earlier accounts for the method to estimate parameters for shallow subsidence can be found in Fokker et al. (2019); the method has also been applied to estimate the parameters for deep subsidence processes (gas production) (e.g. Fokker et al., 2016; Gazolla et al., 2021).

An ensemble refers to a collection of members that are the result of a Monte Carlo analysis. Members are single realizations of the model with specific values for the different parameters. ES-MDA is thus based on a parameter description of the properties that describe the physical processes in the subsurface. A forward model takes the parameters and calculates the subsidence in space and time for each member of the ensemble. The ES-MDA algorithm minimizes the mismatch between the measured data and the estimated subsidence values by changing the parameters of the ensemble members in an organized manner. The multiple data assimilation notion of ES-MDA indicates that the assimilation process is repeated several times. The newly estimated parameters are taken to create a new ensemble of members, with each step increasing the confidence in the parameters.

ES-MDA can be mathematically described as follows. The parameters collected form the vector **m**. The subsidence data is put into a vector **d**, this vector has the length of the number of data points in the area multiplied by the time steps taken at each location. Operation of the forward model is indicated by **G**(**m**); it calculates the subsidence as a function of time for each individual location, based on the parameters in **m**. We want to estimate the vector **m** for which **G**(**m**) has the smallest misfit with the data **d.** To do so, for a single member, as set of prior parameters is created ($\mathbf{m_0}$), with covariance in a matrix $\mathbf{C_m}$. Another covariance matrix is created for the data ($\mathbf{C_d}$). Following Tarantola (2005), the least square solution is acquired by maximizing *J* in the following function:

$$J = \exp\left(-\frac{1}{2}[\boldsymbol{m}-\boldsymbol{m_0}]^T\, \boldsymbol{C}_m^{-1}\, [\boldsymbol{m}-\ \boldsymbol{m_0}] - \frac{1}{2}\, [\boldsymbol{d}-\boldsymbol{G}(\boldsymbol{m})]^T \boldsymbol{C}_d^{-1}[\boldsymbol{d}-\boldsymbol{G}(\boldsymbol{m})]\right) \tag{7}$$

In the ensemble procedure, the values of the members are derived from a prior estimate with a standard deviation of the parameters. An ensemble consists of N_e vectors of **m**; $\mathbf{M} = (\mathbf{m_1}, \mathbf{m_2}, \ldots, \mathbf{m_{Ne}})$. Similarly, an ensemble of data vectors is created by adding random noise to the data following the uncertainty of the data points: $\mathbf{D} = (\mathbf{d_1}, \mathbf{d_2}, \ldots, \mathbf{d_{Ne}})$.

To solve the least square solution for the entire ensemble at once, **GM** replaces **G**(**m**) in equation 5. **GM** is the result of the parameters of all ensemble members operating in the forward model and is the collection of realizations of surface elevations through time. **GM’** is defined as the difference between **GM** and the average of **GM**. **M’** is the difference with the prior mean for each ensemble member: $\mathbf{M'} = \mathbf{M} - \mathbf{m_0}$. The covariance matrix is defined as: $\mathbf{C_m} = \mathbf{M'}\mathbf{M'^T}/(N_e\text{-}1)$. The new set of parameters for the ensemble is given by:

$$\begin{aligned}\widehat{\boldsymbol{M}} &= \boldsymbol{M} + \boldsymbol{M}'[\boldsymbol{GM}']^T(\boldsymbol{GM}'[\boldsymbol{GM}']^T + (N_e-1)\boldsymbol{C}_d)^{-1}(\boldsymbol{D}-\boldsymbol{GM})\\ &= \boldsymbol{M} + \boldsymbol{M}'\left([\boldsymbol{GM}']^T\boldsymbol{C}_d^{-1}\boldsymbol{GM}' + (N_e-1)\mathbf{I}\right)^{-1}[\boldsymbol{GM}']^T\boldsymbol{C}_d^{-1}(\boldsymbol{D}-\boldsymbol{GM})\end{aligned} \tag{8}$$

Depending on the number of parameters versus number of data points one of the two equivalent expressions might be more appropriate to use. $\widehat{\boldsymbol{M}}$ is the estimated ensemble of parameters.

The ensemble smoother technique with a new estimate of parameters can be applied repetitively to obtain a better estimate of parameters in the case of non-linear forward models (Emerick and Reynolds, 2013). The set of parameters is updated with each subsequent step. The data remains the same over the entire procedure. To compensate for the effect of multiple applications with the same data, the covariance of the data is increased with each step of the optimization. This is done with a factor α_i, where the following condition is met: $\sum_{i=1}^{nI}\frac{1}{\alpha_i} = 1$. nI is the number of assimilation steps (Fokker et al., 2019). We used a factor α_i that decreases every step with a factor q to ensure increasing influence of subsequent assimilations.

$$\alpha_i = \alpha_0 \cdot q^i \tag{9}$$

With i being the assimilation step. The above summation condition is met with:

$$\alpha_0 = \frac{1 - q^{nI}}{q^{nI-1} - q^{nI}} \tag{10}$$

To verify the results and determine the actual improvement of the parameter estimation procedure, a test function is applied, considering the covariance of the data and the estimate parameters after the last assimilation step:

$$\chi^2 = \left(\widehat{\boldsymbol{GM}} - \boldsymbol{d}\right)^T (\boldsymbol{C}_d + \boldsymbol{C}_{\widehat{\boldsymbol{GM}}})^{-1} \left(\widehat{\boldsymbol{GM}} - \boldsymbol{d}\right) \tag{11}$$

The outcome of this equation should be around the degree of freedom (N_d), so that $\frac{\chi^2}{Nd} \approx 1$. The parameters for this study are summarized in table 1. The number of grid cells equals the number of lithological and groundwater voxel cells the InSAR data points cover. In the result section, we present key examples of individual voxel cell locations, the values of the optimized parameters and correlations between different parameters.

Table 1: Parameters for the data assimilation procedure of this study.

Number of ensemble members (-)	200
Number of assimilations (-)	4
q (-)	0.666667
Covariance data (m)	0.01
Number of InSAR data points (-)	3747 (descending), 2846 (ascending)
Number of voxel locations (-)	199 (descending), 158 (ascending)
Number of points in time (-)	208 (descending), 212 (ascending)
Number of model parameters	6

3 Results

Our ES-MDA based workflow yielded 357 individual scatter point locations. To provide a representative summary of the results on point location scale, we present 4 key examples below (Fig. 5). Additionally, we present four key indicators for parameter covariance (Fig. 6), values for the estimated parameters (Table 1), and the average contribution to subsidence for clay and peat (Table 2). The estimated parameters consist of the four model parameters for the shrinkage of clay (shrinkage rate and relative residual thickness for clay and sandy clay), and two model parameters for oxidation (oxidation velocity and relative residual thickness of peat).

The four key examples of the results of the simultaneous assimilation are presented in Figure 5. The time series of the prior ensemble is not indicated in Figure 5. Because they have a high variance, they would not fit into the scale of the figure. The red time series in Figure 5 are the 200 modelled surface movement developments for the ensemble of assimilated parameters. The black dots are the InSAR data points, and the grey area represents the uncertainty given to each data point, as described in section 2.1. On the right y-axis in the same plot the phreatic groundwater level variation is plotted. The lithological column and the location of the column with respect to the phreatic groundwater level is indicated on the right of the plot. The time series and the estimated subsidence correspond well, regardless of lithology, except for Figure 5a. The prior and estimated parameters are presented in Table 2.

Table 2 provides the estimates prior and posterior to the data assimilation with their standard deviation. Results are given for the descending and ascending satellite tracks separately. The two tracks provide comparable estimated parameters as a result of the data assimilation. A few of the parameters are plotted against each other in Figure 6. For each assimilation step, the 200 estimates of the parameters are plotted against each other. The figure indicates the ensemble spread in the prior estimates and the operation of the smoother by molding the cloud of parameter values. A clear relationship between different parameters evolves, along the lines of the argument in the previous paragraph: different combinations of the shrinkage and oxidation rate and the associated residual height give identical outcomes, as long as they follow the relationship $R = 1 - \frac{C}{v}$. The final ensembles have been fitted to this relationship, as indicated with the dotted black line. The resulting constant C is given in the figure description.

In summary, Table 3 provides the overview of the average contribution to subsidence in mm for the different lithologies for both the ascending and descending satellite tracks.

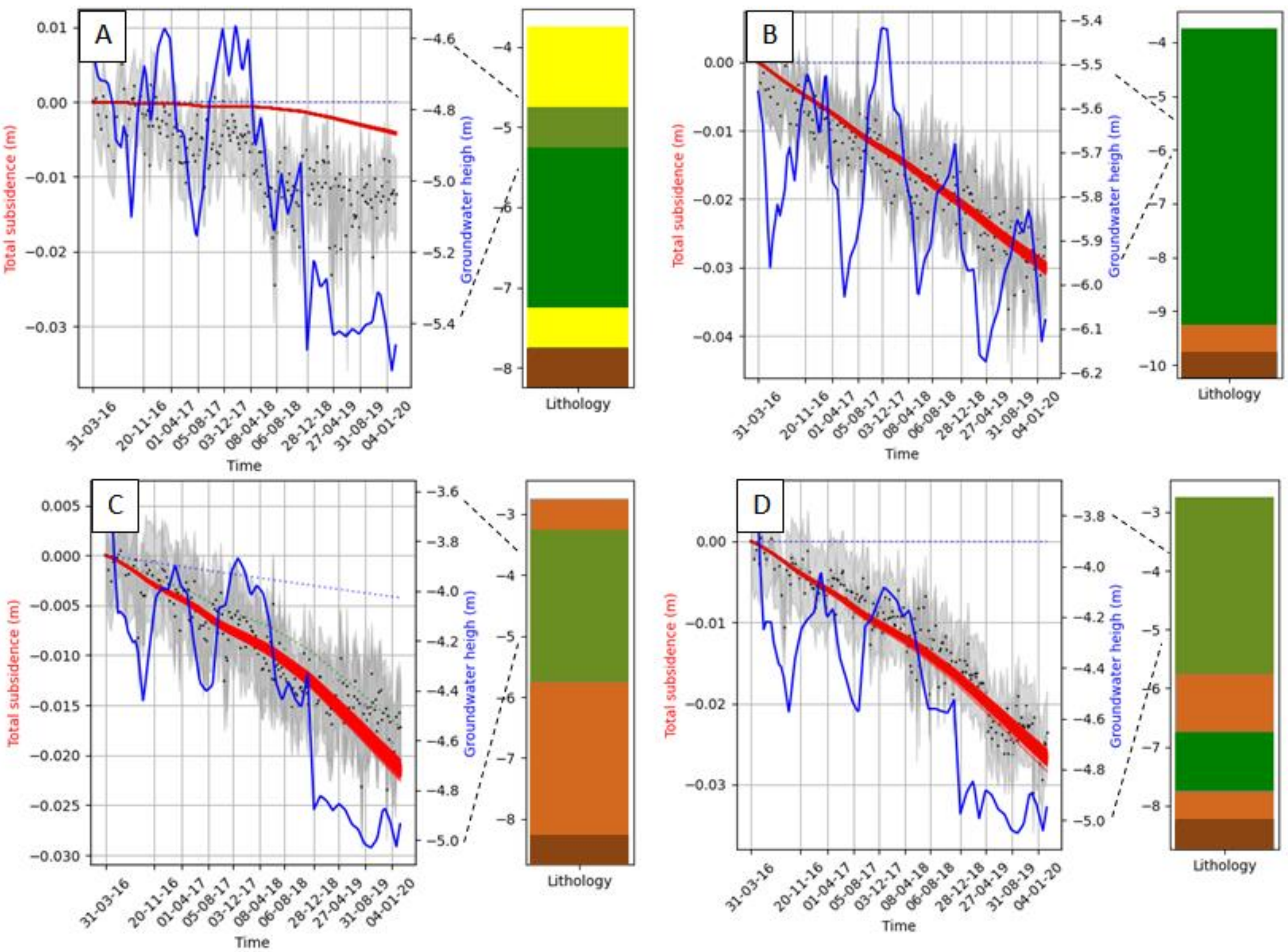

Figure 5: Comparison of surface movements, groundwater levels and lithology for 4 example locations. All figures show the InSAR-derived surface movements (black points) on the scale of the left y-axis. The uncertainty around them is depicted in gray. It was determined as described in section 2.1. The red lines are the 200 ensemble members of the optimized fit after 4 assimilation steps, also on the scale of the left y-axis. The groundwater is the blue line and is with respect to the right y-axis. Next to the graph a stratigraphic column for that specific location is given, according to GeoTOP. The legend of the column is the same as for figure 4. All y-axes are in meters with respect to NAP.

a: descending track, this location shows in increase in subsidence rate once the phreatic surface is below the sandy layers, which happens from spring 2018 onwards. b: ascending track. Shows the fit of subsidence, where the phreatic surface steadily drops under a seasonal trend. There was no significant increase in subsidence rate. d: descending track. Combination of subsidence due to peat and clay. Enhanced subsidence rate from spring/summer 2018 onwards is clear. d: descending track. Seemingly linear subsidence, with a slight acceleration from spring/summer 2018 onwards.

Table 1: The parameters that are optimized in this study for all the locations at the same time. The optimized fit of the ascending and descending track are result of separate data assimilation procedures, but the results are similar. The pre parameters were chosen based on the study of Fokker et al. (2019). The chi-squared error of the ascending track data set has been reduced from 5.2 (prior) to 1.01 (posterior); for the descending track data set it has been reduced from 3.6 (prior) is 3.6 to 0.77 (posterior).

PARAMETER	PRE	POST (ASCENDING)	POST (DESCENDING)
V_{SH} CLAY	0.02 ± 0.005	0.017 ± 0.0012	0.018 ± 0.001
R_H CLAY	0.6 ± 0.05	0.79 ± 0.017	0.78 ± 0.019
V_{SH} SANDY CLAY	0.02 ± 0.005	0.017 ± 0.0015	0.018 ± 0.0016
R_H SANDY CLAY	0.6 ± 0.05	0.77 ± 0.02	0.77 ± 0.025
V_{OX} PEAT	0.01 ± 0.005	0.009 ± 0.003	0.02 ± 0.007
R_H PEAT	0.9 ± 0.05	0.89 ± 0.04	0.88 ± 0.04

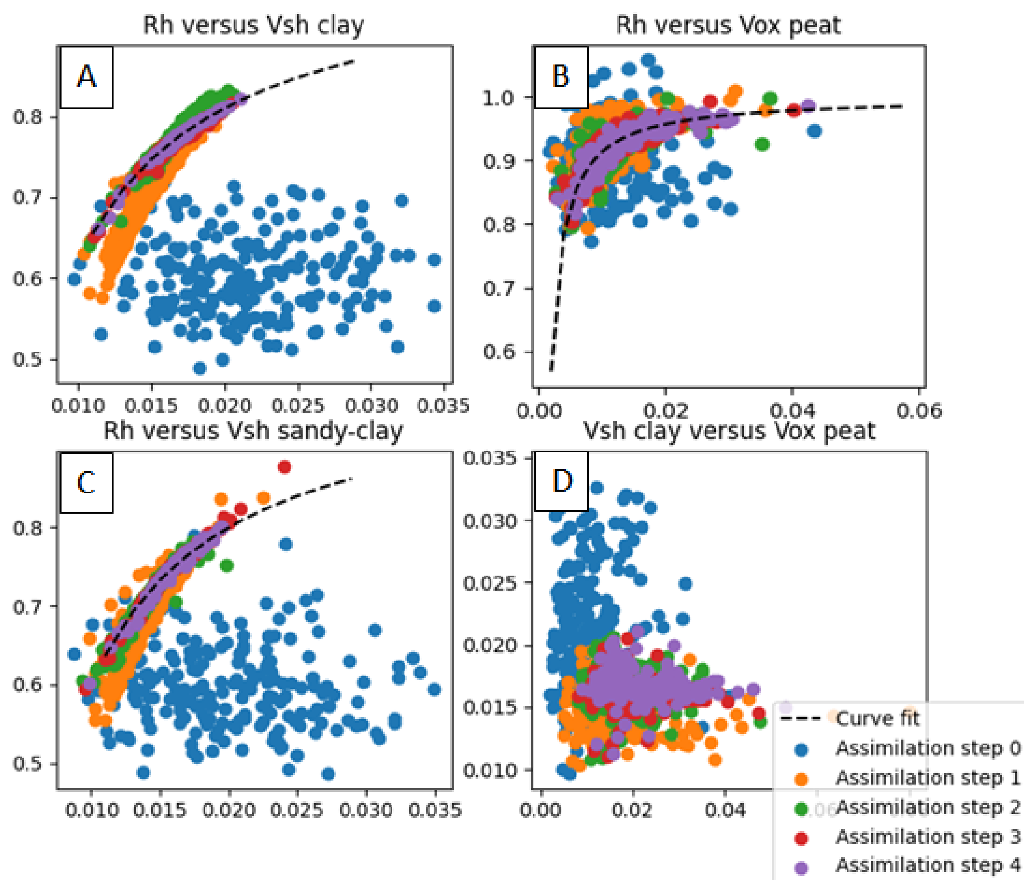

Figure 6: Several of the optimized parameters are plotted against each other for the pre-scenario (assimilation step 0) until the optimized result for the parameters (assimilation step 4) for the ascending satellite track. For all lithoclasses there is a strong correlation between the residual height (Rh) and the rate of subsidence (V). There is no clear correlation between the different lithoclasses, as indicated in figure 6d. For all the lithoclasses the relation of equation 12 is optimized for assimilation step 4, using an automated least squares polynomial fit. The constants for the line in figure a is $\mathrm{C} = \mathrm{v}(1 - \mathrm{R}) = 0.0038\ \mathrm{yr}^{-1}$; for b it is $\mathrm{C} = \mathrm{v}(1 - \mathrm{R}) = 0.0021\ \mathrm{yr}^{-1}$ and for c $\mathrm{C} = \mathrm{v}(1 - \mathrm{R}) = 0.0040\ \mathrm{yr}^{-1}$.

Table 2: The average contribution of clay shrinkage versus peat 21oxidation for all the locations is provided below, in mm/year . Clay incorporates both clay and sandy clay lithoclasses from the GeoTOP model.

	Ascending	Descending
Average contribution clay shrinkage (mm/year)	5.7 ± 2.0	5.8 ± 2.3
Average contribution peat oxidation (mm/year)	0.07 ± 0.17	0.2 ± 0.42

4. Discussion

4.1 Future estimates and spatial pattern of subsidence

This study has demonstrated the possibility to make reliable estimates of subsidence related to phreatic groundwater level changes and lithoclass layering. The study area was the urbanized Almere area of the reclaimed South Flevoland polder. For relatively short timescales, this enables making estimates of future subsidence, providing indications to drivers and hence tools for designing mitigation strategies. To provide information on expected future subsidence rates, four scenarios for the next five years were simulated. The first scenario was to continue the average rate of phreatic groundwater level change towards the future (red in figure 7b), the second scenario was to fix the level at the average height from April 2018 until the end of the research period (blue in Figure 7b) – no more lowering is allowed. The third scenario fixed the phreatic groundwater level at the average height of the phreatic surface for the research period until April 2018 (green in figure 7b): the phreatic level is brought back to higher values. The last scenario, finally, increased the water level even further by adding to the third scenario an extra 20 centimeters. No seasonal trends were added to the scenarios, it is a mere indication of phreatic groundwater level elevation effects on subsidence until 2025.

Figure 7a shows the spatial distribution of the total absolute increase in subsidence since the start of the study related to the different scenarios. The difference between a continuous decrease versus the average level of before March 2018 +0.2 m can be up to 2 centimeters in 5 years. The spatial plotting also makes apparent that most of the subsidence is expected in the southwest and northeast of the city of Almere. The area in the northeast part coincides with the course of the Eem paleovalley (Fig. 1), where the thickest Holocene sequence is present. Naturally, as this study does not provide a continuous image of subsidence, local alternating Holocene sequences are not accounted for. The spatial relation of subsidence with Holocene thickness or groundwater level is not a result straightforward relation, where clay thickness or groundwater level alone determines the subsidence rate. From our results, we see that not one single factor influences the spatial pattern of subsidence. This amplifies our need for subsidence modelling on the urban scale.

Figure 7B provides predictions for one randomly chosen location, to give an idea of what subsidence looks like over time. The phreatic groundwater level is a key factor in the subsidence rates. From our analysis it follows that one meter drop in the phreatic surface will lead to one centimeter of additional subsidence in five years. This relationship can help in decisions concerning groundwater management, the single key factor of human influence on the

730 subsidence rate. The result of this study can be used to support science-based mitigation
731 measures.

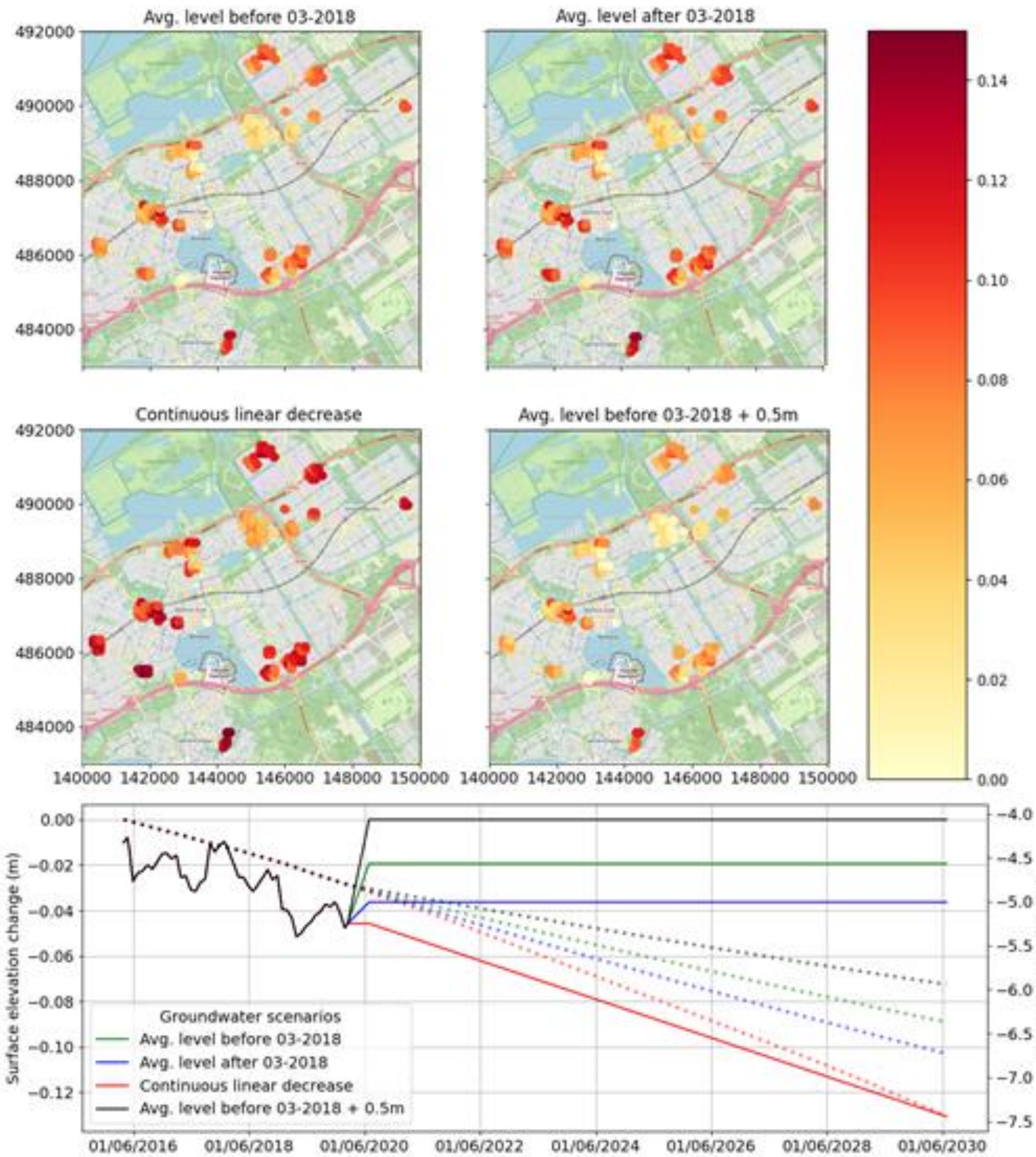

732 Figure 7: Future estimates of subsidence. Figure 7a plots the expected subsidence since the start of the study for
733 different scenarios of groundwater development. The scenarios range from largest to smallest drop in the phreatic
734 surface, and hence largest to smallest expected subsidence. Locations are the same as in Figure 1. 7b shows the
735 subsidence development of one individual location over time, from the start of the study period until 5 years after
736 the end of the study period. The continuous lines show the phreatic surface, on the right y-axis, the dashed line
737 shows the modelled subsidence, with height on the left y-axis In red the continuous decrease of subsidence is

modelled, in blue the average groundwater level from March 2018 until the end of the study period, the green line the average groundwater level of the study period until March 2018 and the black line is the green groundwater level plus 0.2 meters.

4.2 Comparison to other subsidence regions

The Flevoland Polder is unique in the Netherlands in the sense that subsidence is dominated by shrinkage of clay. Clay-shrinkage dominated subsidence is however observed in many other regions in the world. An example is the northern Nile Delta plain in Egypt, where Holocene clay related subsidence is enhanced by climate change that affects the Nile's flow regime (Stanley and Clemente, 2014). There, subsidence ranges from 3.7-8.4 mm/year, which are comparable to the subsidence by clay derived in this study for the South-Flevoland polder.

In and around Venice, Italy there is ongoing subsidence caused by compression of the natural lagoon (0.0-0.5 mm/year). More recently, there is human-induced subsidence (> 2.5 mm/year) due to groundwater withdrawals (Tosi et al., 2013). Parallels with the South Flevoland polder can be found in the reducing natural consolidation over time and significant subsidence induced by groundwater withdrawals. Both areas must deal with irreversible land lowering caused by groundwater withdrawals which are required to prevent the area from flooding.

The same comparison can be made with the Vietnamese Mekong Delta, where groundwater lowering by withdrawals is the main driver of subsidence. The rates of groundwater withdrawal and subsidence are significantly higher in the Mekong Delta. Compaction rates are estimated at an average of 16 mm/year and total subsidence rates, including the subsidence as a result of groundwater withdrawal, can locally be up to 40 mm/year (Erban et al., 2014).

Despite the differences between these areas in rates of subsidence and groundwater withdrawal, the common thread is that all areas are affected by groundwater lowering, either by climate change or anthropogenic causes. Understanding the importance of groundwater level changes to subsidence is therefore of major importance for all these coastal regions across the world. The method presented in this study, and the results in relation to clay behavior of the reclaimed land and the response to groundwater lowering can be of help to tackle this problem.

4.3 Subsidence by drought

In the results, a slight acceleration of subsidence around summer 2018 is visible. This acceleration is related to relative deep lowering of the phreatic groundwater level. At some locations, this acceleration is more profound than in others, as this is influenced by litholoclass and fluctuations of the phreatic levels as well. As shown in Figure 5, this relative low elevation of the phreatic groundwater level influences the processes responsible for subsidence. Namely, due to a lowered groundwater level, deep peat layers are temporarily aerated, resulting in oxidation and volumetric loss. Furthermore, a deeply lowered groundwater level can therefore instigate subsidence at locations that were previously not subsiding.

These temporary deeply lowered phreatic groundwater levels are the results of climate change related drought events, such as the summers of 2018 and 2019 (Hari et al., 2020). Observed accelerated subsidence due to drought is new in the context of the Netherlands. Studies in other (Northwestern) European countries have recently linked drought to increased shrinkage in clay and associated damage to the built environment (e.g. Charpentier et al., 2021; Gruslin et al., 2022). With global warming resulting in more frequent droughts, establishing these relationships becomes increasingly more important.

The results for the effects of drought in this study, however, must be viewed with care. As the number of groundwater datapoints decreases with time, the uncertainty increases. Our results are indicators of drought having an effect, but more extensive and consistent measuring of the phreatic surface is essential to assess groundwater related subsidence. Especially the effect of drought on the phreatic surface height is an important link for future scenarios of subsidence and mitigation strategies.

4.4 Implications

Current governmental attention in the Netherlands for shallow subsidence is predominantly focusing on peat oxidation (Van Nieuwenhuizen Wijbenga, 2019). Therefore, the current study fills a gap in the Netherlands knowledge base. Quantifying the process of clay-driven subsidence is important for optimal decision making regarding shallow subsidence in Almere. Additionally, showing that drought enhances subsidence rates is important for focusing future measures to mitigate subsidence, and connects the problem to climate change. Furthermore, phreatic surface lowering exposing deeper peat beds also increases carbon dioxide emissions by peat oxidation (e.g. Koster et al., 2020).

This study would not have been possible without a structure of nation-wide freely available data on the construction of buildings, relative elevation measurements, geology, and groundwater. Still, more data will help to corroborate our findings. Investments in a network to monitor phreatic groundwater level changes and shallow extensometers able to measure volumetric loss within the Holocene sequence is critical herein (cf. Van Asselen et al., 2020). For improved processing of geodetic data, a network of corner reflectors is required to measure surface movement of the ground level (e.g. Yu et al., 2013). Such investments should be conducted in close collaboration with policy makers and spatial planners.

4.5 A comparison of parameters with previous studies

The South Flevoland polder is unique in the Netherlands with respect to the progressively increasing number of clay and peat beds that encounter contact with atmosphere for the first time since their formation. The estimated subsidence rates are therefore not directly comparable to other polder areas in the Netherlands that have been reclaimed centuries ago.

Earlier studies on subsidence in the South Flevoland polder determined the rates of subsidence due to shrinkage after reclamation estimated based on a few measurements of non-urbanized locations across the South Flevoland polder (De Lange et al., 2012; De Lange, 2015; Fokker et al., 2019). The estimated subsidence in those regions was larger than what we have observed here in the urbanized areas. A reasonable explanation would be that construction has an inhibitory effect on the shrinkage of clay (and when applicable oxidation of organic material) (De Lange, 2015). This study focuses on an urbanized area to estimate the contribution of the different background subsidence processes in urbanized settings.

The residual height estimated by Fokker et al., 2019 lies between 0.50 and 0.67 for clay. However, as mentioned before, the start of modelling subsidence is ~50 years after reclamation in our study, whereas Fokker et al., 2019 start modelling from reclamation onwards, hence the layers still have their original thickness. The values found in this study are higher; ~0.78. Due to the length of the modelling period, only a relation between residual height and reduction rate could be established (Fig. 6). A higher residual height can be explained when layers already have partly undergone shrinkage before the start of the observations. Indeed, in our study, the reference is not at the start of exposure to air but a long time later in the compaction history.

A good match between the estimated parameters and the InSAR time series was found for our spatiotemporal model of subsidence in the city of Almere, quantified with the calculated chi-square error, whilst incorporating groundwater levels, lithology, and the physical models. In line with literature, the shrinkage rates of clay are larger than the oxidation rates of peat (Fokker et al, 2019; Schothorst, 1982).

The same value for uncertainty is currently attributed to each InSAR-derived data point in space and time. There was no covariance matrix available for the dataset. Accurate covariance matrices could increase our ability to fit parameters and models to the data, by reducing the weight given to less reliable data points and incorporating interdependencies.

4.6 Correlations between parameters

We found correlations between the residual height and reduction rate parameters for the same soil types. This correlation could have been expected from the form of their presence in the forward model. The relationship, as shown in Figure 6, helps in future subsidence estimates. By parameterizing the average behavior of the three lithological types, prediction on future behavior with respect to phreatic groundwater changes can be made even when the individual values of the parameters are rather uncertain.

There is no correlation between the shrinkage rate of clay and the oxidation rate of peat (Fig. 6), because lithoclasses act independently. Clay and sandy clay show similar behavior (Figure 6 and Table 2). In the South Flevoland polder, sandy clay is the product of tidal dynamics, and consists of mm-thick alternating clay and sand beds. The comparable behavior between these thin-bedded sandy-clay and clay deposits indicates the dominance of clay shrinkage within the sandy-clay cells. Apparently, the presence of sand is only minimally preventing these deposits from volumetric loss by shrinkage.

Figure 5a shows a scenario in which the average phreatic groundwater level is located within the uppermost sand bed. Here, the model underestimated observed subsidence. We think the mismatch is related to short drought events not captured by our monthly updated groundwater model. Phreatic groundwater levels that are temporally lowered, result in shrinkage of clay directly underneath the upper sand bed, resulting in enhanced subsidence. This explanation is corroborated by the increase in subsidence rate in Figure 5a that coincides with the phreatic surface drop into the clay layer.

5 Conclusions

We have presented a novel data processing and data assimilation workflow with an unprecedented dataset to identify processes resulting in anthropogenically-induced subsidence around the city of Almere in the reclaimed South Flevoland polder in the Netherlands. The workflow integrates lithoclass, phreatic groundwater level changes, and InSAR data, with information on construction dates of structures, and a suite of physical models. The assimilation exercise has enabled us to quantify the drivers of subsidence.

Our results have revealed that shrinkage of shallow clay beds induced by artificial lowering of phreatic groundwater levels is the dominant subsidence process in the South Flevoland polder, with rates up to 6 mm/yr. In line with previous research in the South Flevoland polder, the subsidence rates due to clay shrinkage are significantly higher than those due to peat oxidation, which are up to 0.2 mm/yr. The rates depend critically on the development of phreatic water levels – drought has therefore been identified in this study as an important catalyzer of subsidence. At longer timescales we estimated that one meter drop in groundwater level results in 10 millimeter of subsidence in the urbanized area of Almere.

Groundwater governance is the single human activity influencing land subsidence in Almere. Our study highlights the necessity of high-quality data in order to make trustworthy analyses of subsidence processes and support such governance. Data is obtained by measuring campaigns and continuous monitoring. This includes lithology, groundwater development and surface level changes. Robust analyses of subsidence processes and quality predictions are possible through the application of an approach that integrates all available data with knowledge on physical processes in a dedicated data assimilation procedure.

Acknowledgments

We are grateful to Joana Esteves-Martins for providing aid with the initial InSAR dataset for this study. The research presented in this paper is part of the project Living on soft soils: subsidence and society (grantnr.: NWA.1160.18.259). This project is funded through the Dutch Research Council (NWO-NWA-ORC), Utrecht University, Wageningen University, Delft University of Technology, Ministry of Infrastructure & Water Management, Ministry of the Interior & Kingdom Relations, Deltares, Wageningen Environmental Research, TNO-Geological Survey of The Netherlands, STOWA, Water Authority: Hoogheemraadschap de Stichtse Rijnlanden, Water Authority: Drents Overijsselse Delta, Province of Utrecht, Province of Zuid-Holland, Municipality of Gouda, Platform Soft Soil, Sweco, Tauw BV, NAM.

Open Research

Data from the geological survey of the Netherlands (TNO-GSN, 2022) is used to construct the lithological and groundwater model. Kadaster (2022) has been used to verify the age of the buildings. From Rijkswaterstaat (2022) InSAR data products were retrieved. Figures were made with Matplotlib v.3.4.3 (Caswell et al., 2022) available under the matplotlib license at https://matplotlib.org and QGIS v3.24 (QGIS Development team, 2022).

References

Allison, M., Yuill, B., Törnqvist, T., Amelung, F., Dixon, T.H., Erkens, G., Stuurman, R., Jones, C., Milne, G., Steckler, M., Syvitski, J. & Teatini, P. (2016) Global risks and research priorities for coastal subsidence. *Eos* 97, 22-27. https://doi.org/10.1029/2016EO055013.

Barbour, E.J., Adnan, M.S.G., Borgomeo, E., Paprocki, K., Shah Alam Khan, M., Salehin, M. & Hall, J. W. (2022) The unequal distribution of water risks and adaptation benefits in coastal Bangladesh *Nature Sustainability* 5, 295-302, https://doi.org/10.1038/s41893-021-00846-9

Barciela Rial, M. (2019). Consolidation and drying of slurries: A building with nature study for the Marker Wadden. (Doctoral dissertation) Delft: TU Delft https://doi.org/10.4233/uuid:ae11c3e7-86f2-4c6a-8d53-ee8781d56a72

Barciela-Rial, M., van Paassen, L. A., Griffioen, J., van Kessel, T. & Winterwerp, J. C. (2020). The effect of solid-phase composition on the drying behavior of Markermeer sediment. *Vadose Zone Journal*, 19(1), doi:10.1002/vzj2.20028

Beets, D. & Van der Spek, A. (2000). The Holocene evolution of the barrier and the back-barrier basins of Belgium and the Netherlands as a function of late Weichselian morphology, relative sea-level rise and sediment supply. Netherlands Journal of Geosciences - Geologie En Mijnbouw, 79(1), 3-16. doi:10.1017/S0016774600021533

Bronswijk, J. J. B. & Evers-Vermeer, J. J. (1990). Shrinkage of Dutch clay soil aggregates. *Netherlands Journal of Agricultural Science*, 38(2), 175-194.

Burnol, A., Foumelis, M., Gourdier, S., Deparis, J. & Raucoules, D. (2021) Monitoring of expansive clays over drought-rewetting cycles using satellite remote sensing. *Atmosphere* 12 (10), 1262. https://doi.org/ 10.3390/atmos12101262

Caló, F., Notti, D., Galve, J.P, Abdikan, S., Görüm, T., Pepe, A. & Balik Şanli, F. (2017) DInSAR-based detection of land subsidence and correlation with groundwater depletion in Konya Plain, Turkey. *Remote Sensing Volume* 9 (83). https://doi.org/10.3390/rs9010083

Campello, R.J.G.B., Moulavi, D. & Sander, J. (2013) Density-based clustering based on hierarchical density estimates. *Conference: Pacific-Asia Conference on Knowledge Discovery and Data Mining.* https://doi.org/10.1007/978-3-642-37456-2_14

Candela, T., Chitu, C.G., Peters, E., Pluymaekers, M., Hegen, D., Koster, K. & Peter, A.F. (2022) Subsidence induced by gas extraction: A data assimilation framework to constrain the driving rock compaction process at depth. *Frontiers in Earth Science.* 10. https://doi.org/10.3389/feart.2022.713273

Candela, T. & Koster, K. (2022) The many faces of anthropogenic subsidence. *Science*. 376(6600):1381-1382. https://doi.org/10.1126/science.abn3676.

Chang, H., Chen, Y. & Zhang, D. (2010) Data assimilation of coupled fluid flow and geomechanics using the ensemble Kalman Filter. *SPE Journal*. 15 (2010): 382–394. https://doi.org/10.2118/118963-PA.

Carton, J. A. & Giese, B. S. (2008). A reanalysis of ocean climate using simple ocean data assimilation (SODA), *Monthly Weather Review*, 136(8), 2999-3017. doi:10.1175/2007MWR1978.1.

Castellazzi, P., Martel, R., Galloway, D., Longuevergne, L. & Rivera, A. (2016). Assessing groundwater depletion and dynamics using GRACE and InSAR: Potential and Limitations. *Groundwater.* 54. https://doi.org/10.1111/gwat.12453.

Chaussard, E., Amelung, F., Abidin, H. & Hong, S. (2013) Sininking cities in Indonesia: ALOS PALSAR detects rapid subsidence due to groundwater and gas extraction. *Remote Sensing of Environment.* Volume 218, pp: 150-161. https://doi.org/10.1016/j.rse.2012.10.015

Charpentier, A., James, M.R. & Hani, A. (2021) Predicting drought and subsidence risks in France, *Natural Hazards and Earth System Science Discussions* doi:10.5194/nhess-2021-214

Conroy, P., Van Diepen, S. A. N., Van Asselen, S., Erkens, G., Van Leijen, F. J. & Hanssen, R. F. (2022). Probabilistic Estimation of InSAR displacement phase guided by contextual information and artificial intelligence. *IEEE Transactions on Geoscience and Remote Sensing*, 1-11. https://doi.org/10.1109/TGRS.2022.3203872

CUR (1992). Construeren met grond (In Dutch). CUR Rapport 162, pp. 411

Declercq, P., Gérard, P., Pirard, E., Walstra, J. & Devleeschouwer, X. (2021) Long-term subsidence monitoring of the alluvial plain of the Scheldt river in Antwerp (Belgium) Using Radar Interferometry. *Remote Sensing.* 12, 1160, https://doi.org/10.3390/rs13061160

Deutsch, C. and Journel, A.G. (1998) GSLIB Geostatistical software library and user guide, Second Edition. New York: Oxford University Press.

Dinar, A., Esteban, E., Calvo, E., Herrera, G., Teatini, P., Tomás, R., et al. (2021) We lose ground: Global assessment of land subsidence impact extent. *Science of The Total Environment.* 768, doi:10.1016/j.scitotenv.2021.147415

De Lange, G., Gunnink, J., Houthuessen, Y. & Muntjewerff, R. (2012), Bodemdalingskaart Flevoland. *Grontmij*; GM-0042778.

De Lange, G. (2015), Analyse bodemdaling en zetting Almere. *Deltares Rapport*; 1210761-000.

De Glopper, R.J. (1969) Shrinkage of subaqueuous sediments of Lake IJssel (the Netherlands) after reclamation. *Proceedings First International Symposium On Land Subsidence*, IAH, Tokyo, 192-201

De Glopper, R.J. (1973) Subsidence after drainge of the deposits in the former Zuyder Zee and in the brackish and marine forelands in The Netherlands. *Van Zee tot Land* 50, pp. 205.

De Glopper, R.J. (1984) Subsidence in the recently reclaimed IJsselmeerpolder “Flevoland”. *Proc. Third International Symposium On Land Subsidence*, IAHS, Venice, 487-496

De Glopper, R.J. & Ritzema, H.P. (1994) Land Subsidence. *Drainage Principles and Applications.* vol. 16 (2). ILRI, pp. 41

Den Haan, E. (January 1996). A compression model for non-brittle soft clays and peat. *Géotechnique*, 46(1), 1– 16. https://doi.org/10.1680/geot.1996.46.1.1

Emerick, A. & Reynolds, A.C. (2013), Ensemble smoother with multiple data assimilation, *Computational Geoscience.*, 55, 3-15, doi:10.1016/j.cageo2012.03.011.

Erban, L.E., Gorelick, S.M. & Zebker, H.A. (2014) Groundwater extraction, land subsidence and sea-level rise in the Mekong Delta, Vietnam. *Environmental Research Letters.* 9 https://doi.org/10.1088/1748-9326/9/8/084010

Eslami, S., Hoekstra, P., Nguyen Trung, N., Ahmed Kantoush, S., Van Binh, D., Duc Dung, D., et al. (2019). Tidal amplification and salt intrusion in the Mekong Delta driven by anthropogenic sediment starvation. *Scientific Reports*, 9(1). https://doi.org/10.1038/s41598-019-55018-9

Evensen, G. (2009). *Data assimilation, The Ensemble Kalman Filter* (2nd ed.). Berlin: Springer.

Evensen, G., Vossepoel, F.C. & Van Leeuwen, P.J. (2022) *Data Assimilation Fundementals, A Unified Formulation of the State and Parameter Estimation Problem.* Berlin: Springer. https://doi.org/10.1007/978-3-030-96709-3_1

Fernández Llamas, A., Martínez, D., Hernández, P., Cristóbal, S., Schwaiger, F., Nuñez, J. & Ruiz, J. (2019). Flight Data Monitoring (FDM) Unknown Hazards detection during Approach Phase using Clustering Techniques and AutoEncoders. *Conference paper SESAR* ISSN 0770-1268

Ferretti, A., Monti-Guarnieri, A., Prati, C. & Rocca, F. (2007), InSAR Principles: Guidelines for SAR Interferometry Processing and Interpretation, *ESA Publications*, ESTEC

Fokker, P.A., Wassing, B., Van Leijen, F.J., Hanssen, R.F. & Nieuwland, D. (2016), Application of an ensemble smoother with multiple data assimilation of the Bergermeer gas field, using PS-InSAR. *Geomechanics for Energy and the Environment*, 5, 183-187.

Fokker, P.A., Gunnink, J., Koster, K. & de Lange, G. (2019), Disentangling and Parameterizing Shallow Sources of Subsidence: Application to a Reclaimed Coastal Area, Flevoland, The Netherlands. *Journal of Geophysical Research: Earth Surface*, https://doi.org/10.1029/2018jf004975.

Gazzola, L., Ferronato, M., Frigo, M., Carlo, J., Pietro, T., Zoccarato, C., et al. (2021) A novel methodological approach for land subsidence prediction through data assimilation techniques. *Computational Geoscience. 25*, 1731–1750. https://doi.org/10.1007/s10596-021-10062-1

Ghil, M. & Malanotte-Rizzoli, P. (1991) Data Assimilation in Meteorology and Oceanography. *Advances in Geophysics*. 33, pp: 141-266. https://doi.org/10.1016/S0065-2687(08)60442-2.

Guo, H. & Jiao, J.J. (2007) Impact of Coastal Land Reclamation on Ground Water Level and the Sea Water Interface. *Groundwater.* 45, 3, pp: 362-367. https://doi.org/10.1111/j.1745-6584.2006.00290.x

Hanssen, R. F. (2001). *Radar interferometry: data interpretation and error analysis* (Vol. 2). Springer Science & Business Media.

Hari, V., Rakovec, O. , Markonis, Y. Hanel, M. & Kumar, R. (2020) Increased future occurrences of the exceptional 2018-2019 Central European drought under global warming. *Scientific reports.* 10, 12207. https://doi.org/10.1038/s41598-020-68872-9

Harrison, R., Hol, E.A. & De Graef, M. (2019) On the use of 2D moment invariants in the classification of additive manufacturing powder feedstock. *Material Characterization.* 149, 255-263. https://doi.org/10.1016/j.matchar.2019.01.019

Hoeksema, R. J. (2007). Three stages in the history of land reclamation in the Netherlands. *Irrigation and Drainage*, 56(S1), S113–S126. https://doi.org/10.1002/ird.340

Hoogland, F., Roelandse, A. S., de La Loma González, B., Waterloo, M. J., Mooij, P. W., Verhagen, S. A. & Velstra, J. (2020) Investigating the effectiveness of drain infiltration to minimize peat oxidation in agricultural fields in Flevoland, the Netherlands. *Proceedings of the International Association of Hydrological Sciences.* 382, 747–753, https://doi.org/10.5194/piahs-382-747-2020

Hoogland, T., Van Den Akker, J.J.H. & Brus, D.J. (2012) Modelling the subsidence of peat soils in the Dutch coastal area. *Geoderma* 171-172, 92-97, https://doi.org/10.1016/j.geoderma.2011.02.013

Jones, C.E., An, K., Blom, R.G., Kent, J.D., Ivins, E.R. & Bekaert, D. (2016) Anthropogenic and geologic influences on subsidence in the vicinity of New Orleans, Louisiana. *Journal of Geophysical Research Solid Earth* Volume 121, 5, pp: 3867-3887. https://doi.org/10.1002/2015JB012636

Kadaster (2022) Basisregistratie Adressen en Gebouwen – BAG, URL: www.kadaster.nl/zakelijk/registraties/basisregistraties/bag

Kahloot, K. & Ekler, P. (2019) Improving t-SNE clustering and visualization. *Computer science*, Cropus ID: 229360049

Kim, D. J., Feyen, J., Vereecken, H., Boels, D., & Bronswijk, J. J. B. (1993). Quantification of physical ripening in an unripe marine clay soil. *Geoderma*, 58(1-2), 67–77. https://doi.org/10.1016/0016-7061(93)90085-y

Kooi, H. (2000) Land subsidence due to compaction in the coastal area of the Netherlands: the role of lateral fluid flow and constraints from well-log data. *Global and Planetery Change.* 27, 1-4, pp: 207-222. https://doi.org/10.1016/S0921-8181(01)00067-4

Koster, K., Stafleu, J. & Cohen, K. (2016) Generic 3D interpolation of Holocene base-level rise and provision of accommodation space, developed for the Netherlands coastal plain and infilled palaeovalleys. *Basin Research.* Volume 29. https://doi.org/10.1111/bre.12202

Koster, K., Stafleu, J. & Stouthamer, E. (2018), Differential subsidence in the urbanized coastal-deltaic plain of the Netherlands. *Netherlands Journal of Geosciences*, 1-13. https://doi.org/10.1017/njg2018.11

Koster, K., Stafleu, J., Cohen, K.M., Stouthamer, E., Busschers, F.S. & Middelkoop, H. (2018) Three-dimensional distribution of organic matter in coastal-deltaic peat: Implications for subsidence and carbon dioxide emissions by human-induced peat oxidation. *Anthropocene.* 22, pp: 1-9, https://doi.org/10.1016/j.ancene.2018.03.001

Koster, K., De Lange, G., Harting, R., De Heer, E. & Middelkoop, H. (2018) Characterizing void ratio and compressibility of Holocene peat with CPT for assessing coastal–deltaic subsidence. *Quarterly Journal of Engineering Geology and Hydrogeology*, 51(2), 210–218. https://doi.org/qjegh2017-120

Koster, K., Frumau, A., Stafleu, J., Dijkstra, J., Hensen, A., Velzeboer, I., et al. (2020) Greenhouse Peat: a model linking CO_2 emissions from subsiding peatlands to changing groundwater levels, *Proceedings of* *the International Association of Hydrological Sciences*. 382, 609-614, https://doi.org/10.5194/piahs-382-609-2020

Lambert, J.W.M., Nieal, L., Stoorvogel-van der Horst, S., Verheijen, E. & Woning, M. (2016) Bodemdaling Almere: consequenties voor gemeentelijke infrastructuur. *Rapport Circulair Cities, TO2.*

Li, D., Li, B., Zhang, Y., Fan, C., Xu, H. and Hou, X. (2022) Spatial and temporal characteristics analysis for land subsidence in Shanghai coastal reclamation area using PSInSAR method. Frontiers in Marine Science. 9:1000523. https://doi.org/10.3389/fmars.2022.1000523

Maas, M. (2021) Ook Almere worstelt met bodemdaling. *Binnenlands bestuur* nr. 12

Makaske, B., Van Smeerdijk, D., Peeters, H., Mulder, J., & Spek, T. (2003). Relative water-level rise in the Flevo lagoon (The Netherlands), 5300-2000 cal. yr BC: An evaluation of new and existing basal peat time-depth data. *Netherlands Journal of Geosciences*. 82(2), 115-131. https://doi.org/10.1017/S0016774600020680

Martín-Antón, M., Negro, V., del Campo, J.M., López-Gutiérrez, J.S. & Esteban M.D., 2016. Review of coastal Land Reclamation situation in the World. *Journal of Coastal Research, Special Issue*, No. 75, pp. 667–671. https://doi.org/10.2112/SI75-133.1

Mayoral, J. M., Castañon, E., & Albarran, J. (2017). Regional subsidence effects on seismic soil-structure interaction in soft clay. *Soil Dynamics and Earthquake Engineering*, 103, 123–140. https://doi.org/10.1016/j.soildyn.2017.09.014

Menke, U., van Laar, E. & Lenselink, G. (1999), De Geologie en Bodem van Zuidelijk Flevoland. *Flevobericht* 415, ISBN: 90-3691-2202

Muntendam-Bos, A. G., Kleuskens, M. H. P., Bakr, M., de Lange, G., & Fokker, P. A. (2009). Unraveling shallow causes of subsidence. *Geophysical Research Letters*, 36(10). https://doi.org/10.1029/2009gl037190

Navon, I.M. (2009). Data Assimilation for Numerical Weather Prediction: A Review. In: Park, S.K., Xu, L. (eds) *Data Assimilation for Atmospheric, Oceanic and Hydrologic Applications.* Berlin: Springer. https://doi.org/10.1007/978-3-540-71056-1_2

Neumann, B., Vafeidis, A.T., Zimmermann, J. & Nicholls, R.J. (2015) Future coastal population growth and exposure to sea-level rise and coastal flooding – a global assessment. *PLoS One*, 10 (3), Article e0118571

Nieuwenhuis, H.S. & Schokking, F. (1997) Land subsidence in drained peat areas of the Province of Friesland, The Netherlands. *Quarterly Journal of Engineering Geology and Hydrology*. 30, 37-48, https://doi.org/10.1144/GSL.QJEGH.1997.030.P1.04

Nusantara, R. W., Hazriani, R., & Suryadi, U. E. (2018). Water-table Depth and Peat Subsidence Due to Land-use Change of Peatlands. *IOP Conference Series: Earth and Environmental Science*, 145, 012090. https://doi.org/10.1088/1755-1315/145/1/012090

Peduto, D., Huber, M., Speranza, G., van Ruijven, J., & Cascini, L. (2017). DInSAR data assimilation for settlement prediction: case study of a railway embankment in the Netherlands. *Canadian Geotechnical Journal*, 54(4), 502-517.

Peduto, D., Giangreco, C., & Venmans, A. A. (2020). Differential settlements affecting transition zones between bridges and road embankments on soft soils: Numerical analysis of maintenance scenarios by multi-source monitoring data assimilation. *Transportation Geotechnics*, 24, 100369.

Peeters, J., Busschers, F.S. & Stouthamer, E. (2015) Fluvial evolution of the Rhine during the last interglacial-glacial cycle in the southern North Sea basin: A review and look forward. *Quaternary International.* Volume 357, pp: 176-188. https://doi.org/10.1016/j.quaint.2014.03.024

Pritchard, O.G., Hallett, S.H. & Farewell, T.S. (2015) Probabilistic soil moisture projections to assess Great Britain's future clay-related subsidence hazard. *Climate Change*. 133, 635-650. https://doi.org/ 10.1007/s10584-015-1486-z

Schmidt, C.W. (2015) Delta Subsidence: An Imminent Threat to Coastal Populations. *Environmental Health Perspectives.* 123 (8): A204-A209. https://doi.org/10.1289/ehp.123-A204

Schothorst, C.J., (1982). Drainage and behavior of peat soils. In: *Proceedings of the symposium on peat lands below sea level*, edited by H. de Bakker & M.W. van den Berg. ILRI-publication 30: 130-163.

Schultz, E. (1983). From Natural to Reclaimed Land. *Water International*, 8(2), 55–60. https://doi.org/10.1080/02508068308686007

Spaan, B. (2015). Buildings, *Waag Society*. URL: https://code.waag.org/buildings/

Spikker, M. (2010) Funderen in Almere. *Msc. Thesis TU Delft*

Stanley, J.D. & Clemente, P.L. (2014) Clay Distributions, Grain Sizes, Sediment Thickness and Compaction Rates to Interpret Subsidence in Egypt's Northern Nile Delta. *Journal Of Coastal Research*, 30 (1), 88-101. https://doi.org/10.2112/JCOASTRES-D-13-00146.1

Steckler, M.S., Oryan, B., Wilson, C.A., Grall, C., Nooner, S.L., Mondal, D.R., et al. (2022) Synthesis of the distribution of subsidence of the lower Ganges-Brahmaputra Delta, Bangladesh. *Earth-Science Reviews* 224, https://doi.org/10.1016/j.earscirev.2021.103887

Steenbergen, C., Reh, W., Nijhuis, S. & Pouderoijen, M. (2009) The Polder Atlas of The Netherlands – Pantheon of the Low Lands. *THOTH*, ISBN: 978-90-6868-519-0

Sun, Q., Jiang, L., Jiang, M., Lin, H., Ma, P. & Wang, H. (2018) Monitoring Coastal Reclamation Subsidence in Hong Kong with Distributed Scatterer Interferometry. *Remote Sensing* 10 (11), pp:1738. https://doi.org/10.3390/rs10111738

Syvitski, J., Kettner, A., Overeem, I., Hutton E., Hannon, M., Brakenridge, R., et al. (2009) Sinking deltas due to human activities. *Nature Geoscience* 2, 681–686 https://doi.org/10.1038/ngeo629

Teatini, P., Ferronato, M., Gambolati, G. & Gonella, M. (2006). Groundwater pumping and land subsidence in the Emilia-Romagna coastland, Italy: Modeling the past occurrence and the future trend. *Water Resources Research* 42. https://doi.org/10.1029/2005WR004242.

Thépaut, J. N. (2003). *Satellite data assimilation in numerical weather prediction: An overview. In Proceedings of ECMWF Seminar on Recent Developments in Data Assimilation for Atmosphere and Ocean*, Reading UK: ECMWF. (pp. 8-12).

TNO (2022) REGIS II, hydrogeologisch model (HGM). *Basisregistratie Ondergrond (BRO).* URL: REGIS II, hydrogeologisch model (HGM) - Basisregistratieondergrond

Tarantola, A. (2005), *Inverse Problem Theory and Method for Model Parameter Estimation*. Paris; SIAM.

TNO-GSN (2022) DINOloket, https://www.dinoloket.nl/

Tosi, L., Teatini, P. & Strozzi, T. (2013) Natural versus anthropogenic subsidence of Venice. *Scientific Reports* 3: 2710. https://doi.org/10.1038/srep02710

Van Asselen, S., Stouthamer, E. & Van Asch, Th.W.J. (2009) Effect of peat compaction on delta evolution: A review on processes, respones, measuring and modeling. *Earth-science Reviews* 92-1, pp: 35-51. https://doi.org/10.1016/j.earscirev.2008.11.001

Van Asselen, S., Erkens, G., Stouthamer, E., Woolderink, H.A.G., Geeraerts, R.E.E. & Hefting, M.M. (2018), The relative contribution of peat compaction and oxidation to subsidence in built-up areas in the Rhine-Meuse delta, The Netherlands. *Science of the Total Environment* 636, 177-191. https://doi.org/10.1016/j.scitotenv.2018.04.141

Van Asselen, S., Erkens, G. & de Graaf, F. (2020) Monitoring shallow subsidence in cultivated peatlands. *Proceedings of the International Association of Hydrological Sciences*. 382, 189-194. https://doi.org/10.5194/piahs-382-189-2020

Van den Biggelaar, D.F.A.M., Kluiving, S.J., Van Balen, R.T., Kasse, C., Troelstra, S.R. & Prins, M.A. (2014) Storms in a lagoon: flooding history during the last 1200 years derived from geological and historical archives of Schokland (Noordoostpolder, the Netherlands) *Netherlands Journal of Geosciences.* 93, 175-196, https://doi.org/10.1017/njg.2014.14

Van Dooremolen, W.A., van der Scheer, A. & Winkels, H.J. (1996), Waarnemingen en Prognoses van maaiveldsdaling in Flevoland, *Flevobericht* 388, ISBN: 90-369-1161-3

Van de Kerkhof, B., Pankratius, V., Chang, L, van Swol, R. & Hanssen, R.F. (2020), Individual Scatterer Model Learning for Satellite Interferometry. *IEEE Transactions on Geoscience and Remote Sensing.* 58-2, https://doi.org/10.1109/TGRS.2019.2945370.

Van den Akker, J.J.H., Kuikman, P.J., De Vries, F., Hoving, I., Pleijter, M., Hendriks, R.F. A., et al. (2008) *Emission of CO2 from agricultural peat soils in the Netherlands and ways to limit this emission.* In: Farrell, C., Feehan, J. (Eds.), Proceedings of the 13th International Peat Congress., pp. 1–6.

Van der Maaten, L. & Hinton, G. (2008), Visualizing Data using t-SNE, *Journal of Machine Learning Research* 9, 2579-2605

Van der Meulen, M., Maljers, D., Gesssel, S.F. & Gruijters, S.H.L.L. (2007) Clay resources in the Netherlands, *Geologie en Mijnbouw, Netherlands Journal of Geosciences.* https://doi.org/10.1017/S001677460002312X

Van der Meulen, M., Doornenbal, J., Gunnink, J., Stafleu, J., Schokker, J., Vernes, R., et al. (2013). 3D geology in a 2D country: Perspectives for geological surveying in the Netherlands. *Netherlands Journal of Geosciences - Geologie En Mijnbouw*, 92(4), 217-241. https://doi.org/10.1017/S0016774600000184

Van Hardeveld, H. A., Driessen, P. P. J., Schot, P. P., & Wassen, M. J. (2017). An integrated modelling framework to assess management strategies steering soil subsidence in peatlands. *Environmental Impact Assesssment Review*, 66, 66– 77. https://doi.org/10.1016/j.eiar.2017.06.007

Van Nieuwenhuizen Wijbenga, C. (2019) Rijksbrede inzet op bodemdaling. *Ministerie van Infrastructuur en Waterstaat:* IENW/BSK-2019/135551.

Viscchedijk, M.A.T. & Trompille,V. (2009) MSettle Version 8.2. Emankment design and soil settlement prediction. *Deltares report*

Vos, P.C. (2015), Origin of the Duthc coastal landscape. Long-term landscape evolution of the Netherlands during the Holocene, described and visualized in national, regional and local palaeogeographical map series. (Doctoral Dissertation) Retrieved from: Utrecht University Repository. (https://dspace.library.uu.nl/handle/1874/315553) Utrecht: Utrecht University

Wang, M., Li, T. & Jiang, L. (2016) Monitoring reclaimed land subsidence in Hong Kong with InSAR technique by persistent and distributed scatters. *Natural Hazards* 82, pp 531-543. https://doi.org/10.1007/s11069-016-2196-1

Wang, W., Liu, H., Li, Y. & Su, J. (2014) Development and management of land reclamation in China. *Ocean & Coastal Management* 102B, pp: 415-425. https://doi.org/10.1016/j.ocecoaman.2014.03.009.

Wegmüller, U, Santoro, M., Werner, C. & Cartus, O. (2015) On the estimation and interpretation of Sentinel-1 tops InSAR coherence. *Proc. 'Fringe 2015 Workshop'*

Yu, B., Liu, G., Li, Z., Zhang, R., Jia, H., Wang, X., & Cai, G. (2013). Subsidence detection by TerraSAR-X interferometry on a network of natural persistent scatterers and artificial corner reflectors. *Computers & Geosciences*, 58, 126–136. https://doi.org/10.1016/j.cageo.2013.04.020

Zaadnoordijk, W.J., Bus, S.A.R., Lourens, A. & Berendrecht, W.L. (2018) Automated Time Series Modelling for Piezometers in the National Database of the Netherlands. *Groundwater*. https://doi.org/10.1111/gwat.12819